SUSTAINABLE AND DURABLE INFRASTRUCTURE WITH ADVANCED CONSTRUCTION MATERIALS

A Thesis

by

JENNIFER MICHELLE PROUTY

Submitted to the Office of Graduate and Professional Studies of
Texas A&M University
in partial fulfillment of the requirements for the degree of

MASTER OF SCIENCE

Chair of Committee,	Mary Beth Hueste
Co-Chair of Committee,	Stefan Hurlebaus
Committee Members,	John Mander
	Mohammed Haque
Head of Department,	Robin Autenrieth

August 2014

Major Subject: Civil Engineering

ABSTRACT

Two experimental prestressed concrete bridge girder projects focus on the use of advanced materials including Aramid fiber reinforced polymers (AFRP) bars and self-consolidating concrete (SCC). One specimen is a precast, prestressed concrete bridge girder (TxDOT Type A) reinforced with AFRP that was tested to determine how the girder acts compositely with the bridge deck. The second specimen is a full-scale bridge girder (modified Tx70) constructed using spliced girder technology with SCC precast, prestressed concrete girder segments. The major objectives of this research are: (1) to characterize the concrete and reinforcement materials for the AFRP girder, (2) to characterize the concrete materials for the spliced girder, and (3) to conduct a comparative analysis of the AFRP girder and the spliced girder concrete materials.

AASHTO LRFD (2006), ACI 363 (1992) (revised by Al-Omaishi et al. 2009), ACI 318 (2008), CEB-FIP (2010), and Trejo et al (2008) prediction models were used to conduct a comparative analysis of the behavior of the material properties, such as modulus of elasticity, splitting tensile strength, and modulus of rupture, for both projects. It is important to note that the trends and models discussed in this thesis are limited to the behavior of the concrete tested for this research and the measured experimental data obtained.

Further research into the behavior of SCC, curing conditions, and alternative test methods for mechanical properties of SCC would be beneficial for the future concrete industry. Information concerning the longevity of AFRP use in bridge girder as well as retrofitting existing girders using these construction materials is currently limited. Longer term tests of AFRP and SCC in bridge girders needs to be conducted to discern the behavior of the material after a number of years in service.

ACKNOWLEDGMENTS

I would like to thank my committee chair, Dr. Mary Beth Hueste, and co-chair, Dr. Stefan Hurlebaus, for their guidance and support in this research and the support of my committee members, Dr. John Mander and Dr. Mohammed Haque.

Thank you especially to Dr. Hueste for encouraging me to apply for my master's degree at Texas A&M University. I would also like to thank all the people who have assisted me to get to this point including the faculty and staff at North Carolina State University and Texas A&M University. I would like to thank all of my friends and family for their love and support.

TABLE OF CONTENTS

Page

LIST OF FIGURES

Page

LIST OF TABLES

Page

1. INTRODUCTION

1.1 Background

Advances in knowledge and technology are an important part of growth and preservation of infrastructure. The current methods and materials of construction typically give structures a target life span before repair or replacement is required. It is important to investigate new materials and new ways to construct bridges to promote more sustainable infrastructure that is resistant to loading and natural environmental conditions allowing for longer life spans of these structures.

Two experimental prestressed concrete bridge girder projects focus on the use of advanced materials including Aramid fiber reinforced polymers (AFRP) bars and self-consolidating concrete (SCC). This thesis focuses on investigating short-term and long-term properties of these materials to gain insight and information regarding structural applications specifically for prestressed concrete bridge structures.

The research projects are geared toward implementation. As part of the overall project scopes, full-scale girder specimens have been constructed using these advanced construction materials. One specimen is a precast, prestressed concrete bridge girder (TxDOT Type A) reinforced with AFRP that was tested to determine how the girder acts compositely with the bridge deck. The second specimen is a full-scale bridge girder (modified Tx70) constructed using spliced girder technology with SCC precast, prestressed concrete girder segments.

The first project is focused on assessing the use of AFRP tendons in pretensioned bridge girders. Aramid fiber reinforced polymer tendons, which are inherently corrosion resistant, can be used to replace steel prestressing strands in bridge girders to enhance bridge sustainability. Despite ongoing experimental research, there is a lack of uniformity and consistency in testing procedures, definitions of material characteristics, as well as results.

The second project has an overall objective of developing economical design alternatives for longer span bridges through the use of continuous precast, pretensioned concrete bridge structures that use spliced girder technology. Aesthetic and economic

demands require a need for longer spans, fewer columns and minimal bent cap cross-sections in bridges. Crowded urban areas require long-span bridges in order to cross over major roadways. Current bridge construction practices in many states include prestressed bridges with continuous spans but there has been limited verification of the ability of the connection to provide the predicted continuity. The precast, pretensioned girder segments spliced and tested in this project are fabricated using SCC.

1.2 Research Objectives

The major objectives of this research are: (1) to characterize the concrete and reinforcement materials for the AFRP girder, (2) to characterize the concrete materials for the spliced girder, and (3) to conduct a comparative analysis of the AFRP girder and the spliced girder concrete materials. The data and findings are summarized, conclusions are drawn, and recommendations are provided for future research and implementation.

The first objective is to characterize the concrete and reinforcement materials for the AFRP girder. Samples that were cast and tested for the SCC used in the pretensioned AFRP reinforced girder and the steel reinforced deck provided data on associated material mechanical properties. Fresh properties and hardened properties were tested in accordance with their corresponding ASTM and TxDOT standard procedures. Fresh property tests of the concrete, such as slump flow, unit weight, and concrete temperature were conducted and the test samples were cast for future testing of hardened properties. Hardened property tests, such as compression strength (f'_c), modulus of elasticity (MOE), splitting tensile strength (STS), modulus of rupture (MOR), and shrinkage were performed at a number of test ages. Shrinkage testing was conducted to provide general insight into the long-term characteristics of the concrete. Test results of the AFRP girder materials are analyzed and trends discussed.

The second objective is to characterize the concrete materials for the spliced girder specimen. With the implementation of SCC in the bridge girder segments and high strength high slump conventional concrete (CC) in the connections, material tests are essential to provide data on their expected behavior. The same tests identified for the

AFRP girder concrete are used for the spliced girder. Test results for the spliced girder samples are analyzed and trends discussed.

The third objective is to conduct a comparative analysis of the concrete materials used in the two projects. The SCC samples are also compared and related to the samples of the high strength, high slump concrete used for the connections and the CC used in the deck. The CC used for the spliced girder deck provides a baseline of normal strength concrete, allowing determination of the benefits of high strength concrete and SCC.

From this research, conclusions are made on the observed trends and behavior of the materials used in these projects. Characterization of the AFRP and SCC provide additional data for implementation of these advanced construction materials into current practice and suggest possible aspects for future research.

1.3 Research Tasks

This research study focuses on the properties of SCC and AFRP materials used in precast, prestressed concrete girders. The modified Tx70 and the AASHTO Type I I-Girder (TxDOT Type A) are made using SCC. Fresh property tests of the concrete and fabrication of test specimens for hardened material properties testing were conducted on the day of the concrete pour of the associated full-scale specimen. Hardened properties tests, such as f'_c , MOE, STS, MOR, and shrinkage are measured based on different test sample ages per standard codes of practice (ASTM C39, C78, C496, C469, and C596, respectively). Shrinkage tests provide information on the long-term characteristics of SCC.

The following six major tasks were identified to accomplish the objectives of this research study, as follows:

- Task 1: Literature Review
- Task 2: Concrete Testing Procedures
- Task 3: AFRP Girder
- Task 4: Spliced Girder
- Task 5: Comparative Analysis of Materials
- Task 6: Summary, Conclusions, and Recommendations

1.3.1 Task 1: Literature Review

Literature review was conducted on past research and industry applications for SCC and AFRP. Concrete mechanical properties definitions and equations are presented and discussed.

1.3.2 Task 2: Concrete Testing Procedures

The experimental program included testing fresh and hardened properties of the concrete mixtures used in constructing the full-scale girder specimens for the AFRP girder and spliced girder projects. These results provide insight into the properties of the materials used to understand the associated girder specimen behavior. Fresh properties for the concrete include slump for CC and slump flow for SCC, unit weight, temperature, and air content. Hardened properties include compression strength, MOE, STS, MOR, and shrinkage.

1.3.3 Task 3: AFRP Girder

The AFRP girder materials include SCC and AFRP ARAPREE® bars and prestressed strands. This task defines, in further detail, AFRP and the purpose of its use in the AFRP girder specimen. The grout-coupler system that was designed to overcome the problems encountered in fabrication is also described. In addition, the grout for the coupler prestressing system and the AFRP strands used was also evaluated. Results obtained from materials testing for this task are presented and trends are discussed.

1.3.4 Task 4: Spliced Girder

The spliced girder materials include precast SCC and cast-in-place (CIP) concrete for the connections and the deck. This task defines, in further detail, the materials as well as the mixture proportions for the precast SCC girder (modified Tx70) and the CIP concrete connections. The connection concrete was selected to avoid potential problems during casting such as flowability of the mix for the congested splices. Results obtained from materials testing for this task are presented and trends are discussed.

1.3.5 Task 5: Comparative Analysis of Materials

Task 5 focuses on a comparative analysis of the results from both the AFRP girder and the spliced girder concrete mixtures. Data of the SCC mixtures from two different precast plants are analyzed to compare the mechanical properties of the SCC from the AFRP girder and the SCC and connection concrete mix of the spliced girder. Trends are discussed. Current AASHTO LRFD and ACI 318 prediction equations for mechanical properties of conventional concrete used in industry will be evaluated for their applicability to the data. New expressions are developed as needed.

1.3.6 Task 6: Summary, Conclusions and Recommendations

Based on the design test samples, issues pertaining to design, adoption and implementation of advanced construction materials, specifically SCC and AFRP, are identified. Recommendations for further research are discussed.

1.4 Organization of Thesis

Section 1 provides an introduction to this thesis and outlines the objectives of the research. Section 2 provides a literature review on the mechanical properties of concrete, the background and implementation of SCC, and background and implementation of AFRP. Section 3 provides detailed information on testing procedures and determination of the fresh and hardened properties of concrete. Section 4 and 5 detail the construction process and limitations of the AFRP girder and spliced girder, respectively, and present the sample test results. Section 6 discusses the prediction equations for the various hardened properties compared to the experimental results obtained. Section 7 summarizes the results and findings of this research and provides recommendations for implementation of these advanced construction materials and future research needs.

2. LITERATURE REVIEW

2.1 General

The AASHTO Type I I-Girder and Tx70 modified girder were fabricated using SCC. Mechanical properties of concrete were determined per standard codes of practice. Prior to casting the AFRP girder, tensile tests were conducted to determine the strength of the AFRP material to be used for the prestressing operation in the girder. The following sections discuss key mechanical properties of concrete and AFRP and relevant research studies.

2.2 Prestressed Concrete Girder Design

Prestressed concrete girder design includes both service and strength limit states, along with serviceability checks as specified in the AASHTO Load and Resistance Factor Design (LRFD) Bridge Design Specifications (2012). The service limits for flexure are used to ensure that the girder remains in the uncracked elastic state during pretensioning and construction, and at service under dead and live loads. Typically these service limits governs the design, whereas the deflection limit state serves as a final check for service conditions by considering allowable deflection under live loads. In addition, both flexure and shear are checked to ensure safety at ultimate load conditions. Mechanical properties of the concrete girder and deck are critical to predicting the structural behavior of prestressed concrete girders and to determine appropriate limiting stresses or forces at service and ultimate load conditions. For example, because the cracking moment is directly related to the MOR, the design equation values provide limits to estimate the cracking moment of the beam. A lower bound (LB) estimate of the MOR is relevant when considering service load stress limits, serviceability (to determine if the beam is cracked), and corresponding deflections. The upper bound (UB) MOR equation is to determine the minimum amount of reinforcement, by ensuring that the nominal moment capacity of member is at least 20 percent greater than the cracking moment. If the cracking moment is too close to the nominal moment capacity, the beam could fail in a brittle manner (AASHTO LRFD 2012). In addition, accurate estimates of

the MOE are important for determining elastic shortening losses for the prestressing and deflections of the girder.

2.3 Mechanical Properties of Concrete

Mechanical properties of concrete such as compressive strength, MOE, STS and MOR are useful in predicting the behavior of the full-scale girder specimens. Compressive strength is typically the key mechanical property that is used to estimate MOE, STS and MOR in the absence of additional test data. This research focuses on the use of self-consolidating concrete, or self-compacting concrete, which is a relatively recent advancement in the concrete industry that exhibits a high slump and consolidates under its own weight.

Type III Portland Cement was used in the AFRP SCC girder and SCC deck, as well as the spliced SCC girder and the high strength high slump concrete connections, in order to achieve high early strength and allow the forms to be removed within a day after casting. Knowledge of the compressive strength, MOE, STS and MOR of the concrete used in the girder specimens is important to estimate behavior of the full-scale specimens before and after prestressing. These properties aid in understanding and estimating the camber of the prestressed members at release, elastic deflection caused by dead and live loads, axial shortening and elongation, and prestress losses (Long et al. 2013).

MOE is the ratio between the stress and strain of the concrete, which can be found by taking the initial slope of the stress-strain curve. This ratio is significant for structural design because it represents the maximum allowable stress before the specimen is permanently deformed (Mehta and Monteiro 2006). MOE of concrete is influenced by the porosity of the cement paste, which is a function of the water-to-cement (*w/c*) ratio used, and the relative proportion of cement and aggregate (Gutierrez and Manuel 1995). Typical *w/c* ratios range from 0.4 to 0.6 but for high strength concrete (HSC) lower *w/c* are used with superplasticizers to maintain flowability. It is important for concrete to have ample ability to flow when casting so that the concrete fills the form without any voids as well as passing through the reinforcement.

The tensile strength of concrete is important to predict the initiation of cracking of a concrete member when it is subjected to an external force (Trejo et al. 2008). To estimate the tensile strength of concrete, flexural prisms are used to determine MOR and splitting cylinders are used to determine STS. Studies show that the true tensile strength, as obtained from the STS test, is between 65–75 percent of the MOR for normal concrete. The acceptance of the STS is based on the knowledge that the stress distribution is uniform along the vertical diameter of the cylinder, which is the plane of principle tensile stress for roughly 80 percent of its length (Sesha Phani et al. 2013). The STS can be related to compressive strength by a power function. The ratio of STS to compressive strength results in STS not remaining constant, but rather STS decreases as compressive strength increases (Ozyildirim and Carino 2006).

Research shows that the MOR decreases with increasing beam size. The cause of the size effect on MOR stems from the semi-brittle nature of the material, and particularly the stress redistribution and energy release caused by a fracture with a large fracture process zone (Bazant and Novak 2001).

Curing conditions of the samples can have an effect on the strength of the concrete. There are three main functions of curing concrete: maintaining mixing water of the concrete during early hardening stages, reducing the loss of mixing water from the surface of the concrete, and accelerating strength gain using additional heat and moisture. Precast plants use these methods by covering specimens after casting with burlap and sprayers to keep the concrete moist during initial curing. ACI Committee 301 recommends samples be cured a minimum amount of time in order to reach 70 percent of the specified compressive strength (2010). The effect of moist curing (initially versus entire time before testing) on the compressive strength of concrete samples can be seen in Figure 2.1.

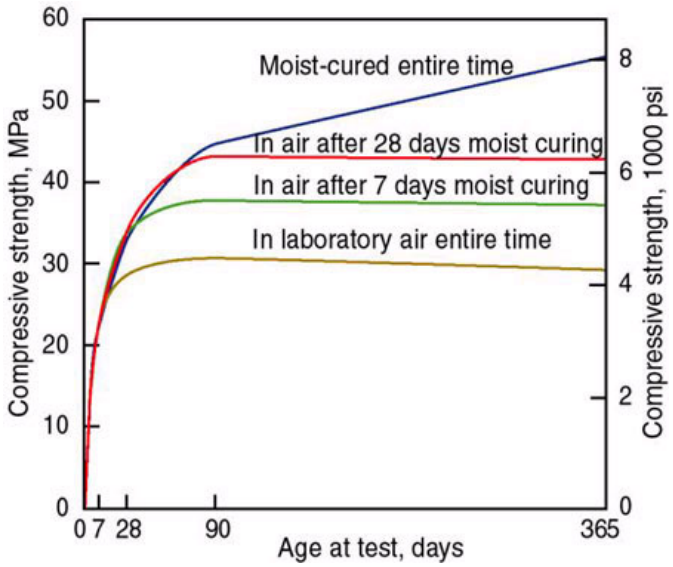

Figure 2.1. Moist Curing and Compressive Strength Gain (Zemajitas 2014).

Hameed (2009) conducted a study on the effect of curing conditions on the compressive strength of HSC by testing moist curing on sample groups for seven days then air drying versus water curing until the day of testing. Hameed found that water curing the samples aided in attaining the objective compressive strength due to the low *w/c* (2009). Newbolds and Olek (2001) performed research on different curing conditions, such as lime bath or sandpit, for samples and the effect it had on the strength properties and maturity development of concrete. It was found that samples had higher flexural strengths when cured in a moist condition (lime bath or sandpit) than air cured samples (Newbolds and Olek 2001). The results also indicated that air cured samples had the most similar compressive strengths to the sandpit cured samples, while the lime bath cured samples exhibited different strengths compared to both the air cured and sandpit cured samples (Newbolds and Olek 2001).

2.4 Self-Consolidating Concrete

SCC exhibits a high slump and consolidates under its own weight. Therefore, it is poured with no mechanical vibration, which allows the mix to be used for heavily congested reinforced shapes, particularly bridge deck girders. The three essential

properties of SCC are filling ability under self-weight, passing ability through congested reinforcement, and segregation resistance (Koehler et al. 2007).

SCC was first used in Japan in the late 1980s and gained wide acceptance for casting congested members as well as concrete placement in difficult-to-access areas, where consolidation may not be feasible. SCC is considered a new class of high performance concrete (HPC) used to facilitate and accelerate concrete placement without hindering in-situ properties and durability (Khayat 1999). The creation of this HPC that no longer requires mechanical vibration allows for less labor and increased worker safety, quicker installations, and reduced construction noise (Okamura and Ozawa 1996).

As SCC has grown to have a wider acceptance, more studies have been conducted in order to better understand the properties and benefits. ACI Committee 237 (2007) reported on SCC as an emerging technology and encouraged the use of it throughout the U.S. According to Daczko (2012), a common list of benefits has been compiled for 60 case studies whose details are published and accessible to the public. The identified benefits can be described using the following categories:

1. Ease of placement in areas with limited access
2. Provide higher in-place quality and aesthetics
3. Ease of placement and consolidation through dense reinforcement
4. Faster speed of construction and time savings
5. Labor savings
6. Ease of placement and consolidation in a complex structure or shape
7. Improved worker safety and noise reduction.

As more research is conducted and standards established by known associations such as the American Society for Testing and Materials (ASTM) and the American Concrete Institute (ACI), SCC has gained more popularity. However, although the benefits are numerous, as of 2008 statistics, only roughly 40 percent of all precast production in the United States uses SCC and even a smaller amount of just 2-4 percent of the cast-in-place industry was using SCC (Daczko 2012). Figure 2.2 shows the

frequency of specific SCC benefits by the precast and cast-in-place (CIP) concrete sectors using the seven factors noted above in relation to the 60 case studies analyzed by Daczko (2012). The statistics for overall concrete construction are also provided.

As seen in Figure 2.2, the three primary advantages for the use of SCC in precast projects are higher in-place quality and aesthetics, faster speed of construction, and time and labor savings. The statistics are not entirely clear if the benefits are because SCC is more widely used in precast sectors currently and if these numbers would change if SCC is used more overall. SCC is beneficial in both precast and CIP sectors for areas of difficult or congested placement and can be economically beneficial by saving on labor and equipment costs.

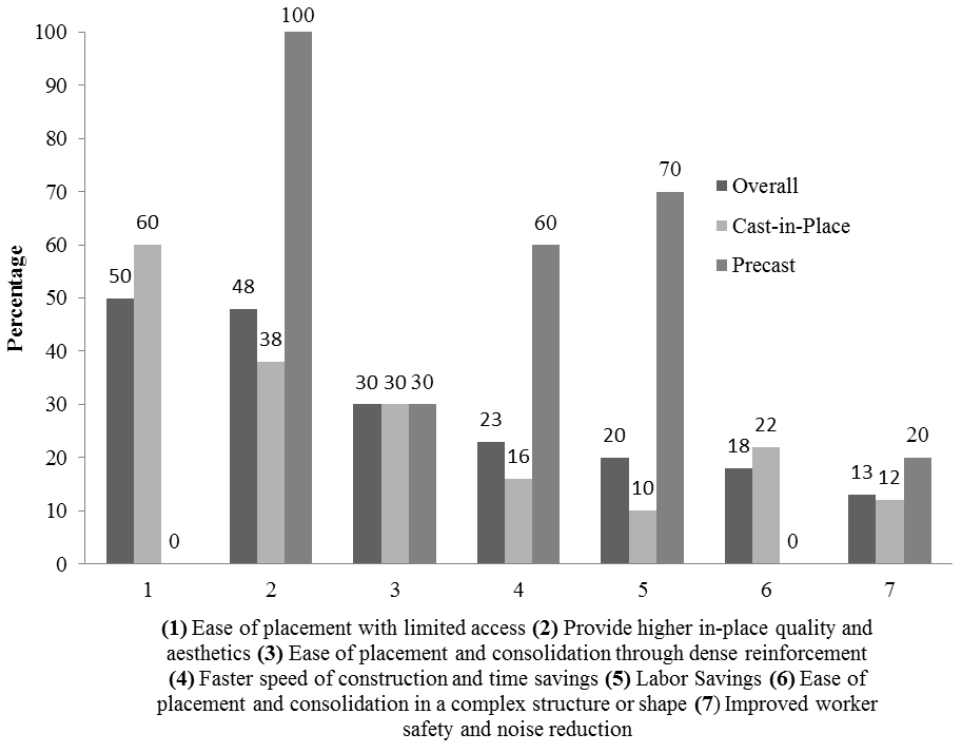

Figure 2.2. SCC Used in Precast and CIP Production (Daczko 2012).

SCC does not come without limitations. There is a possibility of bleeding, segregation, and settlement when using flowing concrete mixtures. However, the design and application of SCC mixes and the evaluation of the fresh properties is important to ensure these characteristics are minimized or eliminated (Mehta and Monteiro 2006, Daczko 2012, Naik et al. 2012). Because of the high flowability of a SCC mixture, limitations may include the inability to immediately withstand self-weight, hold form or shape when pouring on a significant slope, as well as delivery or workability time.

In the modern concrete industry, it has become more common to use a variety of cementitious components, such as fly ash, or chemical admixtures, such as superplasticizers, to give concrete certain desired characteristics. Concrete self-compacting properties can be achieved by: limited aggregate content, low *w/c* ratio, and use of superplasticizers (Okamura and Ouchi 2003, Okamura and Ozawa 1996). However, slump flow does not increase when more high range water reducers (HRWRs) or superplasticizers are added. HRWRs only affect the cement paste portion of a mix; the paste fraction is determined by the *w/c* ratio. Concrete mixture fluidity is determined by the relationship between the *w/c* ratio and the aggregate characteristics (Daczko 2012).

Henault (2014) conducted research on the use of SCC in structural precast operations. Currently the Connecticut Department of Transportation (ConnDOT) only allows the use of SCC for drainage structures, barriers, and retaining walls. The purpose of the research was to gain more knowledge of SCC and the characterization based on material property tests and specifications. As of now, ConnDOT does not have specifications for using SCC, other than what is already required for conventional concrete (Henault 2014). Slump flow tests were observed at each of the five plants that the research team visited in 2008. Currently ConnDOT uses a high slump CC, up to 8 in., that has been used for over two decades in their prestress applications. As a result of this study, Henault recommended that SCC not be used in prestressed elements until ConnDOT enforces a more rigorous SCC mixture proportioning and acceptance process. This process should include workability tests on batches prepared by precast plants and required to meet target test results as specified in NCHRP Report 628 that evaluate

filling ability, passing ability, filling capacity, static stability, and air volume (Henault 2014). Such tests, including but not limited to visual stability index, T20, and J-ring, are described later in this thesis in Section 3, SCC fresh property tests.

Trejo et al. (2008) conducted research on the characterization of SCC for design of precast, prestressed bridge girders. Different SCC mixtures and proportions were evaluated for mechanical properties, shear characteristics, bond characteristics, creep, and durability. The research focused on the evaluation of girders using SCC and determining if the current design prediction equations are applicable or if new or modified equations are needed to estimate mechanical properties. Particular variables of interest for the different mixes included: mixture type (SCC or CC), coarse aggregate type (limestone or river gravel), and coarse aggregate volume (Trejo et al. 2008). Trejo et al. (2008) evaluated existing equations for concrete mechanical properties provided by the American Association of State Highway Transportation Officials (AASHTO) Load and Resistance Factor Design (LRFD) Bridge Design Specifications (2006) and ACI Building Code Requirements for Structural Concrete and Commentary (ACI Committee 318 2005). Applicability of these expressions for SCC mixtures was assessed based on experimental results of compressive strength, MOE, STS, and MOR.

Conclusions were drawn about SCC mixtures and proportions. SCC mixtures tested exhibited higher early strength, workability, and later age strengths than comparable CC mixtures. The volume of coarse aggregate for both river gravel and limestone mixtures was found to have minimal influence on the compressive strength in the Trejo et al. (2008) research. River gravel mixtures exhibited higher values of MOE compared to the limestone mixtures because of the high stiffness of the river gravel itself. In the prediction of MOR and STS for SCC and CC mixtures, the volume of the coarse aggregate was not found to be a statistically significant variable (Trejo et al. 2008). However, according to research conducted by Domone (2007), compressive strength results led to the conclusion that strength difference between mixes with crushed and uncrushed coarse aggregate is lower for SCC than for CC. Trejo et al. (2008) found that CC mixtures exhibit higher MOR values than SCC mixtures. The

MOR values for limestone SCC mixtures were lower than river gravel SCC mixes. STS of the river gravel SCC mixtures was significantly higher than limestone SCC mixtures, which may be attributed to the low strength of limestone aggregate. SCC mixtures predominately had higher STS values than the CC mixtures.

The main two sources for design equations evaluated by Trejo et al. (2008) for SCC were AASHTO (2006) and ACI 318 (2005); these equations can be seen in Table 2.1. The CEB-FIP model code (2010) serves as an international basis for Eurocode design guidelines. Mechanical properties of SCC evaluated in the study led to the development of models for the MOE, MOR, and STS which were compared to AASHTO LRFD and ACI prediction equations. Research performed by Trejo et al. (2008) presented refined equations that may better suit a material such as SCC. The prediction equations are dependent on coarse aggregate types (limestone versus river gravel). Al-Omaishi et al. (2009) commented that the revised ACI 363 committee report (1992) suggests that the MOE may be underestimated with the ACI 318 equations and a new proposed equation may be more suitable for HSC above 6 ksi. The equation is calculated in ksi with a limit of the unit weight between 0.145 and 0.155 kcf.

In Table 2.1, K_1 is the correction factor for source of aggregate and should be taken as 1.0 unless determined by a physical test, w_c is the unit weight in pounds per cubic foot (pcf), and α is 0.9 for limestone and 1.0 for quartzite, or river gravel, aggregates. The CEB-FIB model for MOR is based on beams with a cross-section height and depth of six inches. For Table 2.1 equation calculations f'_c is in psi, except for the AASHTO LRFD (2006) and ACI 363 (2009) equation, where w_c is in kcf and f'_c is in ksi.

Combining the data for river gravel and limestone SCC mixtures, general simplified equations were developed to predict MOE, STS, and MOR. These unified design equations can be seen in Table 2.2. The upper and lower bound equations were obtained from the 95 percent prediction interval for STS and MOR (Trejo et al. 2008). For Table 2.2 equation calculations, f'_c is in psi.

Table 2.1. Prediction Equations for CC Mixtures (Adapted from Trejo et al. 2008).

Equation Source	MOE (psi)	STS (psi)	MOR (psi)
AASHTO LRFD (2006)	$33{,}000 K_1 w_c^{1.5} (f'_c)^{0.5}$	$0.23(f'_c)^{0.5}$	Lower bound, $0.24(f'_c)^{0.5}$
			Upper bound, $0.37(f'_c)^{0.5}$
ACI 318 (2008)	$33 w_c^{1.5} (f'_c)^{0.5}$	$6.7(f'_c)^{0.5}$	$7.5(f'_c)^{0.5}$
CEB-FIP (2010)	$593{,}400\alpha(f'_c/10)^{1/3}$	$8.2[(f'_c - 1160)/10]^{2/3}$	$11.04[(f'_c - 1160)/10]^{2/3}$
ACI 363 (1992)	$(w_c/0.145)^{1.5}(1000 + 1265(f'_c)^{0.5})$	-	-

Table 2.2. Prediction Equations for SCC Mixtures (Trejo et al. 2008).

MOE (psi)	STS (psi)	MOR (psi)
Unified, $267{,}100(f'_c)^{0.343}(w_d/150)^{3.3}$	Lower bound, $6.3(f'_c)^{0.5}$	Lower bound, $0.75(f'_c)^{0.75}$
	Upper bound, $10.2(f'_c)^{0.5}$	Upper bound, $1.15(f'_c)^{0.75}$

2.5 Aramid Fiber Reinforced Polymers

The use of fiber reinforced polymer (FRP) materials in strengthening applications of concrete is becoming more accepted and used by engineers due to the beneficial characteristics such as light weight, high strength, corrosion resistance and the performance uninhibited by harsh conditions. FRP composites consist of fiber reinforcements with high strength and stiffness, and a matrix system that is used to bind the fibers. Different reinforcements are used such as unidirectional fibers, woven fabrics, and braided preforms, which are made of glass, carbon, Kevlar, aramid, or alumina. Application of FRPs in construction, retrofitting, and rehabilitation of structures has grown considerably in recent years (Trejo et al. 2000).

FRP bars may be categorized as aramid (AFRP), glass (GFRP), or carbon fiber polymer (CFRP) bars. ACI 440.1R (2006) recommends only AFRP and CFRP for prestressing applications. GFRP is not recommended because of its large susceptibility to creep rupture. AFRP ARAPREE® bars with diameter of 0.394 in. (10 mm) were used for the AFRP girder project as a substitute for either steel rebar or prestressing strand. Pirayeh Gar et al. (2012) investigated the uniaxial characteristics of 10 mm diameter ARAPREE® bars by conducting material tests including tensile strength, short-term and long-term creep and relaxation, and tension stiffening tests. According to the manufacturer, the bar surfaces were coated with quartz and resin to create a rough surface and increase the bond strength of the bar with a tensile strength of 203 ksi.

3. CONCRETE TEST PROCEDURES

3.1 General

Fresh property tests of the SCC used in this research, such as slump flow and unit weight, and sample fabrication for testing hardened material properties, were conducted on the day of casting the full-scale girder specimens. Representative samples of the concrete mixtures were taken and tested per standard testing procedures (ASTM C172 2010, Tx-407-A 2008). Summaries of the applicable ASTM and TxDOT standards for fresh properties are provided in Table 3.1.

Table 3.1. Overview of Fresh Property Tests for Concrete.

Property	ASTM Standard	TxDOT Standard
Slump	C143 (2012)	Tex-415-A (2008)
Slump Flow	C1611 (2009)	-
Unit Weight	C138 (2013)	Tex-417-A (2008)
Temperature	C1064 (2012)	Tex-422-A (2008)
Air Content	C231 (2010)	Tex-416-A (2008)

Hardened mechanical property tests, such as compression strength, MOR, STS, and MOE are measured based on different test sample ages per standard codes of practice (ASTM C39, C78, C496, and C469, respectively). Shrinkage testing (ASTM C596) was conducted to provide information on the general long-term behavior of the concrete. All laboratory concrete samples were made and cured in accordance with ASTM and TxDOT testing procedures (ASTM C31 2003 and Tex-447-A 2008). Summaries of the applicable ASTM and TxDOT standards for hardened properties are provided in Table 3.2.

Table 3.2. Hardened Property Tests.

Property	ASTM Standard	TxDOT Standard	Recommended Test Age
Compression Strength	C39 (2012)	Tex-418-A (2008)	1, 3, 28, 90 days
Modulus of Elasticity	C469 (2010)	-	As desired
Splitting Tensile Strength	C496 (2011)	Tex-421-A (2008)	28 days
Modulus of Rupture	C78 (2010)	Tex-448-A (2008)	As desired
Shrinkage	C596 (2009)	-	1, 2, 3, 4 weeks

3.2 Fresh Properties

Fresh property tests of the concrete including slump flow, unit weight, and temperature of the concrete were conducted on the day of casting each full-scale specimen. The use of fly ash and chemical admixtures, such as superplasticizers and retarders, are used in SCC mixtures in order to achieve low *w/c* ratios, achieve a high slump, and maintain workability. When determining water content for mixture proportions, one must consider the moisture content in the aggregates and adjust accordingly. Moisture content can be determined by following the testing procedures for coarse and fine aggregates (ASTM C127 2012 and C128 2012, respectively).

3.2.1 Slump Test

The slump of CC mixtures is tested in accordance with ASTM and TxDOT testing procedures (ASTM C143 2012, Tex-415-A 2008). The slump cone is placed on a flat, moist, nonabsorbent and rigid surface. The cone is held firmly in place by either standing on the two foot pieces on either side of the mold or using a base plate with a clamp (the former was used). The cone is filled in three layers of equal volume with an even distribution of the concrete around the sides for each layer. Each layer is rodded 25 times throughout its depth by inclining the rod slightly, making sure to uniformly

distribute the rod each time. This can be done by rodding in a spiral shape from the outside to center. For the second and third layer, the rod should penetrate the previous layer by approximately one inch. If rodding the third layer causes the concrete to fall below the top of the cone, concrete is added to keep an excess above the mold. The rodding count is continued from the value reached before the extra concrete was added. The top surface of concrete is struck off with the rod in a rolling motion. Any concrete collected around the base of the cone is removed, making sure to keep downward pressure on the cone. The cone is lifted in a steady upward direction without twisting and then placed upside down next to the specimen of concrete. The slump test must be conducted from the start of filling to the lifting of the cone in two to two and a half minutes. (ASTM C143 2012).

If a large portion of concrete falls away or shears off from one side or portion of the mass occurs the test is disregarded and conducted again on a new sample of concrete. Examples of possible slump test results can be seen in Figure 3.1. The slump should be measured immediately as the vertical distance between the top of the cone (upside down next to specimen) and the displaced original center of the top surface of the specimen. Slump is typically reported to the nearest quarter of an inch.

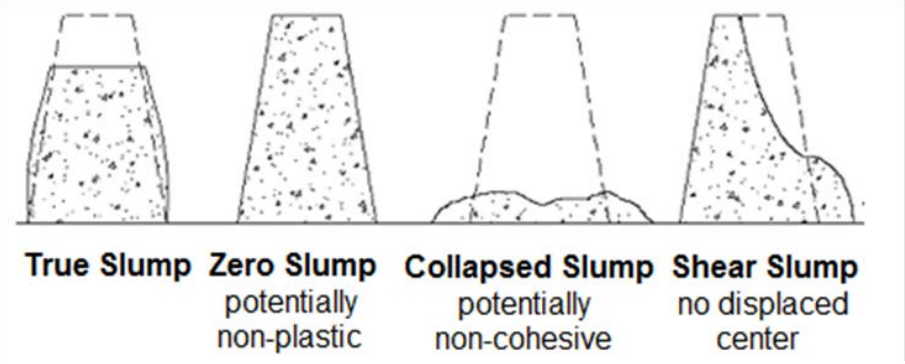

Figure 3.1. Types of Concrete Slump (ACI Committee 238 2008).

3.2.2 Slump Flow

Slump flow of SCC mixtures was tested in accordance with ASTM testing procedures (ASTM C1611 2009). This test is performed using the same slump cone used for the slump test of conventional concrete. The cone can be used in the standard upright position or inverted position (Daczko 2012). Figure 3.2 shows the slump flow testing procedure performed for the spliced girder project at the chosen precast plant. Rather than filling the cone in three lifts with rodding as with CC, the cone is filled in one lift without rodding because the SCC consolidates on its own (see Figure 3.2a).

(a) Filling the cone (b) Lifting the cone (c) Measuring slump diameter

Figure 3.2. Slump Flow Test.

Once the cone is lifted (Figure 3.2b), the diameter that the fresh concrete spreads is measured (Figure 3.2c), rather than the vertical displacement of the concrete measured for conventional slump testing. When performing this test, one must also take care to observe that there is no bleed water around the slump diameter to ensure there is not a segregation of materials and that the concrete is well mixed. Whether the test is conducted by one or several operators, the slump diameters shall not differ by more than three inches (ASTM C1611 2009). The optimum slump diameter to be observed is within the range of 22 to 28 inches.

3.2.3 Unit Weight

The unit weight of the concrete mixtures was determined in accordance with ASTM and TxDOT testing procedures (ASTM C138 2009, Tex-404-A 1999). First the weight of the empty unit weight bucket is determined. The bucket is 0.5 cubic feet allowing for a maximum size coarse aggregate of two inches. The bucket is to be filled in three lifts, each to be rodded 25 times followed by tapping the sides of the bucket with a rubber mallet 10-12 times. The use of a steel or metal bucket is required to ensure that the bucket will not lose the shape or affect the contents that have been prepared before weighing the full bucket. Because SCC consolidates itself, rodding may be deemed unnecessary in this test. The unit weight is calculated by subtracting the weight of the empty bucket from the full bucket weight and dividing by the volume of the bucket. For the purpose of this research a unit weight bucket with a volume of 0.5 cubic feet was used.

3.2.4 Other Tests

Additional fresh property tests are available for SCC including the visual stability index (VSI), T20 test, J-ring, rapid assessment of static segregation resistance of SCC using the penetration test, and static segregation of SCC using the column technique. Table 3.3 summarizes the fresh property tests, target values, and if the test is designated for design or quality control (QC) use.

The VSI and T20 tests are described in the appendix of ASTM C1611 (2009). VSI is a subjective test based on the observations made by the technician performing the slump flow test. The T20 test measures the viscosity of the concrete by measuring the amount of time it takes for concrete in the slump flow test to reach a diameter of 20 in. The J-ring test is performed with the same procedures as slump flow but with a cage of rebar setup around the slump cone. The difference between the J-ring flow and slump flow of SCC is that J-ring is used as an indicator of the passing ability of the concrete (ASTM C1621 2009), the two tests may not differ by more than two inches.

The penetration test is performed on an inverted slump cone with a penetration apparatus centered over the cone to determine a penetration depth to assess static

segregation of the mixture (ASTM C1712 2009). The penetration test does not measure static segregation directly but provides an assessment of the likeliness of static segregation occurring. The static segregation is measured by using the column technique which measures the coarse aggregate content in the top and bottom portions of an 8 in. x 26 in. cylinder sample (ASTM C1610 2010).

Table 3.3. Fresh Property Guidelines (adapted from Henault 2014).

Property	Test Method	Target Values	Design	QC
Filling ability	Slump flow	23.5-29.0 in.	x	x
	T-20	1.5-6.0 sec	x	x
Passing ability	J-ring flow	21.5-26.0 in.	x	x
Filling capacity	Filling capacity	70-100 %	x	
	Slump flow	-		x
	J-ring flow	-		x
Static stability	Column segregation	Column segregation index $\leq$5%	x	
	VSI	0-1 (0 for deep elements)	x	x
Air volume	Air content by pressure method	4.5-7% depending on exposure conditions, MSA, and type of HRWRA. Ensure stable and uniform distribution of small air voids.	x	x

3.3 Hardened Properties

Mechanical properties test results are used for two primary purposes. The first purpose is for engineering design, which can include failure theories based on strength, or deflections based on elastic constants and component geometry. The second purpose is for quality control either by the materials producer to verify the process or by the end user, such as the contractor, to confirm the material specifications. For the purpose of this research, the mechanical properties of the concrete are evaluated with test specimens that include 4 in. x 8 in. cylinders and 6 in. x 6 in. x 20 in. beams as specified in the ASTM standard procedures. All cylinder and beam samples were made in two lifts, each of equal volume. Rodding is not necessary because SCC consolidates on its own. However, after each layer was poured the samples were tapped on the outside of the molds 10-12 times before the second lift as per the standard for fabricating SCC specimens (ASTM C1758 2013).

While these specimens are presumed to have minimal flaws they provide valuable information about the materials used in the full-scale girder specimens. Specimens are fabricated and stored under laboratory conditions as a control group. Through the uniformity of testing, according to ASTM standards, the results should have reliability and repeatability with the same materials. The ASTM standards prescribe the method by which the test specimen is to be prepared and tested, as well as how the test results are to be analyzed and reported.

3.3.1 Specimen Preparation and Curing

All concrete cylinder samples were cured next to the full-scale girder after fabrication. Type III Portland Cement was used in the SCC mixtures to achieve high early strength and allow the precast girder forms and sample molds to be removed within a day after casting. The AFRP girder project girder SCC specimens remained next to the girder after casting for several days until the SCC deck was cast. On the day after casting the deck, all AFRP girder and deck samples were transported from the precast plant to the Texas A&M University laboratory facilities and the molds removed. The spliced girder samples were transported from the precast plant to the Texas A&M University

laboratory facilities one day after casting the girder segments and the molds removed. The connection concrete samples were made and cured in the Texas A&M University Department of Civil Engineering High Bay Structural and Materials Testing Laboratory (TAMU HBSMTL) next to the spliced girder full-scale specimen. The molds were removed on the day after casting.

Once the cylinder and beam samples were de-molded, they were moved to be stored in an environmental curing room of 77°F and greater than 97 percent relative humidity as per ASTM standards (ASTM C31 2012, ASTM C511 2013). The shrinkage prism samples were stored in a separate curing room of 77°F and 50 percent relative humidity as required by the standard. Initially the moist curing room met all ASTM specifications for temperature and relative humidity (RH) and was monitored on a weekly basis. However, due to equipment malfunction the curing room did not remain a consistent humidity four months after the AFRP girder and spliced girder samples were stored and just prior to the storage of the spliced girder connection and deck samples. This malfunction resulted in a lower RH of the room, while the temperature remained at an acceptable constant value. The curing room temperature and RH were continually monitored with an ambient temperature and RH thermometer. Specimens were periodically dipped and sprayed with water to maintain moisture content.

3.3.2 Compressive Strength

Concrete cylinder samples were tested for compressive strength in accordance with ASTM and TxDOT testing procedures (ASTM C39 2004, Tex-418-A 2008). Three 4 in. x 8 in. cylinder samples were tested for each age. Compressive strength was evaluated at 16 hours and 3, 7, 28, 56, and 90 days. The day of large scale specimen tests, and/or 90-day samples, are allowed plus or minus two days to perform the test. All cylinder samples were tested with a 500 kip capacity MTS machine. The cylinders were capped on the top and bottom with steel caps and 70 durometer neoprene pads before loading into the machine for testing. Compressive strength tests were performed with a load rate of 35 psi/s as recommended by ASTM C39 (2012).

The standard test method for determining f'_c of the cylindrical test specimens is defined by ASTM C39 (2012). Cylinder specimens can be either 4 in. x 8 in. or 6 in. x 12 in. For the purpose of this research the specimens used were 4 in. x 8 in. cylinders so that the diameter (d) is four inches and the height is eight inches. Compressive strength is determined by dividing the maximum load (P) applied by the MTS machine by the area of the cylinder face.

$$f'_c = \frac{P}{\pi\left(\frac{d}{2}\right)^2} \tag{3.1}$$

3.3.3 Modulus of Elasticity

MOE of the concrete samples was tested in compression in accordance with ASTM testing procedures (ASTM C469 2010). Three 4 in. x 8 in. cylinder samples were tested for each test age. MOE was evaluated at 7, 28, and 56 days. All cylinder samples were tested with a 500 kip capacity MTS machine. The cylinders were capped on the top and bottom with steel caps and 70 durometer neoprene pads before loading into the machine for testing. MOE testing was displacement controlled with a load rate of 35 psi/s as recommended by ASTM C469 (2010).

Figure 3.3 shows the MOE testing apparatus with two LVDTs mounted on the cylinder at 180 degrees. The metal brackets around the test cylinder are attached by tightening the screws into the concrete cylinder to hold the brackets in place with a four inch gage length for the LVDTs.

Figure 3.3. Modulus of Elasticity Testing Apparatus.

The standard test method for determining the static modulus of elasticity in compression to the nearest 50,000 psi is defined by ASTM C469 (2010). The equation is:

$$E_c = \frac{S_2 - S_1}{\varepsilon_2 - \varepsilon_1} \tag{3.2}$$

where E_c is the Young's modulus of the concrete, S_2 is the stress (psi) corresponding to 40 percent of the ultimate load, and S_1 is the stress (psi) corresponding to the longitudinal strain ε_1 (in./in.) of 0.00005. The longitudinal strain ε_2 (in./in.) is the strain produced by stress S_2.

3.3.4 Splitting Tensile Strength

STS specimens were tested in accordance with ASTM and TxDOT testing procedures (ASTM C496 2011, Tex-421-A 2008). Three 4 in. x 8 in. cylinder samples were made for STS for each test age. The STS was evaluated at 7, 28, and 56 days. All cylinder samples were tested with a 500 kip capacity MTS machine. STS testing was performed with a constant load rate between 100 and 200 psi per minute (approximately 2.5 psi/s) as recommended by ASTM C496 (2011).

As seen in Figure 3.4, STS test is performed with the cylinder on its side. As the force is applied by the MTS machine, a vertical crack should begin to appear and propagate down the vertical diameter of the cylinder. The crack will eventually propagate to failure by splitting the cylinder into two halves.

(a) Cylinder orientation (b) Typical crack propagation

Figure 3.4. Splitting Tensile Test.

The standard test method for the splitting tensile strength is defined by ASTM C496 (2011) and is calculated as:

$$T = \frac{2P}{\pi l d} \tag{3.3}$$

where T is the tensile strength, P is the maximum load applied by the MTS machine (psi), l is the length (in.) and d is the diameter (in.). For the purpose of this research l is eight inches and d is four inches.

3.3.5 Modulus of Rupture

MOR specimens were tested in accordance with ASTM and TxDOT testing procedures (ASTM C78 2010, Tex-448-A 2008). Three 6 in. x 6 in. x 20 in. beam samples were cast for each test age of modulus of rupture. MOR was evaluated at 7, 28,

and 56 days. All beam specimens were tested with a 20 kip capacity MTS machine to evaluate MOR at a load rate of 30 lb/s until failure.

When performing the MOR test, the test is deemed invalid if the beam does not break within the middle third region of the span. For instance, the beams used for this project were 20 in. long. The MOR testing setup and tested beams is shown in Figure 3.5a. The testing apparatus allows for a one inch overhang on either side of the roller supports so that the remaining 18 in. in length is the region of interest. Breaking this length into thirds, the beam must fail with the crack propagation beginning and ending somewhere in the middle 6 in. of the beam (Figure 3.5b).

The standard test method for flexural strength, reported as MOR, is determined by a simple beam third-point loading test. If the fracture initiates in the tension surface within the middle third of the span length when loading the specimen, ASTM C78 (2010), the equation for calculating the MOR is:

$$R = \frac{PL}{bd^2} \tag{3.4}$$

where R is the modulus of rupture (psi), P is the maximum load applied by the MTS machine (lb), L is the span length (in.) of the beam specimen, b is the average width of the specimen (in.), and d is the average depth of the specimen (in.). The specimens were measured before testing and the measured dimensions were used for the MOR calculations. These measurements differed by 0.0625 in. or less from the nominal dimensions of 6 or 18 in. The beams were also measured after each test to ensure the failure occurred within the middle third region of the beam, a minimum of 7 in. to a maximum of 13 in. from the beam end.

(a) Beam orientation (b) Typical cracking behavior

Figure 3.5. Modulus of Rupture Testing Apparatus and Tested Beams.

3.3.6 Shrinkage

Shrinkage samples were fabricated and tested in accordance with ASTM C490 (2011) and C596 (2009). Four 4 in. x 4 in. x 12 in. nominal size prisms were fabricated for the representative batches of the AFRP girder and spliced girder projects. Comparator readings were taken at 1, 2, 3, and 4 weeks per the standard as well as readings between 30 and 40 weeks, shortly after testing the spliced girder. Shrinkage readings were taken by using the length comparator apparatus, zeroing the reference bar (11.625 in.) before each prism reading. The prism was loaded into the apparatus and slowly turned to take measurements for all four sides of the prism to be averaged. The comparator apparatus with a loaded prism sample is shown in Figure 3.6. Readings were taken for each prism and then averaged for each batch

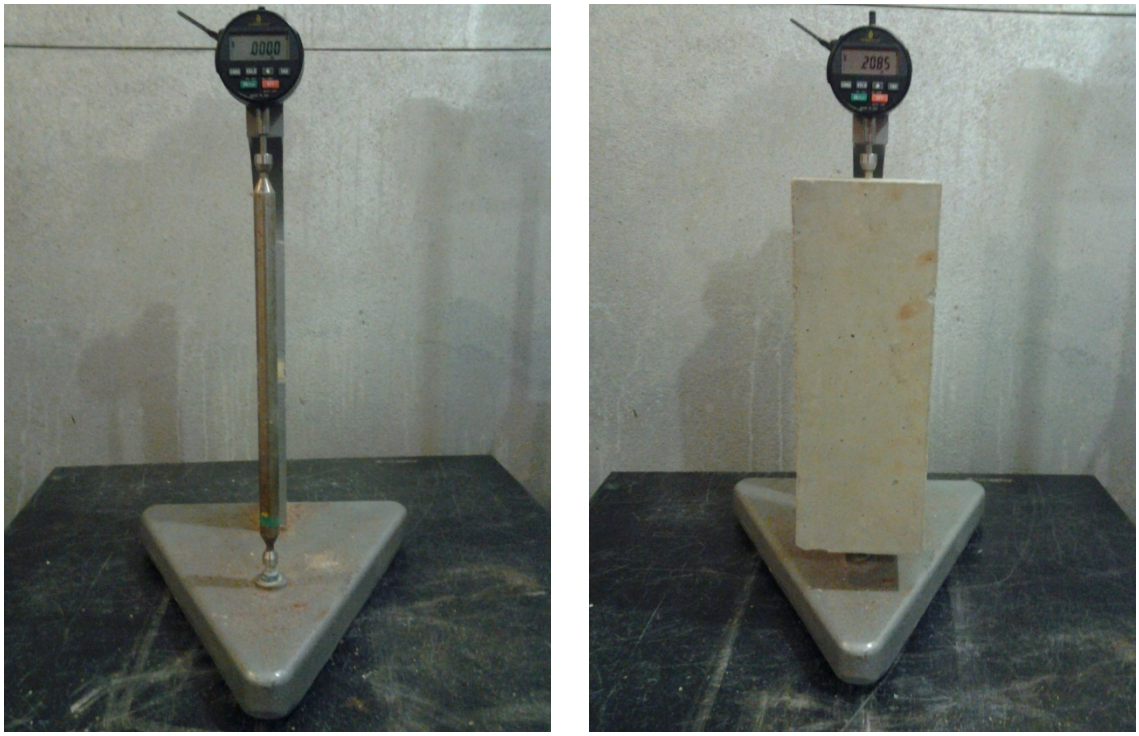

(a) Zeroing with the comparator rod (b) Measuring shrinkage of the sample

Figure 3.6. Apparatus for Measurement of Length Changes for Shrinkage.

4. ARAMID FIBER REINFORCEMENT GIRDER

The AASHTO Type I I-Girder was made using SCC. Fresh property tests of the concrete, such as slump flow and unit weight as well as making the specimens for future mechanical properties testing, were conducted on the day of casting. Mechanical properties tests, such as compression strength, MOE, STS, MOR, and shrinkage are identified based on different test sample ages per standard codes of practice (ASTM C39 2004, C469 2010, C496 2011, C78 2010, and C596 2009 respectively).

4.1 Construction of Specimen

SCC was chosen for the girder and deck so that vibration of the concrete was not necessary to avoid damaging the AFRP strands and reinforcing bars in the girder. However, the steel forms were vibrated in order to rid the concrete of any unwanted air bubbles. The girder was reinforced with prestressed AFRP strands, non-prestressed AFRP bars, and AFRP reinforcement R stirrups, bottom bar, and top side bar. The deck was reinforced with mild steel. The reinforcing layout of the girder and deck can be seen in Figure 4.1.

(a) Girder AFRP reinforcement (b) Deck mild steel reinforcement

Figure 4.1. Reinforcement Layout.

The AFRP was cut to specific lengths to heat and bend into shape for the reinforcement needed for the AFRP girder. Three bar types were made: R stirrups, bottom bar and top side bar. The reinforcement bar fabrication process can be seen in Figure 4.2. Before bending, the bars were heated in order to soften the resin mix coating of the AFRP to allow for ductility of the bar, see Figure 4.2a. Once the bar was heated with the heat gun, a rubber mallet is used to press the bar to soften the resin (see Figure 4.2b). Once the resin coating is softened, it is malleable and can be bent into the desired shape for the stirrups and other reinforcement (see Figure 4.2c and 4.2d).

(a) Heating the resin

(b) Softening the resin

(c) Resin softened and pliable

(d) Reshaping the bar

Figure 4.2. AFRP Bar Bending Process (Pirayeh Gar 2012).

The composite deck was made by leaving the R-shape stirrups exposed after casting the girder so that when the deck was cast the deck SCC would bond to the stirrups and the roughened girder surface. Composite behavior of the girder and deck

was also achieved by using high-strength A490 shear bolts with one inch diameter at approximately every 18 in. The girder and the finished composite deck specimen can be observed in Figure 4.3.

(a) Girder

(b) Girder with composite deck

Figure 4.3. AFRP Girder and Deck.

4.2 Initial Construction Challenges

The project faced several issues involving the prestressing equipment available at the chosen precast plant and the requirements for the scope of this project. The W-line prestressing bed used to prestress standard AASHTO Type I (TxDOT Type A) girders is 75 ft. in length. However, the specimen designed for this project is only 40 ft. in length. AFRP tendons could span the entire length but it would be a waste of costly materials. The course of action to mitigate this problem was to design a splice to join the AFRP strands with conventional steel strands to span the remaining bed length.

4.2.1 Coupler Anchorage System

The couplers used to make the splice were made by grouting a hollow steel pipe, with an inner diameter of 1.5 in. and a wall thickness of 0.2 in., to join conventional steel

strand and the AFRP strand. The prestressing process requires that the coupler must hold a 14 kips prestressing force for three days without failure.

Tests were conducted to determine the compression strength of the grout and tensile strength of the AFRP strands. These separate material tests allow for no ambiguity as to the reason for the failures in prestressing tests of the coupler. These tests also provide results that can be compared with previous research conducted in this field and a similar experiment by Pirayeh Gar (2013).

4.2.1.1 Grout Material Test

Grout sample cubes were made to test the strength of the two types of grout used. Grout "S" was used in previous research by Pirayeh Gar (2013) and grout "K" that has been used in all prestressing tests for this study thus far. The 2 in. x 2 in. x 2 in. cubes were made in accordance with ASTM C305 (2013) and ASTM C109 (2013) for mixing of mortar and casting cubes, respectively. Results from compression tests performed on these samples at age seven days are shown in Table 4.1

Table 4.1. Grout Strength Results.

Grout Type	**S**			**K**		
Sample #	1	2	3	1	2	3
Ultimate Stress (ksi)	7.66	7.77	4.00	4.24	5.91	-

When removing grout cubes from the molds the third grout type "K" specimen broke, therefore only two specimens were tested. The first two specimens for grout type "S" remained consistent with strength of approximately 7.7 ksi while the third specimen was half the strength. Even though the grout type "K" had a large range for the two specimens tested, the grout was found to have a satisfactory strength.

4.2.1.2 AFRP Material Test

The AFRP underwent a tensile strength test by grouting the ends of a 56 in. length piece of AFRP with 18 in. long steel pipes with the same diameter and thickness as used for the coupler tests. The AFRP strand was embedded the full length of each pipe, leaving roughly 20 in. of the AFRP exposed. The specimen was then loaded into the MTS machine as seen in Figure 4.4. The MTS tensile test of the two specimens yielded consistent results with an average of 18 kips axial force.

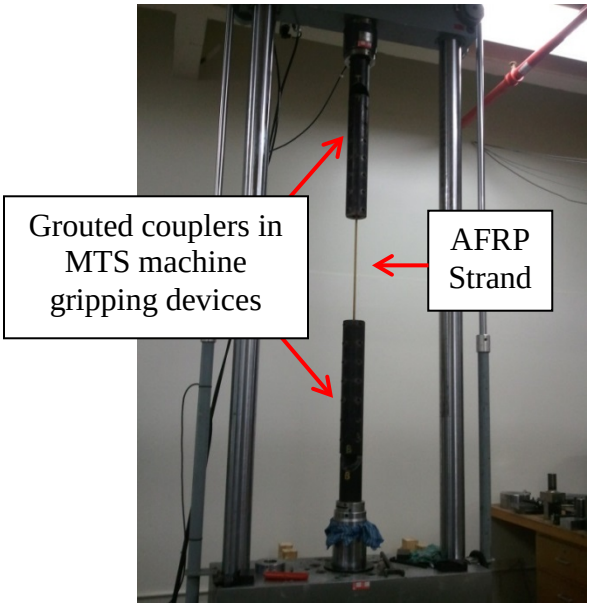

Figure 4.4. AFRP Strand Tensile Test.

4.2.1.3 Coupler Tests

The coupler tests required equipment available from the HBSMTL, the initial test setup can be seen in Figure 4.5. Once a specimen passed the short term test, immediate jacking to failure, the next step was to undergo a long term test, jacking and holding the prestressing force for three days, to see if the coupler-splice solution could withstand the required prestressing force for a prolonged period of time.

Several options were designed and fabricated to undergo short term tests, the first four options used AFRP strand and conventional steel strand:

- Specimen 1 was made by grouting a normal steel pipe.
- Specimen 2 was made by first cleaning the inside of the pipe with a wire brush and using a grout mix that was determined to be optimal, with an 3:8 water-to-grout powder ratio.
- Specimen 3 was fabricated by cleaning the inside of the pipe and then crimping the pipe every two inches at 90 degree turns.
- Specimen 4 was made with a welded end of the pipe and sealing the other end by using epoxy adhesive to attach a washer.
- Specimen 5 welded the ends of the 36 in. long each coupler and dead end pipes, no plastic end caps or epoxied on washers were used. Threaded rod was used, rather than conventional steel strand, to minimize torsion of the pipe with the steel-grout bonded end.

Specimen 1 exhibited grout pullout and AFRP slip at less than 10 kips force provided by jacking the material. It was assumed that perhaps the grout mixture was too inconsistent and perhaps the residue in the pipe before grouting contributed to the slipping. The initial coupler design for Specimens 1, 2, and 3 can be seen in Figure 4.6.

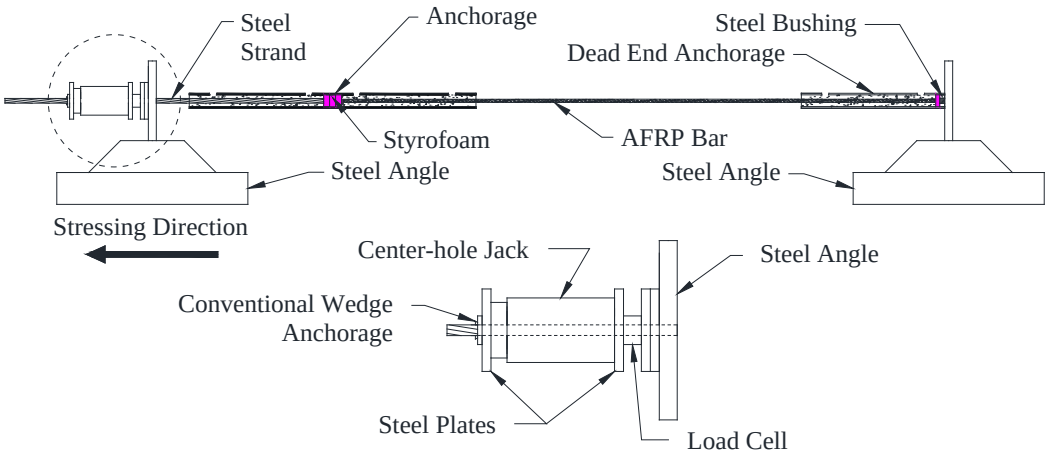

Figure 4.5. Initial Coupler Test Setup (Hurlebaus et al. 2014).

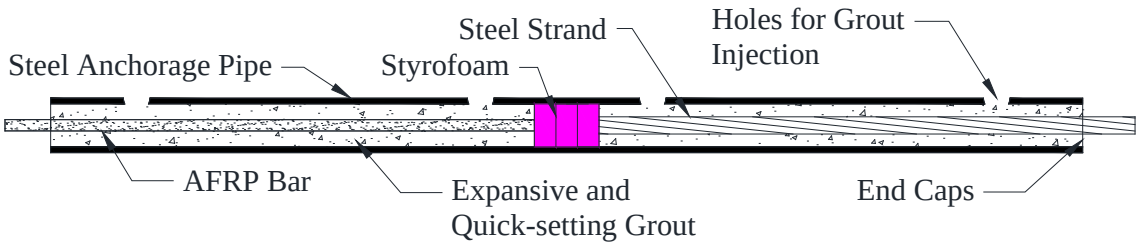

Figure 4.6. Initial Coupler Design for-Specimens 1, 2, and 3 (Hurlebaus et al. 2014).

Specimen 2 used an optimal grout mixture with a water-to-grout powder ratio of 3:8, and this ratio was used for all subsequent tests. The second specimen tested experienced grout pullout at less than 10 kips force. It was determined that the friction between the grout and inner wall of the pipe was insufficient. The grout slippage can be observed in Figure 4.7.

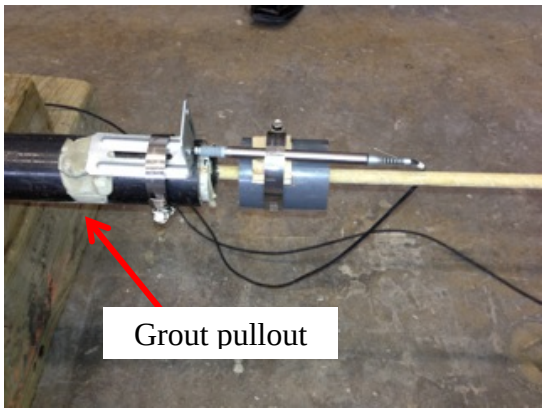

Figure 4.7. Grout Pullout During Short Term Coupler Test.

The crimping process for Specimen 3can be observed in Figure 4.8. The pipe was then grouted using the determined optimal grout mixture. Specimen 3 tested achieved a jacking force of 24 kips before AFRP pullout from the grout was observed.

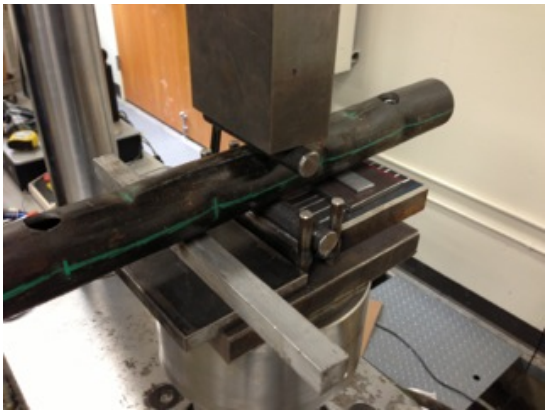

Figure 4.8. Crimping Pipe Every 2 in. at 90° Turns.

The successful tensile test of the AFRP strands, allowed the team proceeded with making the new dead end and coupler for Specimen 4. Specimen 4 was made with a welded end of the pipe and sealing the other end by using epoxy adhesive to attach a washer. The 36 in. long pipes for the dead end and the coupler were not crimped. The short term test failed. The specimen was stressed by the jack then released to set it and fell to 8 kips, not the prestressing force of 14 kips. The jack was then reconnected in attempts to stress the specimen a second time to obtain a higher force on the strand but the torsion of the steel spinning the steel-end of the coupler caused the exposed AFRP to twist, as seen in Figure 4.9. Figure 4.9b is a zoomed in look of the AFRP shown in Figure 4.9a.

Specimen 5 was made with a modified design to counteract the torsional problem encountered by the previous test. The ends of the 36 in. long each coupler and dead end pipes were all welded, no plastic end caps or epoxied on washers were used. Rather than using a steel strand, a threaded rod was used to minimize torsion of the pipe with the steel-grout bonded end. A 75 in. AFRP strand was used, embedded the full length of the dead end and embedded 18 in. into the coupler leaving 20 in. of exposed strand. The specimen was stressed to 18 kips and held without grout or AFRP pullout. The ends were then set and the jack removed. The specimen held an average of 16.5 kips of axial force for the entire three day long term test.

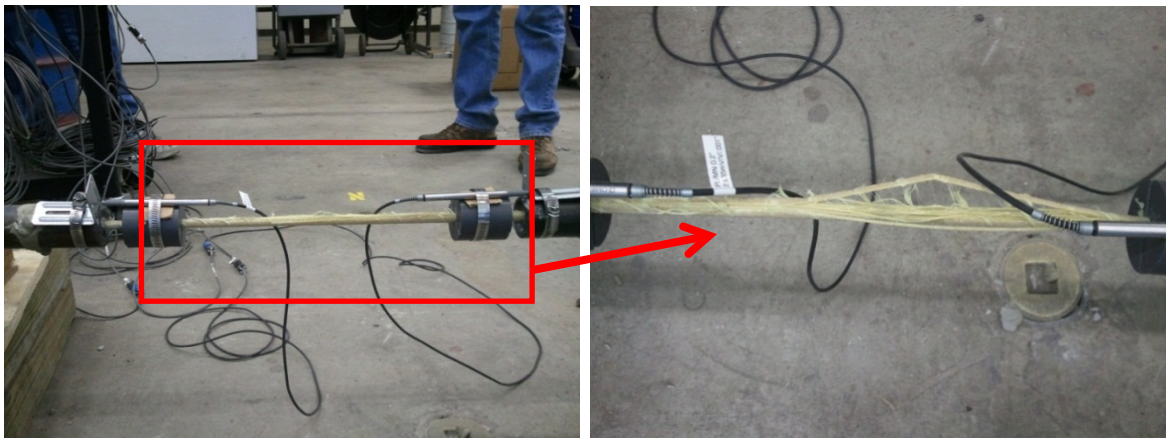

(a) AFRP torsion (b) AFRP rupture

Figure 4.9. AFRP Coupler Short Term Test.

A second long term test was performed to ensure reliability of the Specimen 5 coupler set up. The second test held an average axial force of 15 kips. The final coupler design and setup can be seen in Figure 4.10 and Figure 4.11, respectively.

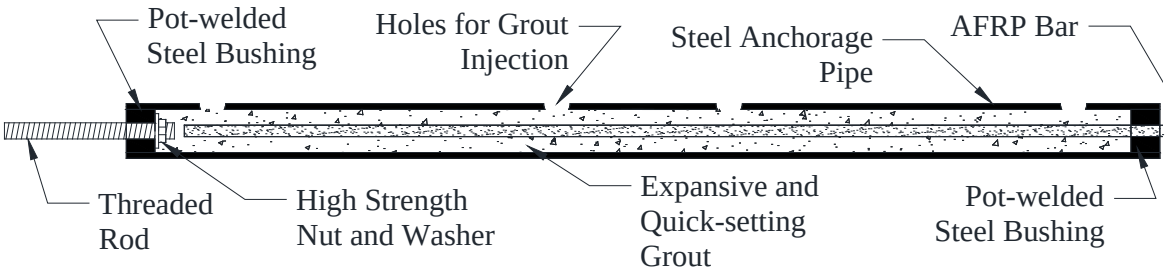

Figure 4.10. Final Design of Coupler Anchorage System, Specimen 5 (Hurlebaus et al. 2014).

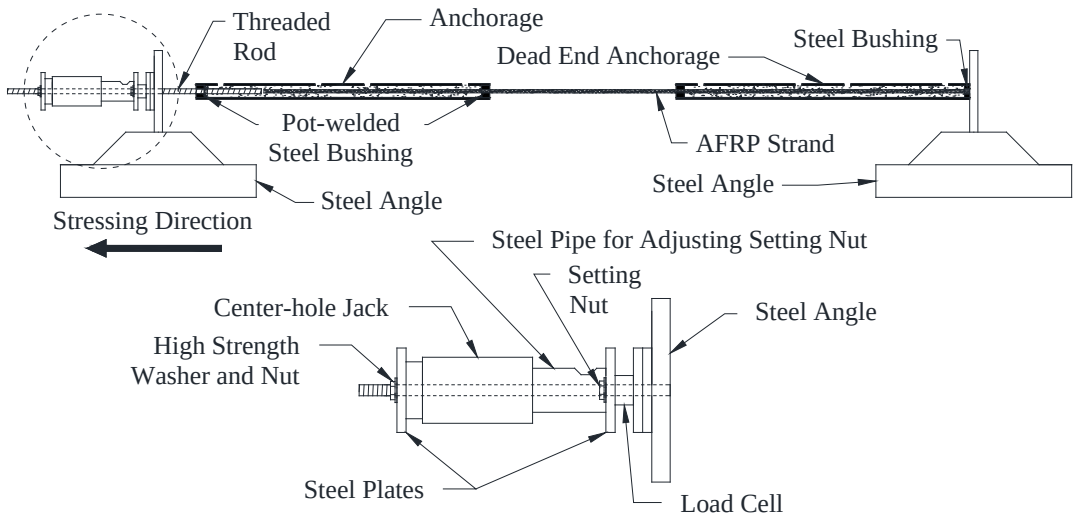

Figure 4.11. Final Coupler Test Setup (Hurlebaus et al. 2014).

4.2.2 Extending the Prestressing Plate

The other issue involving the prestressing equipment at the chosen precast plant was the prestressing plate for this size girder and the predetermined locations of the holes made in the plate for prestressing strands. The project specimen requires an extra row of ARFP to be prestressed, the location of this row is above the prefabricated prestressing plate of the W-line provided. The project design layout can be seen in Figure 4.12 and the prestressing plate provided can be seen in Figure 4.13.

Increasing the height of the prestressing plate required reaching the two prestressing strand locations indicated in the design plan. The proposed mitigation plan was to attach steel plates to the prestressing end plates at both ends of the W-line. The steel plates are 4 in. x 18 in. with 2 in. thickness and were attached to the end plates by threaded steel rods, with a diameter of 9/16 in., bolted in the existing top row of holes. The AFRP strands were then passed through the holes fabricated at the top of the steel plates, allowing the strands to be prestressed at the desired location for the design. Figure 4.14 shows the prestressing layout and results from morning of stressing the strands at the precast plant.

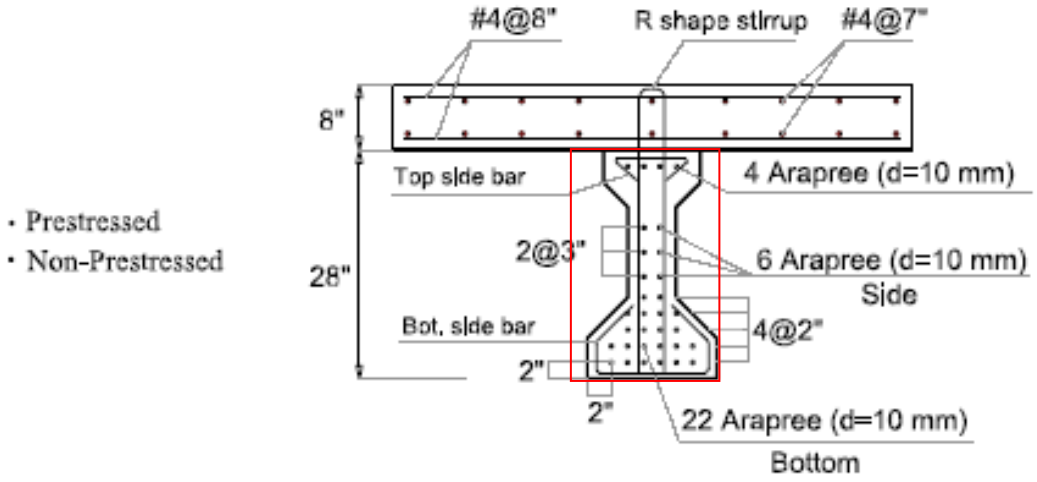

Figure 4.12. AFRP Specimen Design (Pirayeh Gar 2013).

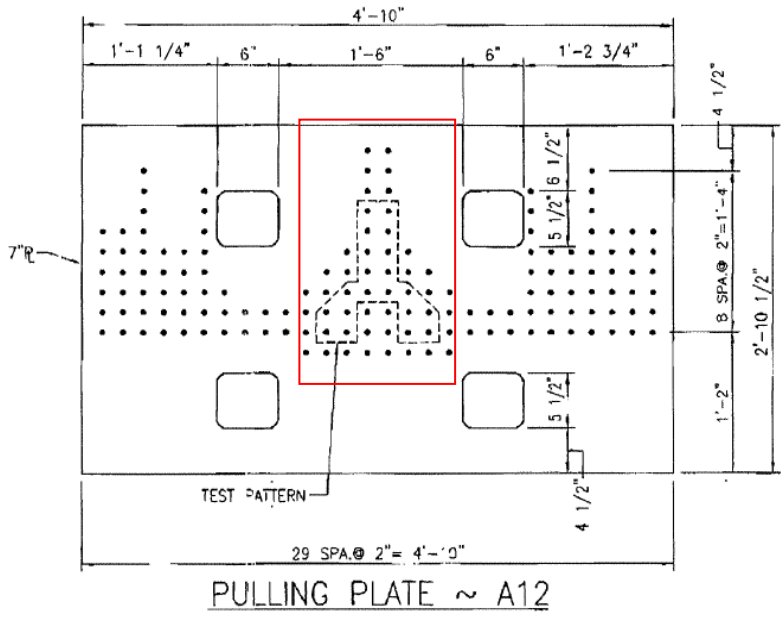

Figure 4.13. Prestressing End Plate for Prestressing Bed (Provided by precast plant).

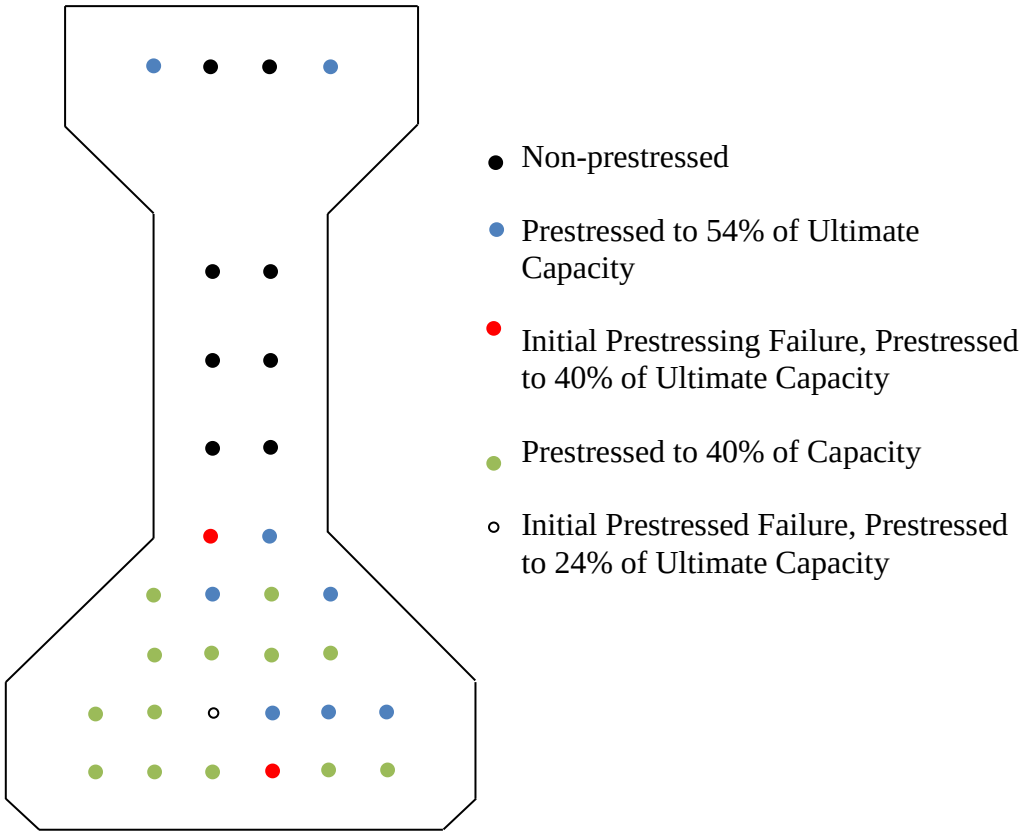

Figure 4.14. Prestressing Layout.

During the prestressing process some strands slipped in the couplers but held the force so they were deemed satisfactory and left intact. Three of the AFRP strands failed during prestressing. New couplers had to be grouted and AFRP strands inserted at the precast plant and then prestressed again. With these failures it was later determined to only partially prestress the remaining strands so that casting of the specimen could stay on schedule for that afternoon.

4.3 Materials Testing Program

The SCC mixture proportions, for saturated surface dry (SSD) conditions, used for the AFRP SCC girder and SCC deck are shown in Table 4.2. The *w/c* ratio was 0.31

with target 7-day compressive strength of 8.9 ksi. The aggregate properties are provided in Table 4.3.

Table 4.2. SCC Mixture Proportions Summary.

Materials		Type	Supplier	Quantity
Cement (lb/yd^3)		III	Capitol	640
Fly Ash (lb/yd^3)		Class F	-	213
Water (lb/yd^3)		-	-	264
Aggregate (lb/yd^3)	Coarse (MNAS 3/4 in.)	Concrete Rock	Capitol-Marble Falls	1712
	Fine	Washed River Sand	Capitol-Austin River	1240
Admixtures (oz/yd^3)		HRWR	Sika 4100	51
		Retarder	Sika Plastiment	17

The values reported are based on tests performed by the precast plant on a pilot test batch. Type III Portland cement was used in order to achieve high early strength and allow the forms to be removed within a day after casting. Fly ash is used in order to decrease the required cement amount, to reduce heat of hydration in hot weather, and is cost effective. Fly ash and chemical admixtures, such as superplasticizers and retarders, are used in SCC mixtures in order to achieve low water-to-cement ratios, achieve a high slump, and maintain workability.

The SCC girder was cast in August 2013 and the deck was cast three days later. The girder was cast with one batch and the deck was cast with two batches, each batch having a maximum volume of four cubic yards (cyd). Due to the scheduling of casting, the girder samples were left to cure next to the full-scale specimen for four days. The deck was cast three days after the girder and the samples were left to cure beside the full-

scale specimen for one day before all SCC samples were transported to the Texas A&M University campus facilities for storage and testing.

Table 4.3. Aggregate Specific Gravity and Absorption.

Aggregate	Specific Gravity	Absorption
Coarse	2.78	15.41
Fine	2.58	30.13

4.3.1 SCC Girder and Deck

Table 4.4 and Table 4.5 summarize the test matrix for the girder and the deck, respectively. Samples were made on each day of casting to test the fresh and mechanical properties of the girder and deck concrete. Three samples were made of each batch for each test age. The second batch deck samples were used primarily as a reliability check of the compressive strength of the first batch.

Table 4.4. Girder Test Matrix.

Age of Samples	f'_c	MOE	MOR	STS
1 day	G1	-	-	-
3 days	G1	-	-	-
7 days	G1	G1	G1	G1
28 days	G1	G1	G1	G1
Test Day (42 days)	G1	-	-	-
56 days	G1	G1	G1	G1

Table 4.5. Deck Test Matrix by Batch.

Age of Samples	f'_c	MOE	MOR	STS
1 day	D1	-	-	-
3 days	D1	-	-	-
7 days	D1, D2	D1	D1	D1
28 days	D1, D2	D1	D1	D1
Test Day (42 days)	D1	-	-	-
56 days	D1	D1	D1	D1

4.4 Results

4.4.1 Fresh Properties

On the day of casting the girder, the unit weight of the girder SCC was tested in accordance with ASTM 318 (2009) and calculated to be 0.148 kcf. A slump flow test was performed on the girder SCC mixture in accordance with ASTM 1611 (2009) and determined to be 23 in. The ambient air temperature on the day of casting the SCC deck was 97°F with a relative humidity in the air of 34 percent. The fresh property values on day of casting for the pilot test batch results provided by the chosen precast plant are shown in Table 4.6.

Table 4.6. SCC Mixture Fresh Properties (Provided by Precaster).

Parameter	Value
Slump Flow (in.)	24
Air Temperature (°F)	97
Concrete Temperature (°F)	93
Actual Unit Weight (kcf)	0.151

4.4.2 Hardened Properties

The results from the SCC sample tests of the girder and the deck were plotted and compared. The SCC mixture and samples were tested in accordance with all the appropriate ASTM standards and procedures for mechanical properties such as compressive strength, MOE, STS, and MOR.

4.4.2.1 Compressive Strength

Compressive strength specimens were made for the girder and both deck batches. Due to the previous mentioned schedule for the girder and deck castings, the 16-hour release strength of the girder and deck SCC samples as well as the 3-day compressive strength of the girder SCC samples were tested by the precaster at their laboratory facilities. The development of compressive strength from 1 day to 56 days and the ratio of the strength at each test age compared to the 28-day strength of the corresponding batch can be seen in Figure 4.15. The average f'_c experimental results by batch are shown in Table 4.7.

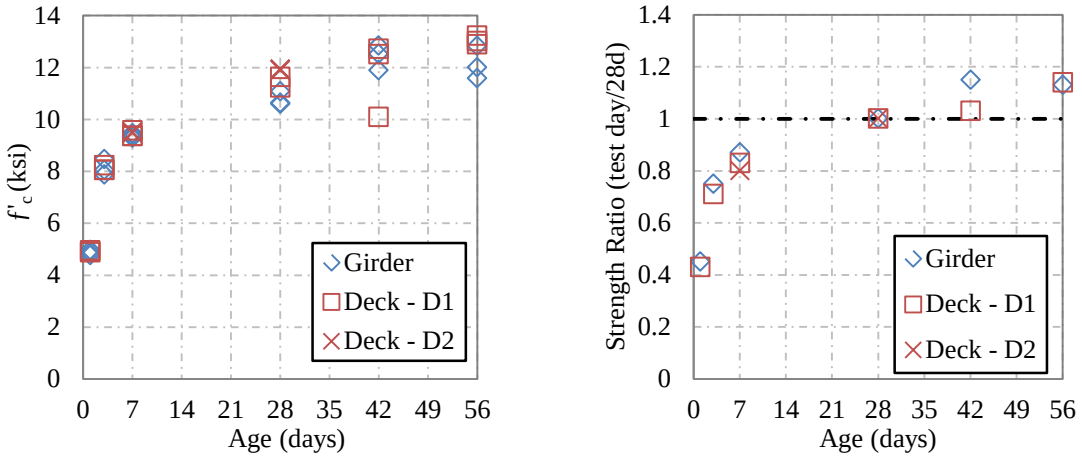

(a) f'_c gain over time (b) Compressive strength ratio

Figure 4.15. Girder and Deck Compressive Strength Experimental Data.

Table 4.7. Average Measured Compressive Strength (ksi) by Batch.

Age	Girder	Deck
7 days	9.38	9.43
28 days	10.8	11.4
56 days	12.1	13.0

The high early strength achieved at three days is approximately 75 percent of the 28-day strength of each batch. The average compressive strength gain can be seen in Figure 4.16. The average release strength for both the girder and deck SCC was almost 5 ksi. The target concrete strength of 10 ksi was exceeded for the girder and both deck batches up to 2 ksi. The 28-day compressive strength for the girder batch was 10.8 ksi and the first and second deck batches reached 28-day strength of 11.4 ksi and 11.9 ksi respectively. The compressive strength of the girder and deck concrete at 56 days was 12.1 ksi and 13.0 ksi.

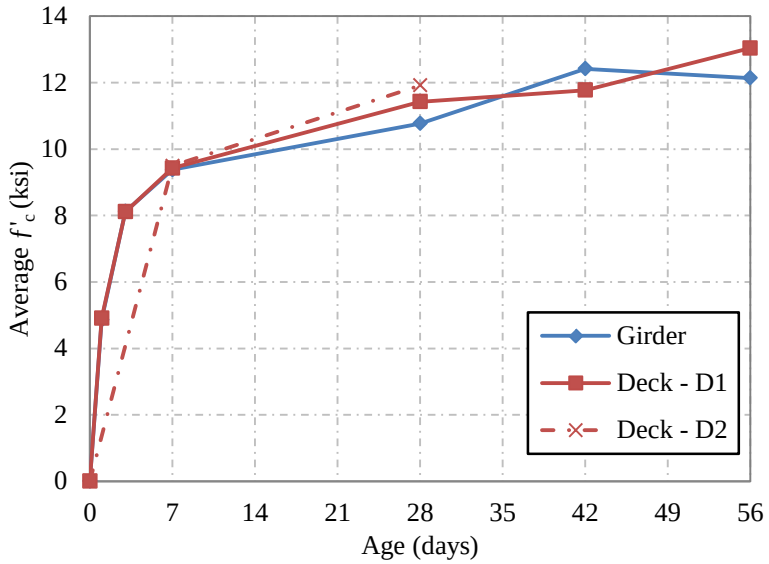

Figure 4.16. Girder and Deck Average Compressive Strength Experimental Data.

4.4.2.2 Modulus of Elasticity

Modulus of elasticity specimens were made for the girder and the first deck batch. The development of MOE from 7 days to 56 days can be seen in Figure 4.17. The average MOE experimental results by batch are shown in Table 4.8.

Table 4.8. Average Measured MOE (ksi).

Age	Girder	Deck
7 days	5898	6036
28 days	5653	6412
56 days	6820	6811

Only three data points are presented for the girder 28-day and 56-day MOE because the third sample test results for each age of testing were outside the acceptable coefficient of variation. MOE is a function of unit weight and compressive strength of concrete therefore unit weight and f'_c are correlated proportionally to MOE as seen in Figure 4.17.

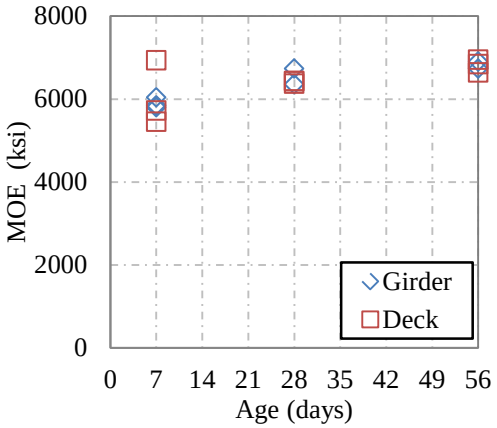

(a) MOE versus time

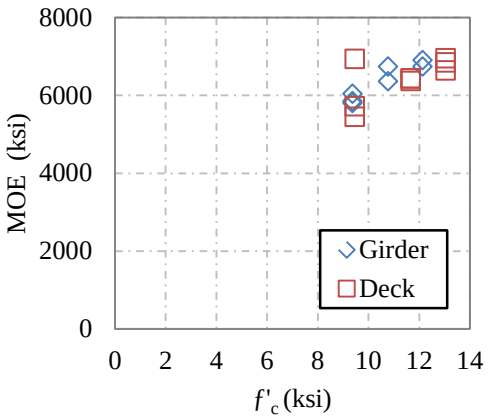

(b) MOE versus f'_c

Figure 4.17. Girder and Deck MOE Experimental Data.

4.4.2.3 Splitting Tensile Strength

STS specimens were made for the girder batch and the first deck batch. The development of STS from 7 days to 56 days and the development of STS in correlation with the average compressive strength at each age can be seen in Figure 4.18. The average STS experimental results by batch are presented in Table 4.9.

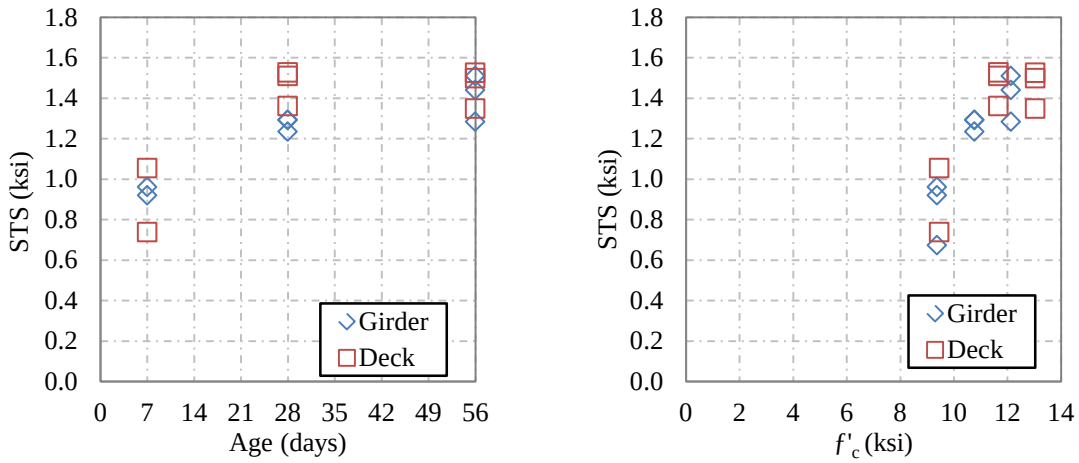

(a) STS versus time (b) STS versus f'_c

Figure 4.18. Girder and Deck STS Experimental Data.

Table 4.9. Average Measured STS (ksi).

Age	Girder	Deck
7 days	0.852	0.897
28 days	0.127	0.147
56 days	0.141	0.146

4.4.2.4 Modulus of Rupture

MOR specimens were made for the girder batch and the first deck batch. The development of MOR from 7 days to 56 days can be seen in Figure 4.19 and the

development of MOR in correlation with the average compressive strength at each age can be seen in Figure 4.19. The experimental MOR results of both the girder and deck batches were lower than the experimental STS results of the associated batches. The 28-day MOR of the girder was over 0.1 ksi lower than the STS while the deck MOR was over 0.4 ksi lower than the STS of the respective batches. The average MOR experimental results by batch are shown in Table 4.10.

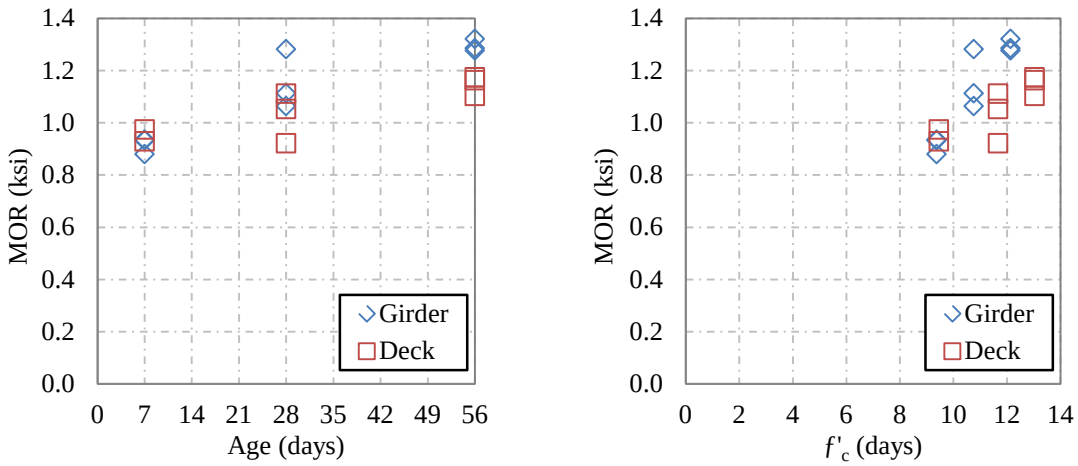

(a) MOR versus time (b) MOR versus f'_c

Figure 4.19. Girder and Deck MOR Experimental Data.

Table 4.10. Average MOR (ksi).

Age	Girder	Deck
7 days	0.915	0.951
28 days	0.115	0.103
56 days	0.129	0.115

4.4.2.5 Shrinkage

Shrinkage readings were averaged from four prisms for both the girder Batch 1 and deck Batch 1. Figure 4.20 expresses the average shrinkage per batch. Shrinkage readings are reported as positive values.

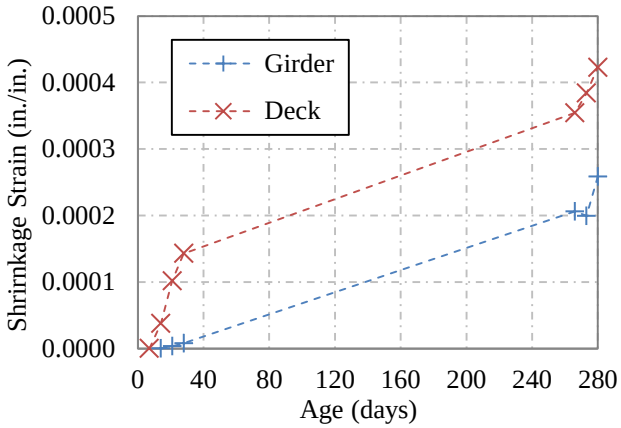

Figure 4.20. Girder and Deck Measured Shrinkage Data.

4.5 Summary

The AFRP girder project faced several construction challenges. A coupler anchorage system was devised in order to lengthen the AFRP strands to span the length of the prestressing bed without wasting costly materials. The research team created a method to overcome the predetermined holes in the prestressing plate in order to fit the project design. By seven days the concrete compressive strength reached 75 percent of the 28-day strength of the SCC used in the girder and deck. The average 28-day compressive strength was determined to be 11.4 ksi, with a 56-day compressive strength of 12.6 ksi. The overall average for MOE, STS, and MOR at 28-days was determined to be 6500 ksi, 0.140 ksi, and 0.105 ksi, respectively.

5. SPLICED GIRDER

The modified Tx70 girder segments were fabricated using SCC and cast at the chosen precast plant. Note that this plant was not the same as the one used for the AFRP girder. The CC connections and deck were cast in the TAMU HBSMTL. Fresh property tests of the concrete, such as slump flow (or slump for CC), unit weight, and temperature, as well as making the specimens for future mechanical properties testing, were conducted on the day of casting. Mechanical properties tests, such as compression strength, MOE, STS, MOR, and shrinkage are identified at certain test sample ages.

5.1 Construction of Specimen

The four girder segments for the spliced girder specimen were cast with eight 4 cyd batches of SCC at the chosen precast plant in August 2013. The two outside segments were modified with thickened end blocks for the post-tensioning anchorages. Conventional mild steel reinforcement was used and the steel strands were prestressed prior to casting the girder. Figure 5.1 shows the reinforcement layout for one of the interior girder segments before casting.

The SCC used for the girder segments was designed by the precast plant to meet the project specified concrete compressive strength requirements of 6 ksi at release and 8.5 ksi at service. The mixture proportions are presented later in Section 5.2. Preparation and fabrication of samples can be seen in Figures 5.2, 5.3, and 5.4.

All cylinder and beam test samples were covered and left to cure overnight next to the full-scale specimen. The following day the samples were transported back to the TAMU laboratory facilities. The samples were de-molded and moved to the appropriate curing room environments as mentioned in Section 3.3.

(a) Interior segment reinforcement

(b) End block reinforcement

Figure 5.1. Reinforcement in Girder Segment.

Figure 5.2. Preparation for Fabrication of Girder Test Samples.

(a) Sample of batch concrete fills 3 to 4 wheelbarrows

(b) Making MOR beam samples

Figure 5.3. Fabrication of Girder Test Samples.

(a) Finished beam samples

(b) Finished cylinder samples

Figure 5.4. Girder Test Samples.

Three weeks after casting, the girder segments were transported from the precast plant to the TAMU HBSMTL. The flatbed trucks carrying the segments were backed

into the laboratory and the laboratory crane was used to lift and place the segments on the concrete pedestals and temporary wooden supports. This process can be seen in Figure 5.5. The four segments were carefully aligned guided by pre-marked positions, spacing distance between segments, and with the laser level. The final alignment can be seen in Figure 5.6.

Formwork and scaffolding was designed and built by the research team for the connections and the deck. The connections and deck were reinforced with mild steel. The forms and reinforcement layouts for a connection and the deck can be seen in Figure 5.7.

(a) Girder segments with lifting points

(b) Placing girder segments

(c) Verifying segment spacing and placement

Figure 5.5. Placing Girder Segments.

(a) Top view girder alignment

(b) Side view girder alignment

Figure 5.6. Final Alignment of Girder Segments.

(a) Center splice connection

(b) Deck

Figure 5.7. Reinforcement Layout.

Mixture proportions for CC used in the connections were tested to find the optimum mix. The mix was selected to be practical to mix at the TAMU laboratory facilities, have a 28-day compressive strength of at least 8.5 ksi to provide similar mechanical properties as the girder, and have an acceptable high slump to flow through the congested reinforcement in each connection. The proportions for these trial batches are discussed later in this thesis. Once mixture proportions were chosen, the connections were cast on-site in the TAMU HBSMTL four months after the girder segments were cast.

The connection mix was adjusted for aggregate moisture correction factors. The aggregates and approximately one-third of the water were transported in a mixing truck from a local quarry to the campus facilities. The Type III cement, superplasticizer admixture, and remaining water were added on site.

The cement powder was measured by weight into a one cubic yard hopper. The cement was added to the mix by backing the mix truck into the TAMU HBSMTL and using the laboratory crane to lift the hopper above the truck and deposit the cement. Water was added to the truck monitored by the truck volume meter by gallons. The amount of cement required was more than one cubic yard, so the process was repeated as efficiently as possible in order to maintain even distribution and avoid clumping of the cement between hopper loads while mixing. One-third of the remaining water was added in between hopper loads to help with the mixing. The superplasticizer was mixed with water separately in nine 5-gallon buckets and then added manually to the truck between loading the cement. Figure 5.8a depicts adding pre-measured barrels of cement powder to fill the hopper. Figure 5.8b illustrates the first hopper of cement powder being added to the concrete mix truck. Figure 5.8c displays the addition of the superplasticizer water being added to the mixture after the first hopper of cement was added. The concrete was mixed in the truck continually throughout the process for a total of 28 minutes.

(a) Measuring cement into hopper

(b) Adding cement to truck

(c) Adding admixture-water mix to truck

Figure 5.8. Adding Materials to Concrete Mixture.

A sampling of the fresh concrete was taken and the slump was measured to be 10 in. The concrete was observed to not be mixed adequately so the concrete was mixed for three to five more minutes and the slump measured again. The slump was 9.75 in., and by observation the mix was acceptable to begin the process of pouring the connections. The one cubic yard hopper was filled with the fresh concrete and then the hopper was lifted by the crane over the splice connection to fill the form. Each connection has an approximate volume of 0.6 cyd so the hopper had to be filled twice to pour all three splices. The truck mixer was continually rotating between hopper loads.

Fresh concrete for the test samples were taken directly from the truck into wheelbarrows as needed throughout the pour. Slump was continually monitored. The connections pour and sample fabrication can be seen in Figure 5.9 and Figure 5.10. All connection concrete samples were cured and stored with the same specifications as the girder samples. However, due to unforeseen maintenance issues with the curing room sprayers the connection samples were not kept at a constant high humidity and some moisture was lost. The temperature and RH of the room was monitored. The temperature stayed constant ± 34°F and the research team periodically wet the samples down.

The deck was cast one week after the connections were cast. The deck pour can be seen in Figure 5.11. The deck samples faced similar issues with curing of samples and moisture loss.

(a) Casting connection

(b) Casting connections complete

Figure 5.9. Connection Pour.

(a) Making cylinder samples

(b) Making beam samples

Figure 5.10. Connection Sample Fabrication.

The formwork for the deck and connections was removed approximately one month after the deck pour. The spliced girder full-scale specimen, including girder segments, connections, and the deck, were then post-tensioned and the ducts were grouted. The post-tensioning and grouting process was performed three months after the connections were poured and can be seen in Figure 5.12.

(a) Casting the deck

(b) Finishing the deck

Figure 5.11. Deck Pour.

(a) Top view post-tensioning girder

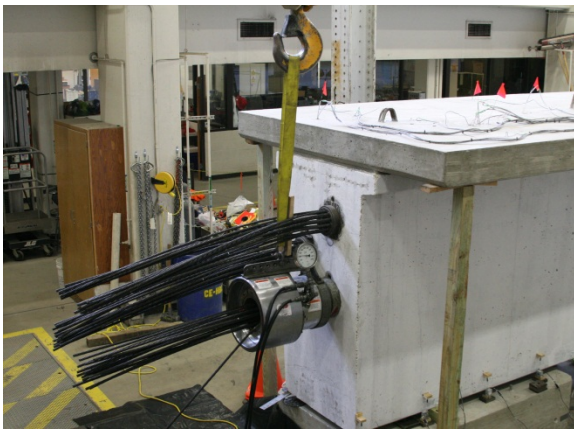

(b) Post-tensioning jack and strands

Figure 5.12. Post-Tensioning Spliced Girder Specimen.

5.2 Materials Testing Program

The SCC and CC mixtures and samples for the girder, connections, and the deck were tested in accordance with all the appropriate ASTM standards and procedures. Fresh property tests were performed including slump and slump flow for quality control. Hardened property tests were conducted to learn more about the mechanical properties of the specimen.

5.2.1 Spliced Girder Segments

The SCC mixture proportions, for SSD conditions, used for the girder segments was provided by the precast plant is shown in Table 5.1. The *w/c* ratio was 0.36 and the target 7-day compressive strength of 9.4 ksi. The precast plant mixed a pilot test batch with these mixture proportions and the measured slump flow was 26 in. and the unit weight was 144.5 pcf. Type III Portland cement was used to achieve high early strength and allow the forms to be removed within a day after casting.

Table 5.1. Girder SCC Mixture Proportions Summary.

Materials		**Type**	**Supplier**	**Quantity**
Cement (lb/yd^3)		III	Alamo Cement	564
Fly Ash (lb/yd^3)		Class F	-	188
Water (lb/yd^3)		-	-	266
Aggregate, lb/yd^3	Coarse (MNAS 3/4 in.)	Limestone	Vulcan (1604 plant)	1499
	Fine	Manufactured Sand	Vulcan (1604 plant)	1359
Admixtures (oz/yd^3)		HRWR	Sika 4100	29.9
		Retarder	Sika	9.0

Samples were made for all batches to test compression strength at 28 days. Because casting the girder required numerous batches, Batches 1, 3, and 5 were selected for representative samples for fresh properties while Batches 2, 4, and 6 were treated as representative batches for fabricating mechanical property samples. When the hopper truck for each batch arrived, a sampling of the SCC was taken to fill wheelbarrows to test fresh properties and fabricate the test samples.

Table 5.2 summarizes the test matrix and the test ages of each mechanical property test conducted for the girder concrete by batch. Three samples were made for each test age. MOE and STS samples were made for Batches 2, 4, and 6. Batches 4 and 6 were chosen to be representative for MOR samples. However, on the day of casting, when Batch 4 arrived, not enough concrete was taken out before the next batch arrived for sample making so only three MOR beam samples were made for Batch 4 instead of the originally planned nine samples.

Compression strength tests were performed at 13 hours and at release (37 hours) by the precaster. Day of testing samples were tested two days prior to the first full-scale specimen test for the purpose of refining design calculations and predictions for the loads corresponding to different failure modes.

Table 5.2. Test Matrix for Spliced Girder Segment Concrete by Batch.

Age	f'_c	MOE	MOR	STS
3 days	B2, B4, B6	-	-	-
7 days	B1 - B8	B2, B4, B6	B6	B2, B4, B6
28 days	B1 - B8	B2, B4, B6	B4, B6	B2, B4, B6
56 days	B2, B4, B6	B2, B4, B6	B6	B2, B4, B6
91 days	B2, B4, B6	-	-	-
Test Day (222 days)	B2, B4, B6	-	-	-

5.2.2 Spliced Girder Connections

The CIP concrete for the splice connections was designed with slump, strength, and practical fabrication requirements. The concrete required a high slump in order to flow through the reinforcement between the girder segments. The connections also needed to reach at least the 8.5 ksi compressive strength at service that was specified for the girder segments. CC mixture proportions used in a study performed by Trejo et al. (2008) were adapted and tested to find an acceptable connection concrete mix.

5.2.2.1 Trial Batches

The connection concrete was mixed and cast on-site at the TAMU HBSMTL. Therefore a high strength high slump CC needed to be designed. Ten trial batches were mixed to test the mechanical properties, primarily the compressive strength. Batches were made with coarse aggregate (limestone or river gravel) and fine aggregate (sand) procured from local batch plants. The coarse aggregates were chosen to have a maximum nominal aggregate size (MNAS) of 0.75 in. to ensure flowability through the closely spaced reinforcement. The mixture proportions used for the trial batches are provided in Table 5.3. The target 7-day compression strength for mixes C5G and C5L, C7G and C7L, provided by Trejo et al. (2008), were 5 ksi and 7 ksi, respectively. All mixes had a target slump between seven to eight inches. Table 5.4 summarizes the fresh properties and the 7-day compressive strength of the trial batches. The development of compressive strength of the trial batches can be seen in Figure 5.13.

Trial batches 1 to 5 used an adaptation of the C5L or C5G mixture proportions from Trejo et al. (2008). Batches 1 to 3 used Type I/II cement, which does not set as quickly as Type III. These batches remained workable for a longer period of time and were relatively easy to mix, but they did not have the high early strength advantage provided by Type III. Batches 4 and 5 used Type III cement, which decreased the workability time of the fresh concrete. Batches 1 to 5 were tested for compressive strength, MOE, STS, and MOR. However due to time constraints, it was decided that the primary concern for the mixture proportions for trial Batches 6 to 10 was compressive strength.

Table 5.3. Connection Concrete Trial Batch SSD Mixture Proportions.

Materials		Type	Mix ID				
			C5G	**C5L**	**C7G**	**C7L**	**C8L**
Cement (lb/yd^3)		I/II	-	-	-	-	658
		Class F Fly Ash	-	-	-	-	165
		III	625	600	700	680	-
w/c ratio		-	0.36	0.42	0.29	0.33	0.45
Water (lb/yd^3)		-	225	252	200	224	250
Aggregate (lb/yd^3)	Coarse (MNAS 3/4 in.)	Limestone	-	1750	-	1752	1937
		River Gravel	1935	-	1935	-	-
	Fine	Mfd. Sand	1232	1380	1232	1382	1166
HRWRA/Superplasticizer (oz/yd^3)		PS 1466	56	37	91	68	33

Trial Batches 6 and 7 were adapted from the mix designated C8L. This design incorporated fly ash, which decreased the amount of cement required. The design did not achieve the desired slump so other designs were considered.

Trial Batches 8 to 10 used an adaptation of Trejo et al.'s (2008) C7G mixture proportions. Batches 8 and 9 used Type III cement for high early strength. When mixing Batch 8, the batch did not mix thoroughly; therefore, it was decided to try the same mix again for Batch 9. Batch 9 achieved the desired early strength gain. Batch 10 was made to match the Batch 9 mix, but using Type I/II cement instead.

Table 5.4. Trial Batch Properties.

Batch #	Mix ID	Cement Type	f'_c at 7 days (ksi)	Coarse Aggregate Type	Slump (in.)	Unit Weight (pcf)
1	C5L	I/II	5.28	Limestone	9.50	145.0
2	C5L	I/II	5.03	Limestone	7.50	146.0
3	C5L	I/II	5.70	Limestone	7.50	-
4	C5L	III	5.74	Limestone	7.00	144.1
5	C5G	III	5.70 (5 days)	River Gravel	8.00	149.6
6	C8L	I/II + Fly Ash	6.65	Limestone	4.00	-
7	C8L	I/II + Fly Ash	6.60	Limestone	4.00	-
8	C7G	III	7.33	River Gravel	8.00	-
9	C7G	III	6.00	River Gravel	7.75	-
10	C7G	I/II	6.56 (5 days)	River Gravel	7.25	-

It was unknown at the time of selecting the mixture proportions for the connections if Batch 10 would reach the desired strength. It was found that river gravel mixtures had higher slumps on average while maintaining high strength. Therefore, the C7G mix using Type III cement, as tested with Batch 9, was chosen to ensure the strength was achieved. Due to time and material constraints, fewer samples were made for the later trial batches (Batches 8, 9 and 10); therefore, there were not enough samples from Batch 9 to tests compressive strength at later ages. Batch 10 was later tested after the connections had been poured and found to have achieved 8 ksi by 28 days.

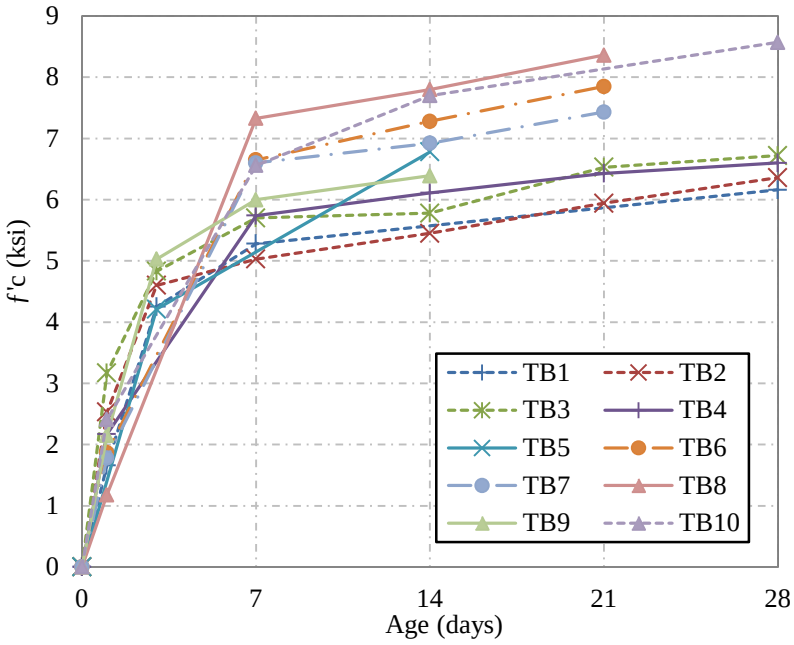

Figure 5.13. Trial Batches Average Experimental Compressive Strength Data.

5.2.2.2 Final Connection Mixture Proportions

The CC mixture proportions chosen for the connections were an adaptation of Trejo et al. (2008) mix designated as C7G and shown previously in Table 5.6. The connections were cast in one 4 cyd batch.

Samples were fabricated for future mechanical property tests. Table 5.5 summarizes the test matrix and the test ages of each mechanical property test conducted for the connection concrete. Three samples were made of each batch for each test age.

Due to scheduling of the connection pour, 3-day sample testing was not performed and 5-day testing was conducted instead. Day of testing samples were tested two days prior to the first full-scale specimen test for the purpose of refining design calculations and predictions for the loads required for the different failure modes. STS was tested prior to day of full-scale testing because the three splice connections were the areas of interest for the flexural tests.

Table 5.5. Connection Concrete Test Matrix.

Age of Samples	f'_c	MOE	STS	MOR
1 day	B1	-	-	-
5 days	B1	-	-	-
7 days	B1	B1	B1	B1
28 days	B1	B1	B1	B1
56 days	B1	B1	B1	B1
Day of Test	B1	-	B1	-

5.2.3 Spliced Girder Deck

The deck was cast with two batches on site at the TAMU HBSMTL. The deck concrete mixture was proportioned and poured by a local ready mix company to meet TxDOT Class S requirements for CC with a specified compressive strength of 4 ksi. Samples were fabricated for future mechanical property tests. Table 5.6 summarizes the test matrix and the test ages of each mechanical property test conducted for the deck concrete by batch.

Table 5.6. Deck Concrete Test Matrix.

Age	f'_c	MOE	STS	MOR
1 day	D1, D2	D1	D1	-
14 days	D1, D2	-	-	D1
28 days	D1, D2	D1, D2	D1, D2	D1
56 days	D1, D2	D1	D1, D2	D1
Day of Test	D1, D2	-	-	-

Three samples were made from each batch for each test age. Due to scheduling of the deck pour, 7-day sample testing was not performed. The testing resumed on the first day available at 14 days.

5.3 Results

5.3.1 Fresh Properties

5.3.1.1 Girder Segments

Fresh properties of the SCC and ambient conditions are summarized in Table 5.7.

Table 5.7. Summary of Girder Concrete Fresh Properties.

Batch	Slump (in.)	Unit Weight (kcf)	Air Content (%)	Concrete Temperature (°F)	Ambient Temperature (°F)	RH (%)
B1	26.5	-	8	96	107.4	24.4
B3	26.0	0.146				
B5	22.0	0.144				

5.3.1.2 Connections

The fresh properties tested for the connections were unit weight and slump. The initial slump was 9.75 in. with a unit weight of 0.151 kcf. The slump was monitored throughout the pour at certain time intervals and recorded in Table 5.8.

Table 5.8. Slump of Connection Concrete.

Time	Slump (in.)	Notes
3:50 pm	9.75	Begin casting, sampled from truck
4:03 pm	9.50	Sampled from truck
4:17 pm	9.25	Sampled from truck
4:38 pm	9.25	End of casting, sampled from hopper

5.3.1.3 Deck

Fresh properties for the CIP deck concrete were monitored and recorded in Table 5.9.

Table 5.9. Deck Concrete Fresh Properties.

Batch	Slump (in.)	Unit Weight (kcf)	Air Content (%)	Concrete Temperature (°F)	Ambient Temperature (°F)	RH (%)
B1	4.5	0.144	5.0	68	70	48
B2	3.0	0.147	5.2	67		

5.3.2 Hardened Properties

5.3.2.1 Compressive Strength

Compressive strength samples were fabricated and tested for the girder, connection, and deck concrete. All batches have been graphed and the overall f'_c of the spliced girder is illustrated in Figure 5.14. The relationships of strength gain are broken down further in the next sections of this thesis.

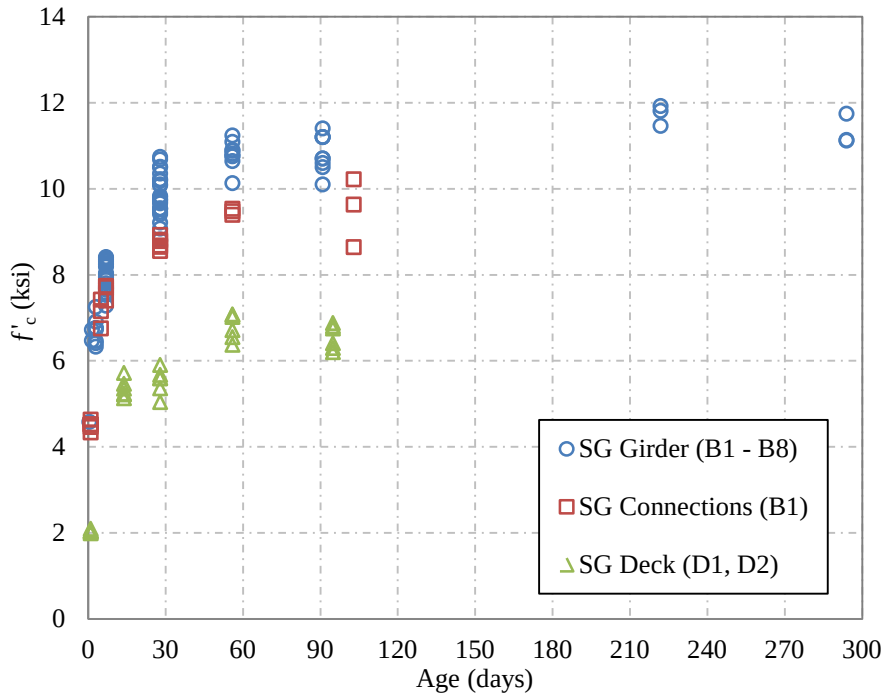

Figure 5.14. Spliced Girder Compressive Strength.

5.3.2.1.1 Girder Segments

Compressive strength samples were made for all eight girder batches. The development of compressive strength from 1 day to 91 days and the ratio of compression strength at each test age compared to the average 28-day strength of the corresponding batch can be seen in Figure 5.15. The high early strength achieved at 3 days is approximately 70 percent of the 28-day strength of each batch. The average compressive strength gain can be seen in Figure 5.16.

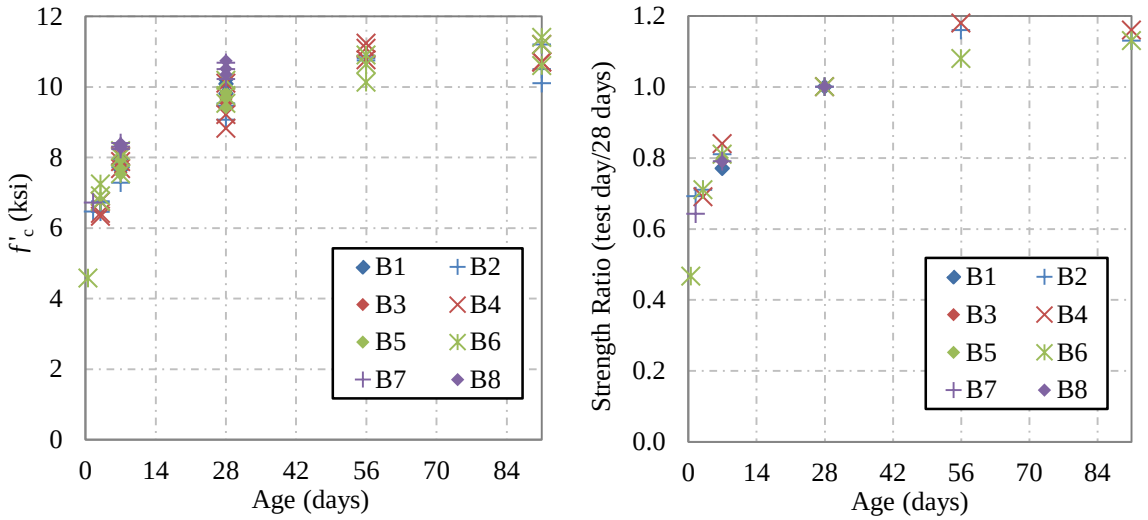

(a) f'c versus time (b) Compressive strength ratio

Figure 5.15. Girder Concrete Compressive Strength Experimental Data.

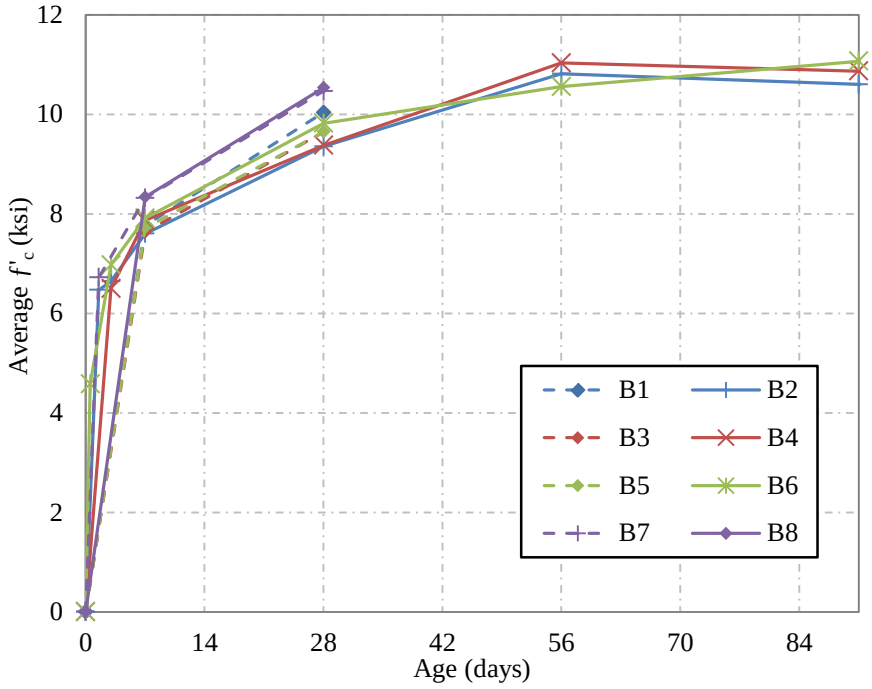

Figure 5.16. Girder Concrete Average Compressive Strength Experimental Data.

The average 3-day compressive strength for girder Batches 2, 4, and 6 was almost 7 ksi. The target concrete compressive strength at service of 8.5 ksi was exceeded for all batches up to 2 ksi. The 7-day, 28-day, and 56-day compressive strengths for Batch 2, 4, and 6 are reported in Table 5.10. The average compressive strength of the girder concrete reached by 91 days was 10.8 ksi.

Table 5.10. Girder Concrete Average Measured Compressive Strength (ksi).

Age	B1	B2	B3	B4	B5	B6	B7	B8
13 hours	-	-	-	-	-	4.58	-	-
At Release (37 hours)	-	6.47	-	-	-	-	6.72	-
3 days	-	6.65	-	6.50	-	6.97	-	-
7 days	7.77	7.60	7.63	7.87	7.72	7.91	8.32	8.34
28 days	10.0	9.35	9.65	9.38	9.65	9.82	10.5	10.5
56 days	-	10.8	-	11.0	-	10.6	-	-
91 days	-	10.6	-	10.9	-	11.1	-	-
Day of Test (222 days)	-	11.7	-	-	-	-	-	-
After Testing (294 days)	-	-	-	11.4	-	11.1	-	-

5.3.2.1.2 Connections

Compressive strength development from 1 day to 56 days can be seen in Figure 5.17. All specimens were fabricated from the same batch. On the day of testing for the spliced girder, the compressive strength of the connection concrete samples (test age of 103 days) was 9.5 ksi.

The benefit of the use of Type III cement for high early strength can be seen in Figure 5.17. Within three days the compressive strength was already 50 percent of the 28-day strength. The strength increase was rapid; the 7-day compressive strength was 87 percent of the 28-day strength. It is noted that typical field applications generally call for Type I/II cement, which provides longer workability. Table 5.11 provides the average compressive strength results at each age.

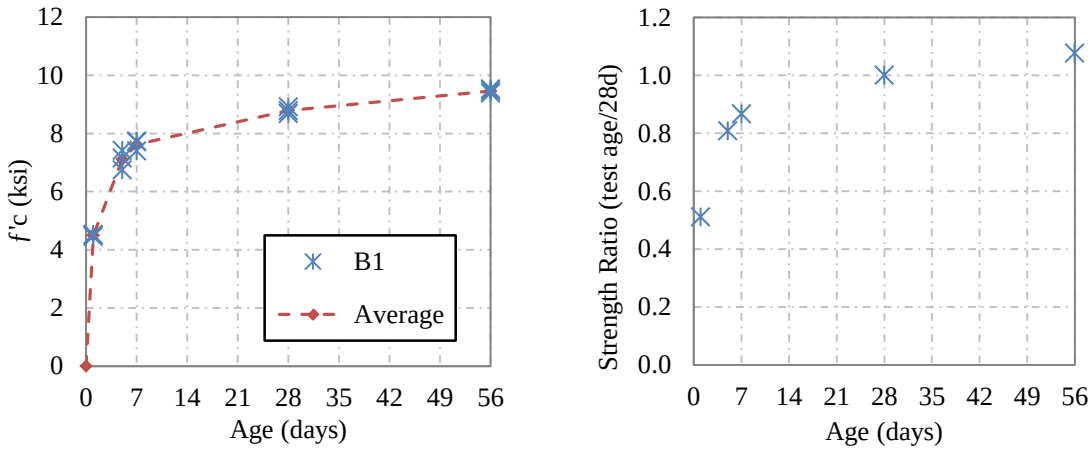

(a) f'_c versus time (b) Compressive strength ratio

Figure 5.17. Connection Concrete Compressive Strength Experimental Data.

Table 5.11. Connection Concrete Average Measured Compressive Strength.

Age	f'_c (ksi)
1 day	4.50
5 days	7.11
7 days	7.62
28 days	8.79
56 days	9.46
Day of Test (103 days)	9.50

5.3.2.1.3 Deck

The development of compressive strength from 1 day to 56 days and the ratio of compression strength at each test age compared to the average 28-day strength of the corresponding batch can be seen in Figure 5.18.

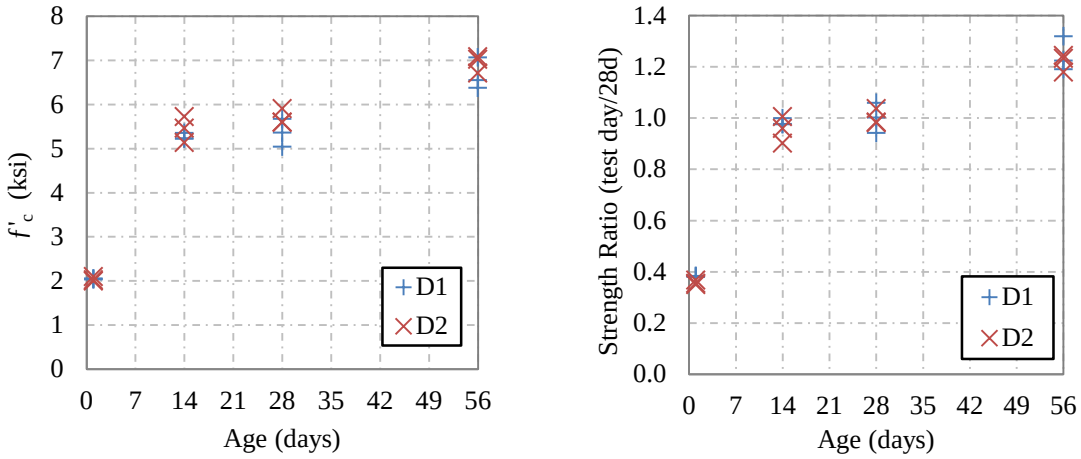

(a) f'_c versus time (b) Compressive Strength Ratio

Figure 5.18. Deck Concrete Compressive Strength Experimental Data.

Samples of the CC used for the CIP deck were tested for a baseline comparison of normal CC to the HSC connections and the girder SCC. On the day of testing for the spliced girder, the compressive strength of the deck concrete (test age of 95 days) was an average of 6.56 ksi. The 1-day compressive strength of the deck concrete was 40 percent of the 28-day; and by 14 days the deck concrete achieved at least 90 percent of the 28-day compressive strength. Table 5.12 reports the average compressive strength results for the deck batches.

Table 5.12. Deck Concrete Average Measured Compressive Strength.

Age	B1 (ksi)	B2 (ksi)
1 day	2.04	2.03
14 days	5.27	5.44
28 days	5.36	5.70
56 days	6.66	6.94
Day of Test (95 days)	6.81	6.30

5.3.2.2 Modulus of Elasticity

MOE samples were fabricated and tested for the girder, connection, and deck concrete. All batches have been graphed and the overall MOE of the spliced girder is illustrated in Figure 5.19.

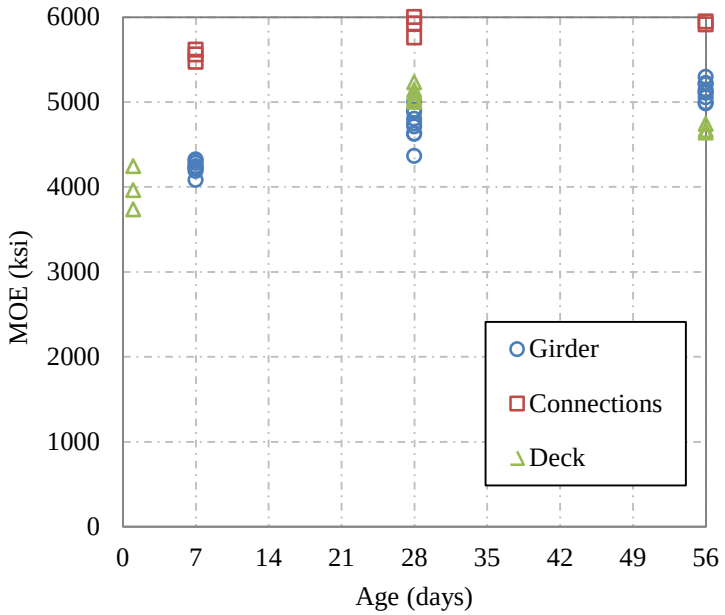

Figure 5.19. Spliced Girder MOE Experimental Data.

5.3.2.2.1 Girder Segments

MOE samples were made for the precast girder Batches 2, 4, and 6. Batch 4 samples yielded more consistent results at each age than the other two batches. Figure 5.20 shows the MOE development of the samples over time and compares the MOE to the average compressive strength at each age. The experimental data shows that by seven days, the MOE was over 4000 ksi and only increased by 1000 ksi between 7 and 56 days. The average experimental MOE values for each batch and age tested are reported in Table 5.13.

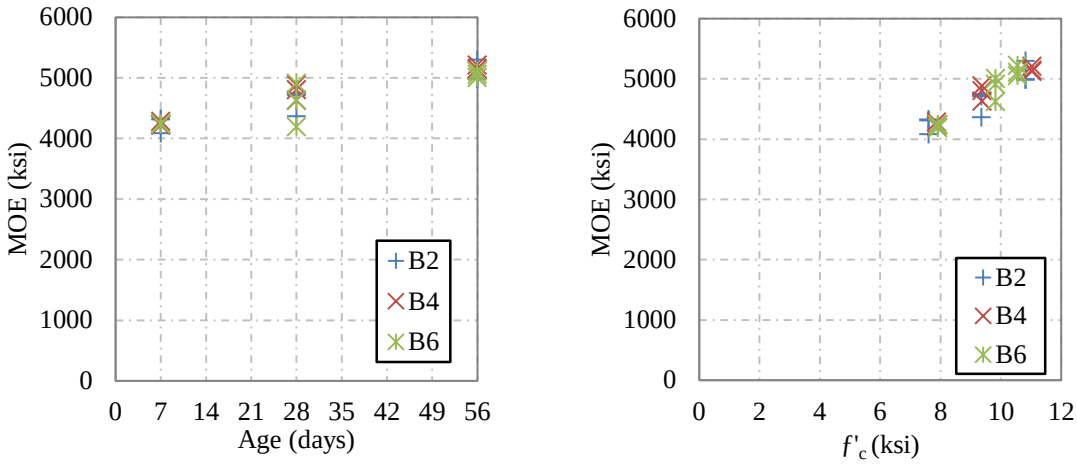

(a) MOE versus time (b) MOE versus f'_c

Figure 5.20. Girder Concrete MOE Experimental Data.

Table 5.13. Girder Concrete Average Measured MOE (ksi) by Batch.

Age	B2	B4	B6
7 days	4239	4240	4224
28 days	4607	4772	4845
56 days	5091	5158	5128

5.3.2.2.2 Connections

The development of MOE from 7 days to 56 days can be seen in Figure 5.21. The connection CC 28-day MOE was over 1000 ksi higher than the girder SCC MOE values. All specimens are from the same batch.

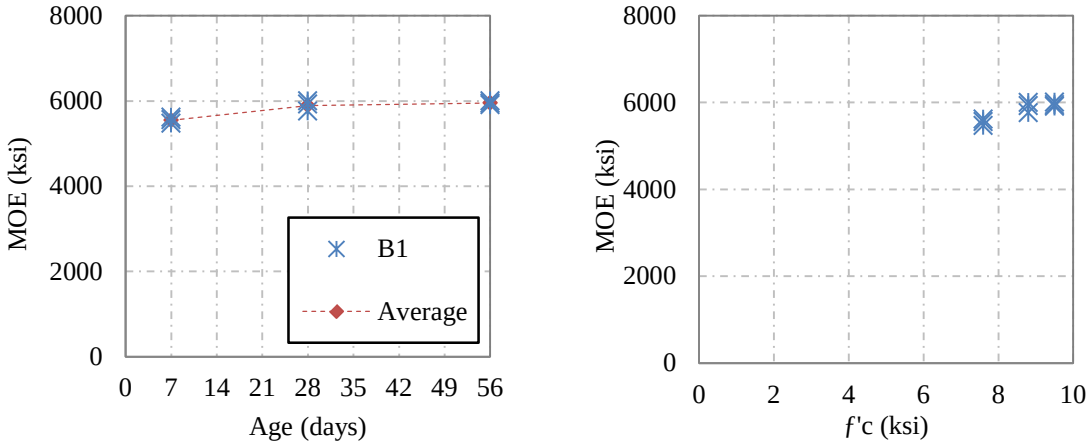

(a) MOE versus time (b) MOE versus f'_c

Figure 5.21. Connection Concrete MOE Experimental Data.

The experimental data shows that by seven days, the MOE was over 5500 ksi and increased by less than 500 ksi between 7 and 56 days. The average experimental MOE values for each age tested are reported in Table 5.15.

Table 5.14. Connection Concrete Average Measured MOE.

Age	MOE (ksi)
7 days	5548
28 days	5895
56 days	5954

5.3.2.2.3 Deck

The development of MOE from 7 days to 56 days can be seen in Figure 5.22. The average experimental MOE values for each age tested are reported in Table 5.16.

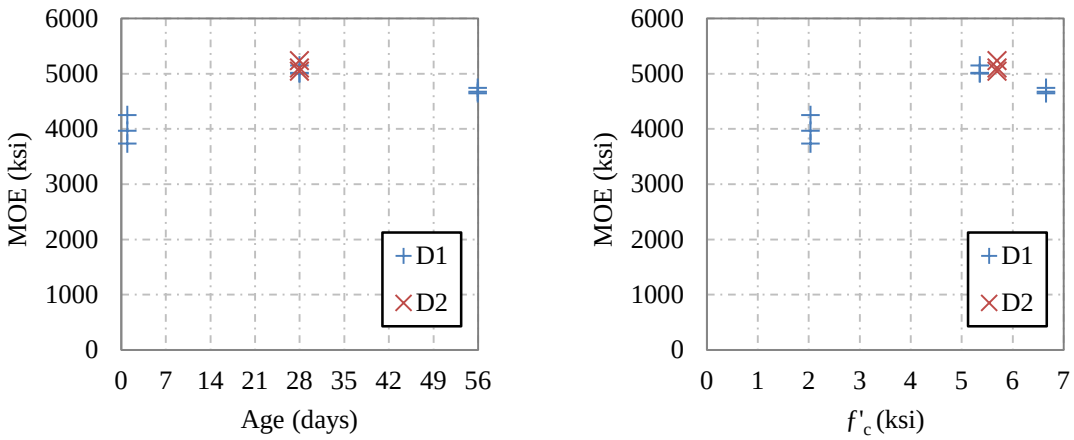

(a) MOE versus time (b) MOE versus f'_c

Figure 5.22. Deck Concrete MOE Experimental Data.

The experimental data shows the initial MOE by one day was almost 4000 ksi and increased over 1000 ksi by 28 days. The MOE decreased by 500 ksi between 28 and 56 days. This trend was observed by averaging three samples at each age, each experimental value was within the acceptable coefficient of variation.

Table 5.15. Deck Concrete Average Measured MOE (ksi) by Batch.

Age	B1	B2
1 day	3981	-
28 days	5052	5125
56 days	4684	-

5.3.2.3 Splitting Tensile Strength

All batch STS samples for the girder, connection, and deck concrete have been graphed and the overall STS of the spliced girder is illustrated in Figure 5.23.

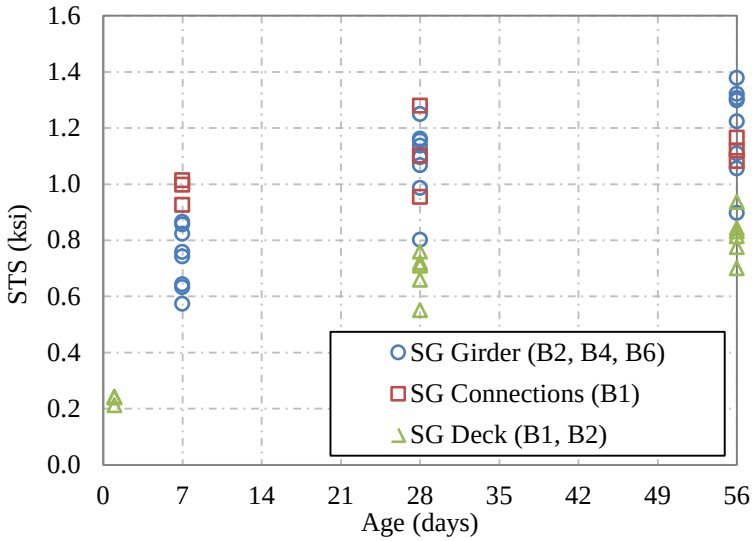

Figure 5.23. Spliced Girder STS Experimental Data.

5.3.2.3.1 Girder Segments

STS samples were made for girder Batches 2, 4, and 6. Figure 5.24 shows the development of STS over time as well as the development of STS versus the average compressive strength at each age.

Although Batch 6 had a lower average STS at seven days, it had the highest average STS at 28 and 56 days. Batch 2 consistently had the minimum single STS value at each test age. The average experimental STS values for each batch and age tested are reported in Table 5.16.

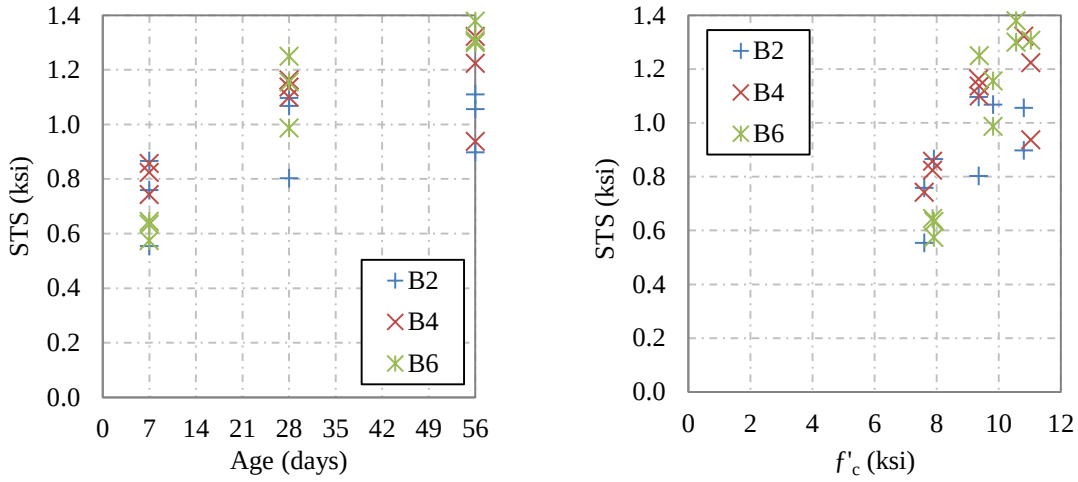

(a) STS versus time (b) STS versus f'_c

Figure 5.24. Girder Concrete STS Experimental Data.

Table 5.16. Girder Concrete Average STS (ksi) by Batch.

Age	B2	B4	B6
7 days	0.726	0.807	0.617
28 days	0.988	1.13	1.13
56 days	1.02	1.16	1.33

5.3.2.3.2 Connections

The development of STS for the connection concrete from 7 days to 56 days can be seen in Figure 5.25. The average experimental STS values for each age tested are reported in Table 5.17.

The STS on day of testing the spliced girder (test age of 103 days) was 1.0 ksi. All specimens are from the same batch. By seven days the connection concrete STS achieved almost 1 ksi and gained 0.1 ksi by 56 days. Observing the 7-day to 56-day experimental data, the trend of STS grew and remained almost asymptotic between 28

and 56 days. However, the STS of the connection concrete on the day of the girder test was 0.1 ksi lower than the average at 56 days. As discussed by Ozyildirim and Carino (2006), the STS when compared to compressive strength does not remain constant but decreases as compressive strength increases.

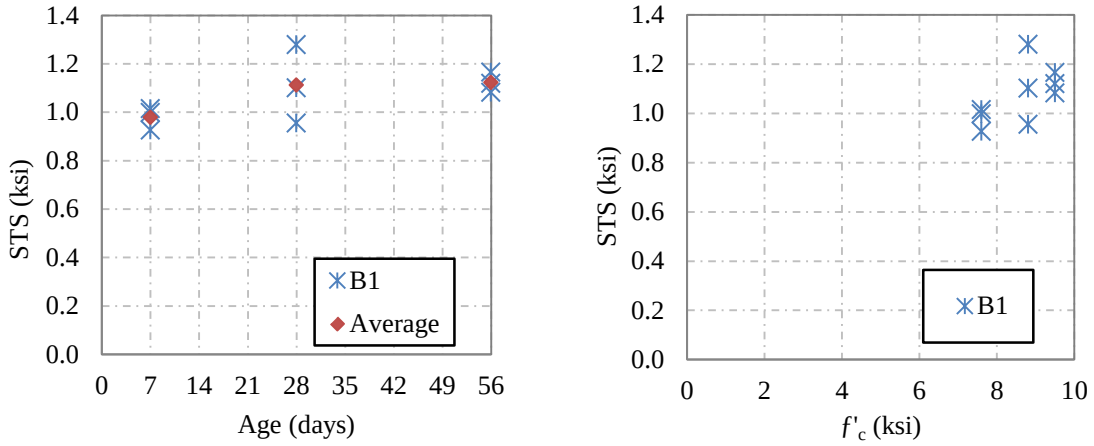

(a) STS versus time (b) STS versus f'_c

Figure 5.25. Connection Concrete STS Data.

Table 5.17. Connection Concrete Average Measured STS.

Age	STS (ksi)
7 days	0.979
28 days	0.111
56 days	0.112
Day of Test (103 days)	0.999

5.3.2.3.3 Deck

The development of STS for the deck concrete from 7 days to 56 days can be seen in Figure 5.26. The average experimental STS values for each age tested are reported in Table 5.18.

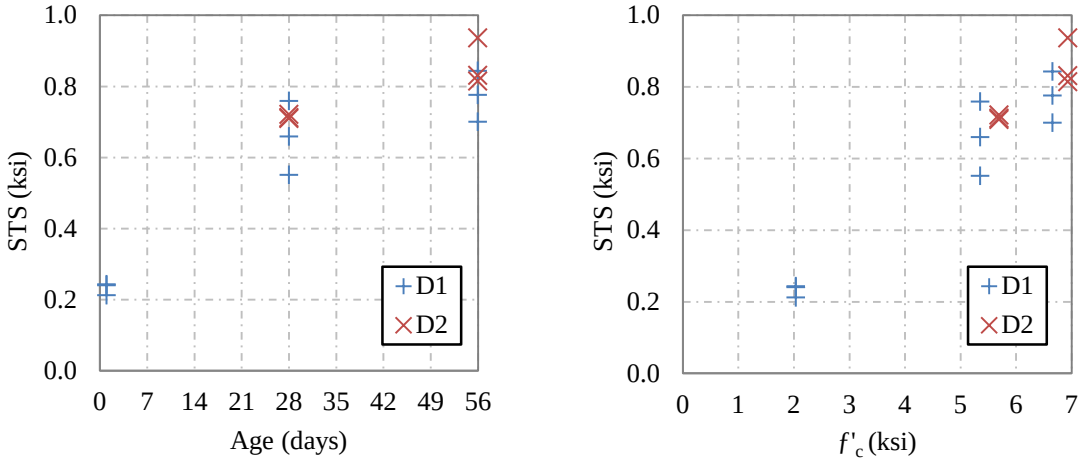

(a) STS versus time (b) STS versus f'_c

Figure 5.26. Deck Concrete STS Experimental Data.

Table 5.18. Deck Concrete Average Measured STS (ksi) by Batch.

Age	B1	B2
1 day	0.232	-
28 days	0.656	0.714
56 days	0.773	0.860

The experimental data depicts the initial STS of the deck concrete at one day was slightly over 0.2 ksi and increased 0.45 ksi by 28 days. The STS continued to increase steadily so that by 56 days, the STS increased by 0.13 ksi between 28 and 56 days.

5.3.2.4 Modulus of Rupture

MOR samples were fabricated and tested for the girder, connection, and deck concrete. All batches have been graphed and the overall MOE of the spliced girder is illustrated in Figure 5.27.

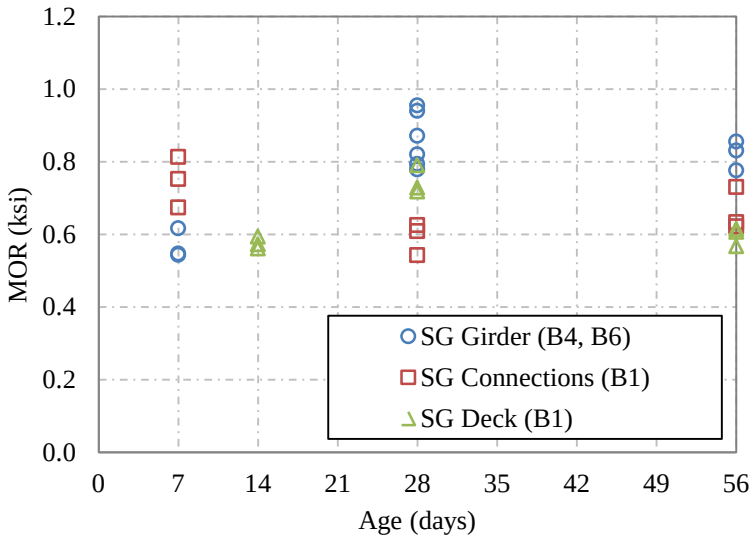

Figure 5.27. Spliced Girder MOR Experimental Data.

5.3.2.4.1 Girder Segments

MOR samples were made for Batch 4 at 28 days and Batch 6 at 7, 28, and 56 days. Figure 5.28 shows the development of MOR over time as well as the development of MOR versus the average compressive strength at each age. MOR for Batch 6 increased by 75 percent from 7 to 28 days but then unexpectedly dropped when tested at 56 days. The average experimental MOR values for each batch and age tested are reported in Table 5.19.

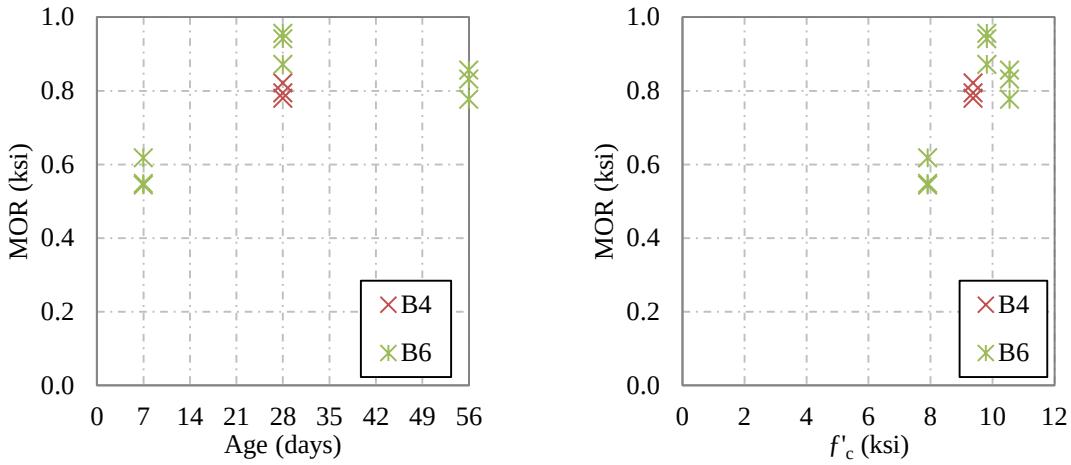

(a) MOR versus time (b) MOR versus f_c

Figure 5.28. Girder Concrete MOR Data.

Table 5.19. Girder Concrete Average MOR (ksi) by Batch.

Age	B4	B6
7 days	-	0.570
28 days	0.798	0.923
56 days	-	0.821

5.3.2.4.2 Connections

The development of MOR for the connection concrete batch from 7 days to 56 days can be seen in Figure 5.29. The average experimental MOR values for each age tested are reported in Table 5.20. All specimens are from the same batch.

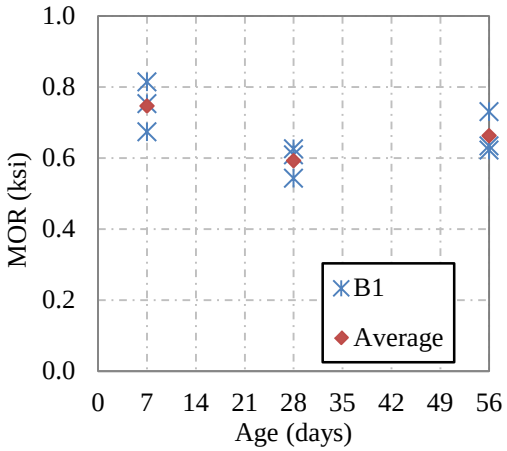

(a) MOR versus time

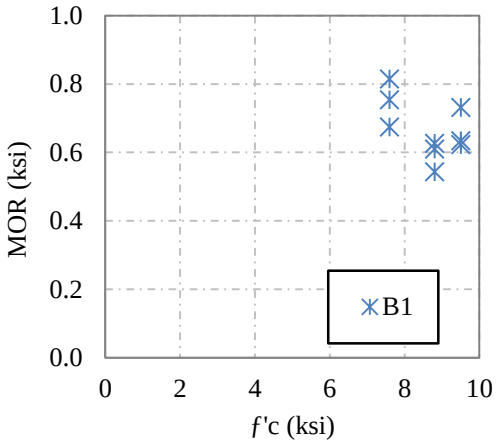

(b) MOR versus f'_c

Figure 5.29. Connection Concrete MOR Data.

Table 5.20. Connection Concrete Average Measured MOR.

Age	MOR (ksi)
7 days	0.747
28 days	0.593
56 days	0.662

5.3.2.4.3 Deck

The development of MOR for the deck concrete Batch 1 from 7 days to 56 days can be seen in Figure 5.30. The average experimental MOR values for each age tested are reported in Table 5.21.

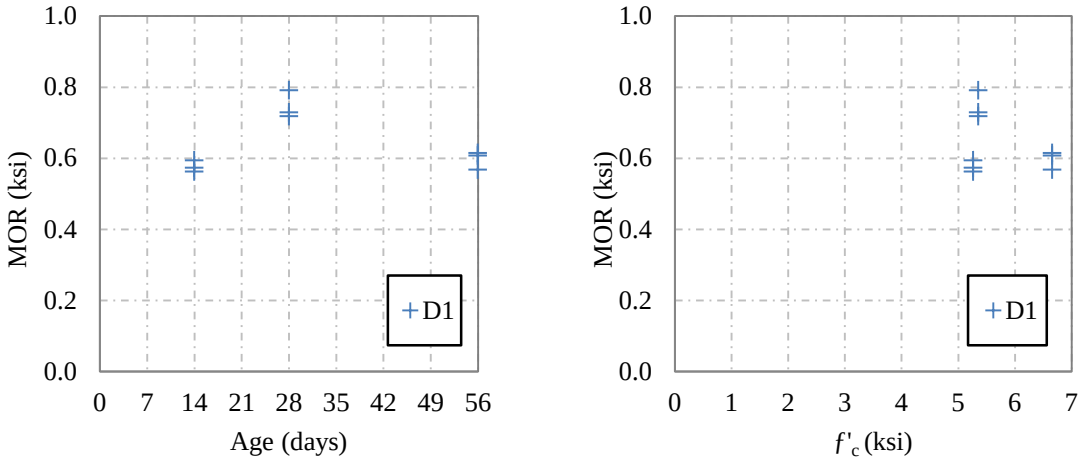

(a) MOR versus time (b) MOR versus f'_c

Figure 5.30. Deck Concrete Batch 1 MOE Experimental Data.

Table 5.21. Deck Concrete Average Measured MOR (ksi).

Age	B1
14 days	0.576
28 days	0.746
56 days	0.597

5.3.2.5 Shrinkage

Four prisms for shrinkage testing were cast for each of girder Batches 2, 4, and 6. However, only three prisms were tested for Batch 6 because the embedded screws were too short in the fourth sample. The shrinkage results are plotted in Figure 5.31. Shrinkage readings are reported as positive values. Negative values indicate initial expansion of the concrete at early ages.

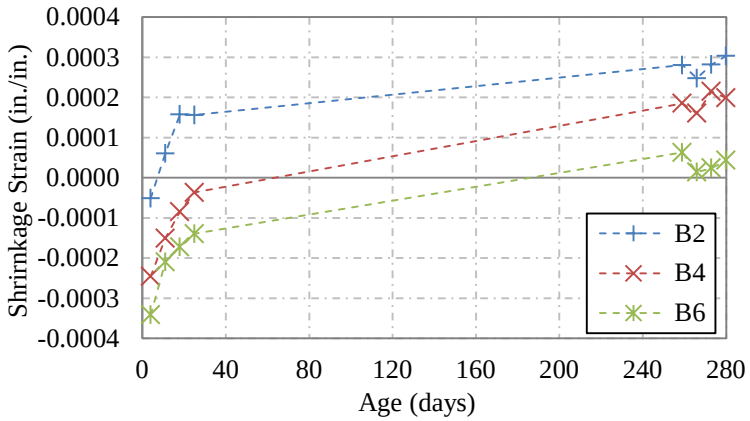

Figure 5.31. Spliced Girder Shrinkage Data.

5.4 Summary

The spliced girder segments were precast four months prior to the assembly and casting of the CIP splice connections and deck. By seven days the concrete compressive strength reached 80 percent and 86 percent of the 28-day strength of the SCC used in the girder segments and the CC used in the connections, respectively; while the CC used for the deck reached 36 percent by one day and 98 percent by fourteen days. The increased strength gain for the girder segments and the connections can be attributed to the use of Type III cement. The average 28-day compressive strength was determined to be 9.86 ksi, with a compressive strength at 56 days of 10.8 ksi for the girder. The overall averages for MOE, STS, and MOR for the girder at 28 days was determined to be 4740 ksi, 1.08 ksi, and 0.860 ksi, respectively. The average 28-day compressive strength was determined to be 8.73 ksi, with a compressive strength at 56 days of 9.46 ksi for the connection concrete. The overall average of MOE, STS, and MOR for the connection concrete at 28 days was determined to be 5900 ksi, 0.111 ksi, and 0.593 ksi, respectively. The MOE for the girder SCC was lower than the MOE for the connection concrete. Research suggests that the lower MOE for SCC could be attributed to a lower coarse aggregate content in SCC than a CC high strength mixture (Al-Omaishi et al 2009, Yang et al. 1997). Also, the coarse aggregate for the girder was limestone and the connection concrete used river gravel.

6. COMPARATIVE ANALYSIS OF MATERIALS

6.1 General

A comparative analysis was conducted on the experimental data for the AFRP girder concrete and the spliced girder concrete. Current AASHTO LRFD and ACI 318 prediction equations for mechanical properties of conventional concrete used in industry were evaluated for their applicability to the data and compared to a power regression model for best fit. Curves of the prediction models were overlaid with the experimental data of the AFRP girder and spliced girder project. Relationships between different mechanical properties, such as compressive strength versus MOE, STS, or MOR were observed.

The prediction equations were calculated based on the average compression strength of each specified batch at 7, 28, and 56 days. The average compressive strengths for the AFRP SCC girder and first deck batches are reported in Table 4.7. The average compressive strengths for the spliced girder SCC girder segment Batches 2, 4, and 6 are reported in Table 5.11. The ACI 318 and AASHTO LRFD design equations each have a coefficient that relates the MOE with the square root of the compressive strength. These coefficients have been calculated for each age, by batch, to relate the MOE at time t, in days, to the square root of the 28-day compressive strength.

6.2 Compressive Strength

According to the precast plant data for the SCC mix, the AFRP girder project SCC expected a target 28-day compressive strength of 10.9 ksi. The spliced girder project SCC was required to have a f'_c of 8.5 ksi at 28 days, but according to the precast plant design the expected target 28-day compressive strength is 10.1 ksi. The AFRP girder reached an average 28-day strength of 10.8 ksi and the deck had a 28-day strength of 11.4 ksi. Spliced girder Batches 2, 4, and 6 reached a 28-day strength of 9.35 ksi, 9.38 ksi, and 9.82 ksi, respectively. Table 6.1 shows the ratio of the measured average 28-day strength to the expected mixture strength and the required design strength. The AFRP girder batches had measured f'_c values closer to the expected 28-day f'_c as

compared to the spliced girder batches. The spliced girder batches did not reach the expected 28-day f'_c but they exceed the design strength. The AFRP girder and spliced girder compressive strength versus age can be seen in Figure 6.1.

Table 6.1. Comparison of Expected to Measured 28-Day Compressive Strength.

SCC Mixture	Batch	28-Day Design f'_c (ksi)	28-Day Expected f'_c (ksi)	Measured 28-Day f'_c (ksi)	Ratio (Measured/ Design)	Ratio (Measured /Expected)
AFRP Girder	G1	6.00	10.9	10.8	1.80	0.99
	D1			11.4	1.91	1.05
Spliced Girder	B2	8.50	10.1	9.35	1.10	0.92
	B4			9.38	1.10	0.93
	B6			9.82	1.16	0.97

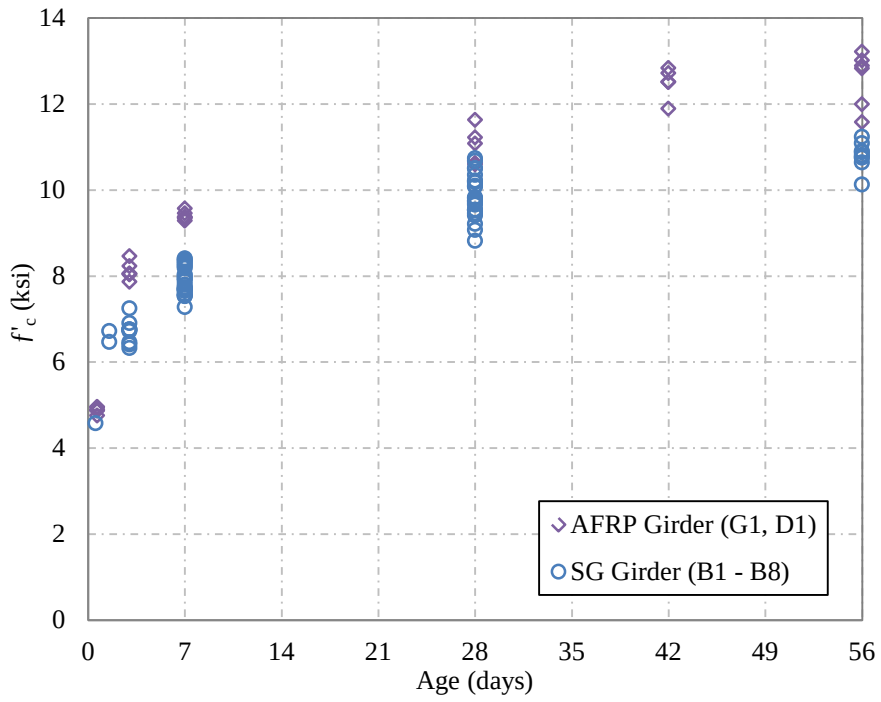

Figure 6.1. AFRP Girder and Spliced Girder Compressive Strength Comparison.

The ACI 209 model (2010) for evaluating the compressive strength gain over time is provided by Equation 6.1.

$$\frac{f'_{c_t}}{f'_{c_{28}}} = \frac{t}{a + \beta t} \tag{6.1}$$

where the relationship of the compressive strength at time t, in days, (f'_{ct}) is compared to the 28-day compressive strength (f'_{c28}). The ACI 209 model was applied to the data to find the best fit based on the optimum a and β values. By evaluating f'_{ct}/f'_{c28} at t equals 28 days, the ratio is set to 1; therefore, the value of a is dependent on β as β is varied to find the best fit model. Typical β values for moist-cured concrete are 0.85 and 0.92 for Type I and Type III cement, respectively (ACI 209 2010). For steam-cured samples, typical values for β are 0.95 and 0.98 for Type I and Type III cement, respectively (ACI 209 2010). Therefore, Equation 6.1 can be rewritten as Equation 6.2.

$$\frac{f''_{c_t}}{f'_{c_{28}}} = \frac{\left(\frac{t}{28}\right)\left(\frac{f_{c_\infty}}{f_{c_{28}}}\right)}{\left(\frac{f_{c_\infty}}{f_{c_{28}}}\right) - 1 + \left(\frac{t}{28}\right)} \tag{6.2}$$

The power regression model, proposed by Mander (2014), was developed by analyzing Equation 6.3 and finding the optimum power value, p, to determine the expression that best fits the data where $f'_{c\infty}/f'_{c28}$ is taken between 1.05 and 1.25 or the inverse of the β value, a typical value when evaluating time t as ∞.

$$\frac{f'_{c_t}}{f'_{c_{28}}} = \frac{\left(\frac{t}{28}\right)^p \left(\frac{f_{c\infty}}{f_{c_{28}}}\right)}{\left\{\left(\frac{t}{28}\right)^{10p} + \left(\frac{f_{c\infty}}{f_{c_{28}}}\right)^{10}\right\}^{0.1}} \tag{6.3}$$

Figure 6.2 and Figure 6.3 shows all f'_c experimental results for the AFRP girder and spliced girder SCC data, respectively, with the best fit ACI 209 model and power regression model by batch. Figure 6.4 displays the f'_c experimental results for spliced girder CC data for the connection concrete and the deck concrete with the best fit ACI 209 model and power regression model.

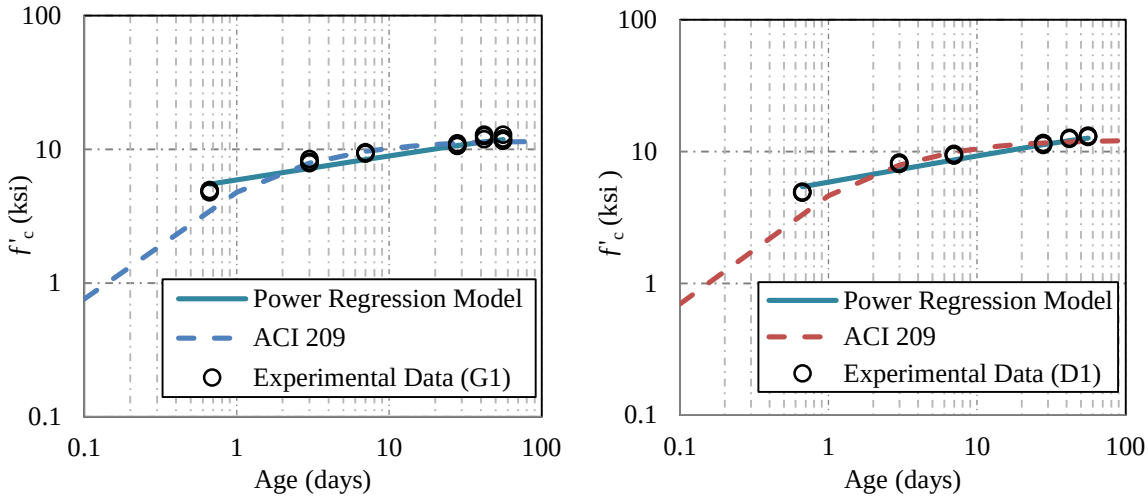

(a) Girder (b) Deck

Figure 6.2. AFRP Girder SCC - ACI 209 and Power Regression Models by Batch.

When analyzing the spliced girder concrete by batch, the optimum β value was higher in order for the model to go through the experimental data point range at all ages. However, if the model was applied, and the early ages neglected (by not including 3-day or 7-day data in the model calculations), the optimum β values were lower.

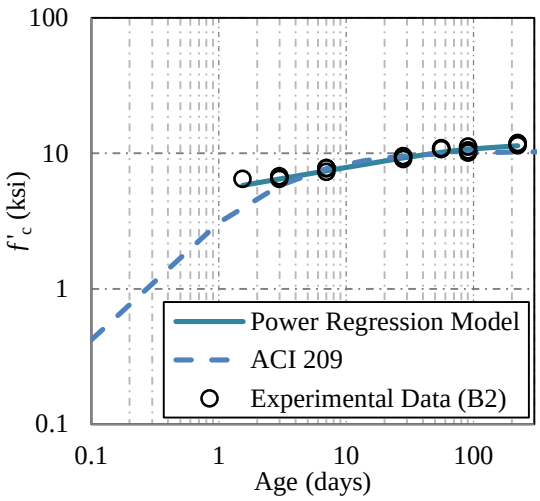

(a) Batch 2

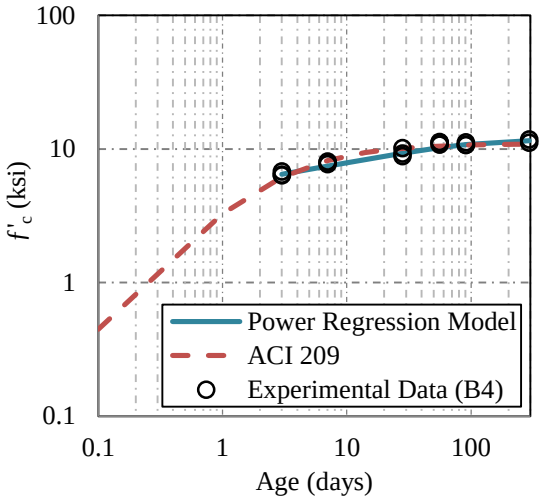

(b) Batch 4

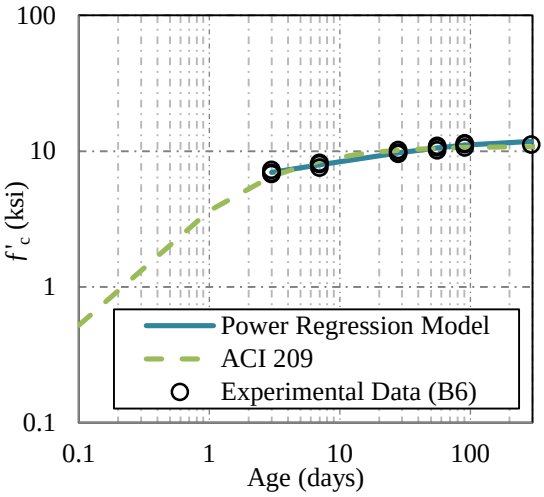

(c) Batch 6

Figure 6.3. Spliced Girder SCC - ACI 209 and Power Regression Models by Batch.

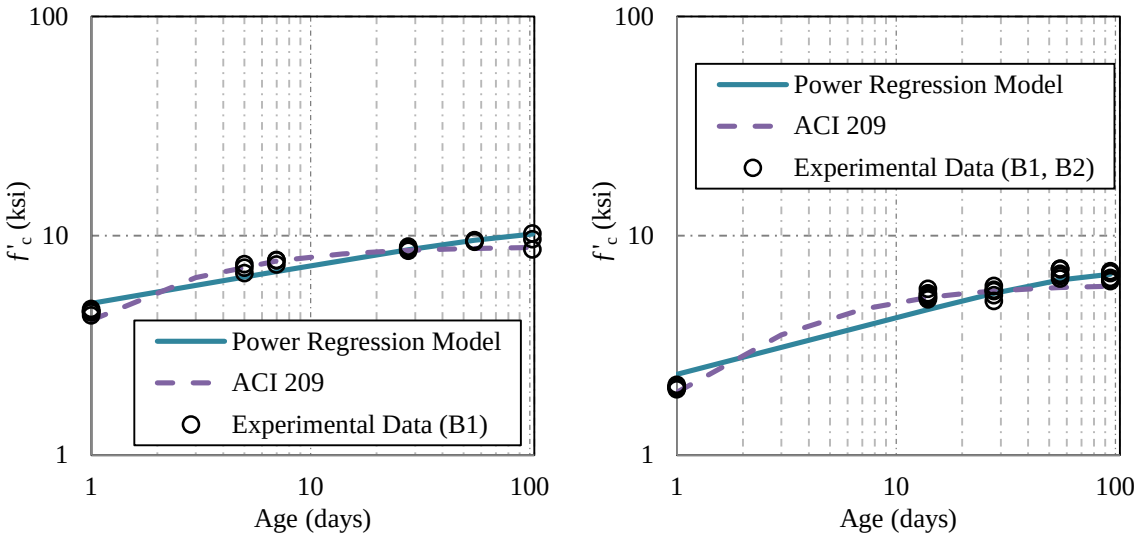

(a) Connections Batch 1 (b) Deck Batch 1 and 2

Figure 6.4. Connection and Deck CC - ACI 209 and Power Regression Models.

Figure 6.5 and Figure 6.6 shows all f'_c experimental data for the AFRP girder and spliced girder project, respectively, and the corresponding best fit ACI 209 model and best fit power regression model.

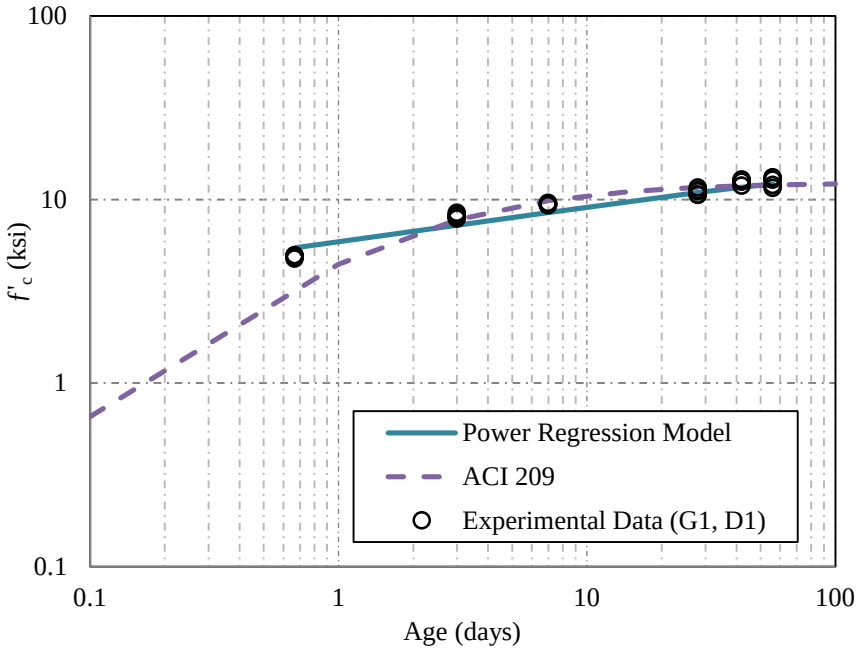

Figure 6.5. AFRP Girder Project - ACI 209 and Power Regression Models.

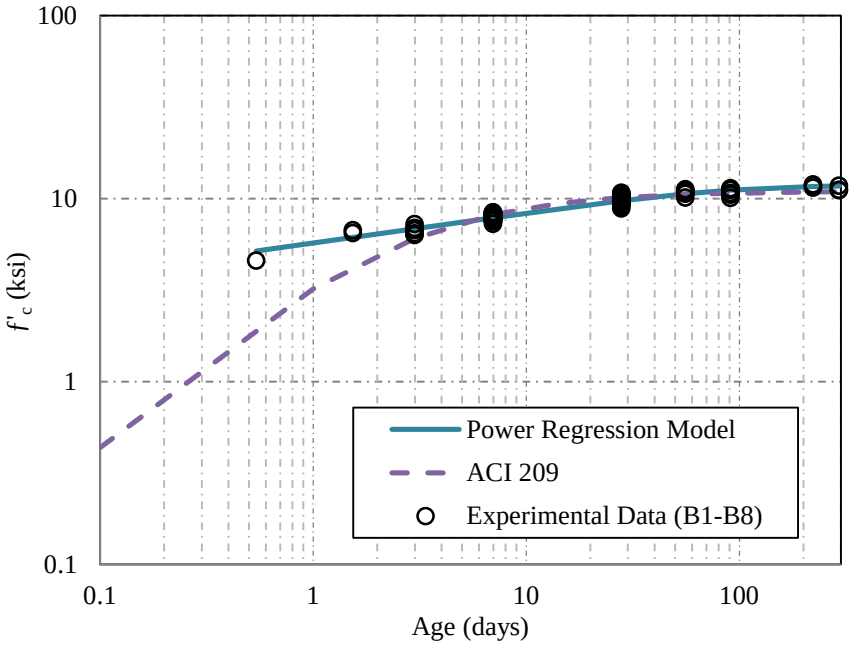

Figure 6.6. Spliced Girder Project - ACI 209 and Power Regression Models.

Tables 6.2 and 6.3 provide the optimum values found for the AFRP girder and spliced girder projects SCC and CC, respectively, for both the ACI 209 model and the power regression model.

Table 6.2. Optimum Model Variable Values for Spliced Girder SCC.

Batch		**ACI 209 Model**		**Power Regression Model**	
		β	a	$f_{c\infty}/f_{c28}$	p
AFRP Girder	G1	0.95	1.37	1.25	0.18
	D1	0.94	1.57	1.25	0.20
	All	0.94	1.68	1.25	0.19
Spliced Girder	B2	0.92	2.18	1.25	0.16
	B4	0.92	2.16	1.25	0.17
	B6	0.93	1.86	1.22	0.15
	All	0.92	2.23	1.20	0.27

Table 6.3. Optimum Model Variable Values for Spliced Girder CC.

Batch	**ACI 209 Model**		**Power Regression Model**	
	β	a	$f_{c\infty}/f_{c28}$	p
Connection	0.96	1.12	1.25	0.17
Deck	0.93	1.96	1.25	0.26

Figure 6.7 shows the combined SCC data for both projects and the corresponding best fit power regression model and ACI 209 model. The model values β, a , $f_{c\infty}/f_{c28}$, and p for the combined data are 0.94, 1.81, 1.25, and 0.16, respectively.

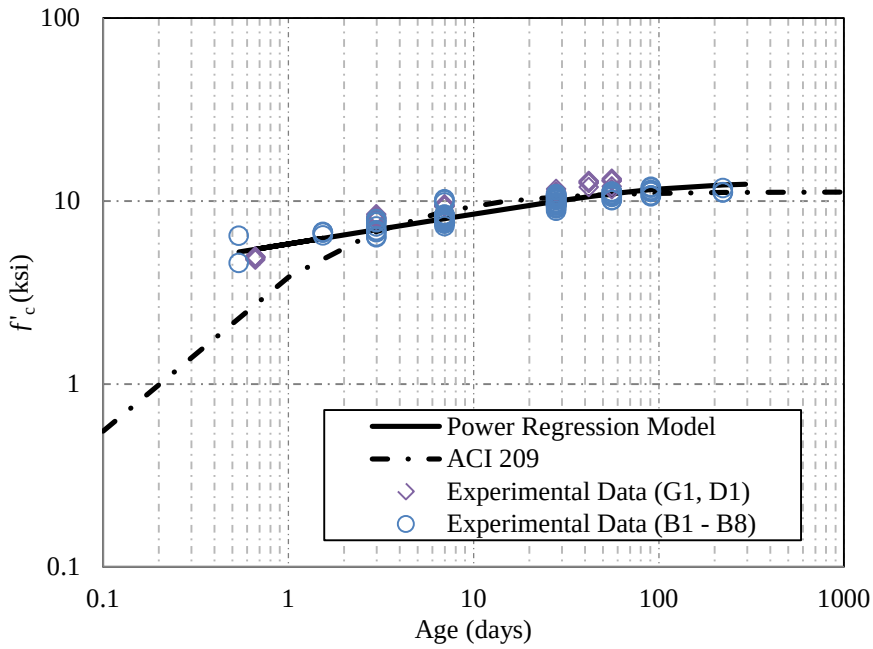

Figure 6.7. Combined SCC Experimental Data Compressive Strength Gain Models.

6.3 Modulus of Elasticity

MOE samples were fabricated and tested for the AFRP girder and deck SCC and the spliced girder SCC. The measured MOE for all batches of the AFRP girder and spliced girder projects have been graphed versus time and compressive strength, as illustrated in Figure 6.8.

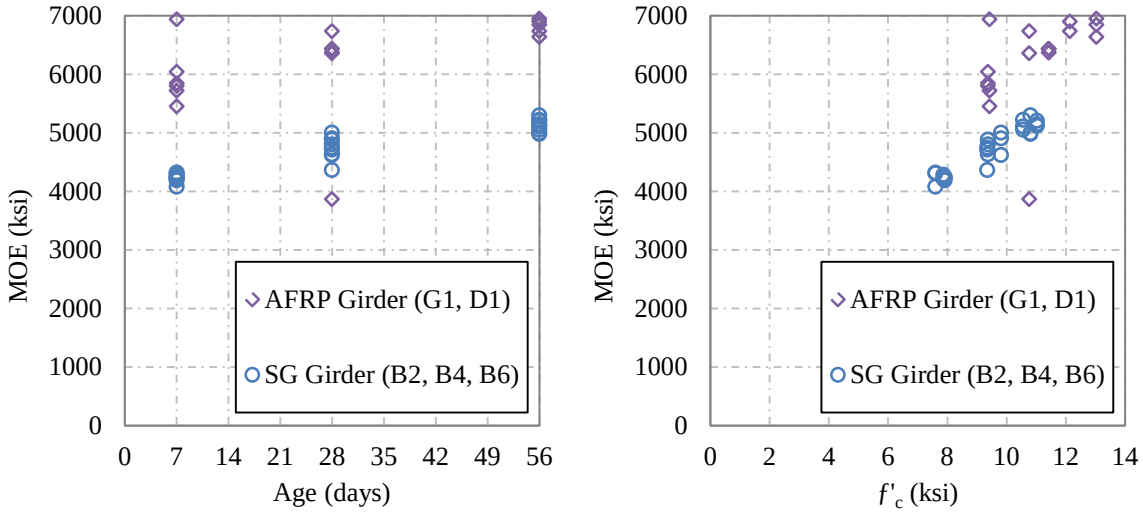

(a) MOE versus time (b) MOE versus f'_c

Figure 6.8. Measured MOE Experimental Data for SCC.

6.3.1 AFRP Girder

The predicted MOE values were calculated based on the average compression strength of the AFRP girder and first deck batch of SCC at 7, 28, and 56 days. The average experimental MOE data and the predicted values from 7 to 56 days for the girder and deck batches are presented in Figure 6.9. The ratios of the experimental MOE to the predicted MOE versus the compressive strength are shown in Figure 6.10. The relative scatter of the ratios compared to the horizontal line at 1.0 provides a measure of the goodness of fit for the prediction equations.

The unified Trejo et al. (2008) equation was used in this evaluation because the mixture proportions provided by the precaster stated that the coarse aggregate used was concrete rock without specifying limestone or other types. As seen in the calculations for 7, 28, and 56 days for the Trejo et al. prediction equations, the limestone equation was more accurate than the unified equation when predicting the girder MOE at 7 and 28 days. However, at 56 days the unified prediction equation was closer to the girder experimental results. The Trejo et al. (2008) MOE unified prediction equation was more accurate than the limestone equation when predicting the deck MOE at all test ages. The

prediction equations from Tables 2.1 and 2.2 were applied to the girder and deck MOE data and the percent error can be seen in Table 6.4 at 28 days.

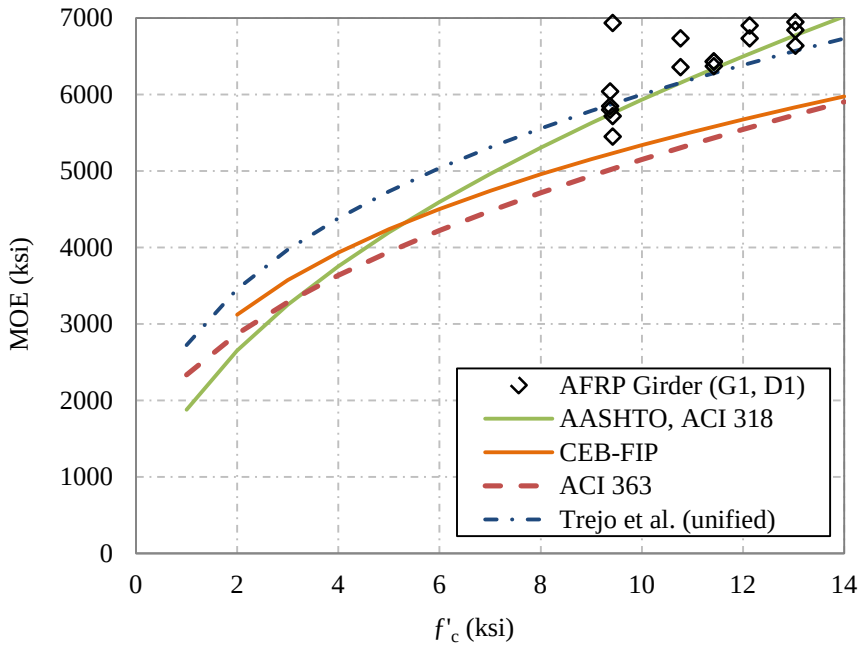

Figure 6.9. AFRP Girder and Deck Predicted and Experimental MOE versus f'_c.

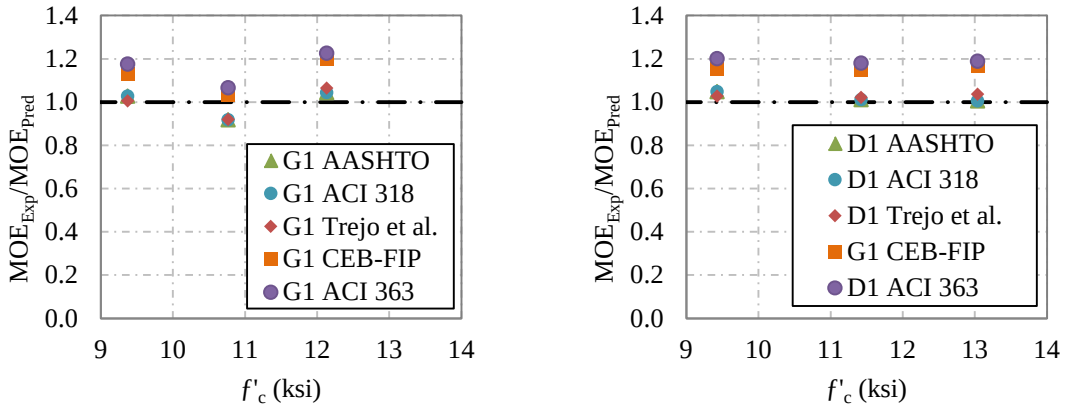

(a) Girder (b) Deck

Figure 6.10. AFRP Girder and Deck – Experimental-to-Predicted MOE Ratios.

Table 6.4. AFRP Girder and Deck Predictions for 28-Day MOE.

Equation Source		Girder, ksi (% error)	Deck (D1), ksi (% error)
Average Experimental Results		5650	6410
AASHTO (2012), ACI 318 (2011)		6160 (8.9)	6340 (-1.1)
ACI 363 (1992)		5300 (-6.2)	5430 (-15)
CEB-FIP (2010)		5470 (-3.2)	5580 (-13)
Trejo et al. (2008)	Limestone	6160 (8.9)	6300 (-1.8)
	Unified	6160 (8.9)	6280 (-2.0)

The basic ACI 318 relationship for MOE is $57{,}000(f'_c)^{1/2}$ for normal strength concrete, calculated with the 28-day f'_c in psi. The AASHTO LRFD MOE relationship is $1820(f'_c)^{1/2}$ for normal strength concrete, calculated with the 28-day f'_c in ksi. The corresponding coefficients were calculated based on the measured MOE values for each age, by batch, and are illustrated in Figure 6.11. For comparison, the ACI 318 and AASHTO LRFD coefficients are shown with a horizontal line.

The ACI 318 and AASHTO LRFD design equation coefficients are generally lower than the coefficients calculated for the experimental data of the AFRP girder and deck SCC. The ACI 318 and AASHTO LRFD design equations slightly underestimate the measured experimental MOE of the girder and deck SCC at early ages, which is generally conservative. Nevertheless, the design equations provide a relatively close estimate of the measured MOE values.

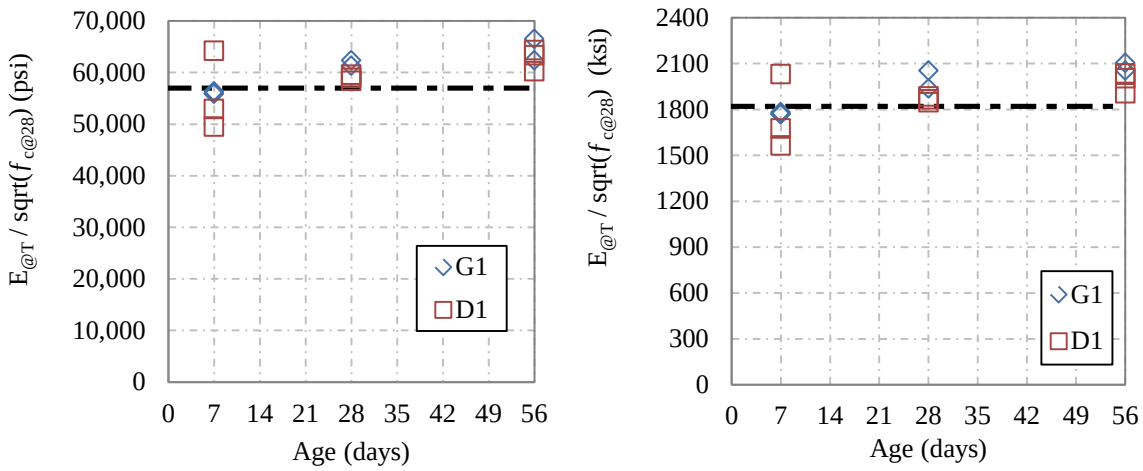

(a) ACI 318 (psi) (b) AASHTO LRFD (ksi)

Figure 6.11. AFRP Girder and Deck MOE Coefficients.

6.3.2 Spliced Girder

6.3.2.1 Girder Segments

The predicted MOE values were calculated based on the average compression strength of the spliced girder batches of SCC at 7, 28, and 56 days. The experimental MOE data and the prediction equation values from 7 to 56 days are presented in Figure 6.12. The Trejo et al. (2008) equation for limestone aggregate was used because the mixture proportions provided by the precaster stated the coarse aggregate used was crushed limestone. The Trejo et al. (2008) equation for limestone was more accurate than the unified equation, as seen in Table 6.5. The experimental MOE values were approximately 1000 ksi lower than the AASHTO (2012), ACI 318 (2011), and Trejo et al. (2008) predicted MOE values for Batches 2, 4, and 6 at all test ages. Figure 6.13 shows the experimental MOE to the predicted MOE ratios versus the compressive strength for Batches 2, 4, and 6.

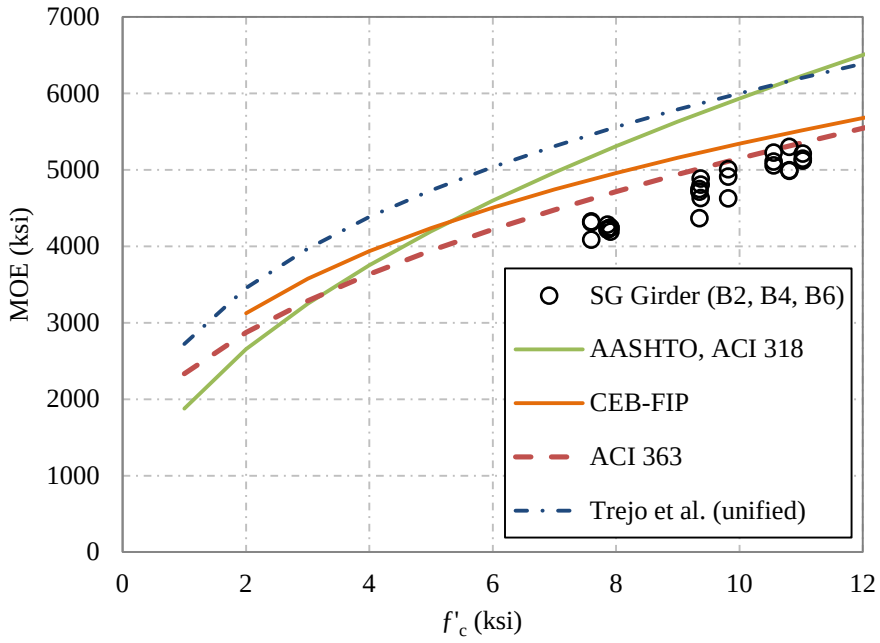

Figure 6.12. Spliced Girder Predicted and Experimental MOE versus f'_c.

Table 6.5. Spliced Girder Predictions for 28-Day MOE.

Equation Source		**Batch 2 ksi (% error)**	**Batch 4 ksi (% error)**	**Batch 6 ksi (% error)**
Average Experimental Results		4610	4770	4850
AASHTO (2012), ACI 318 (2011)		5740 (25)	5750 (20)	5880 (21)
ACI 363 (1992)		5010 (8.8)	5020 (5.2)	5110 (5.5)
CEB-FIP (2010)		5220 (13)	5230 (9.5)	5310 (9.6)
Trejo et al. (2008)	Limestone	5830 (27)	5840 (22)	5940 (23)
	Unified	5870 (27)	5870 (23)	5960 (23)

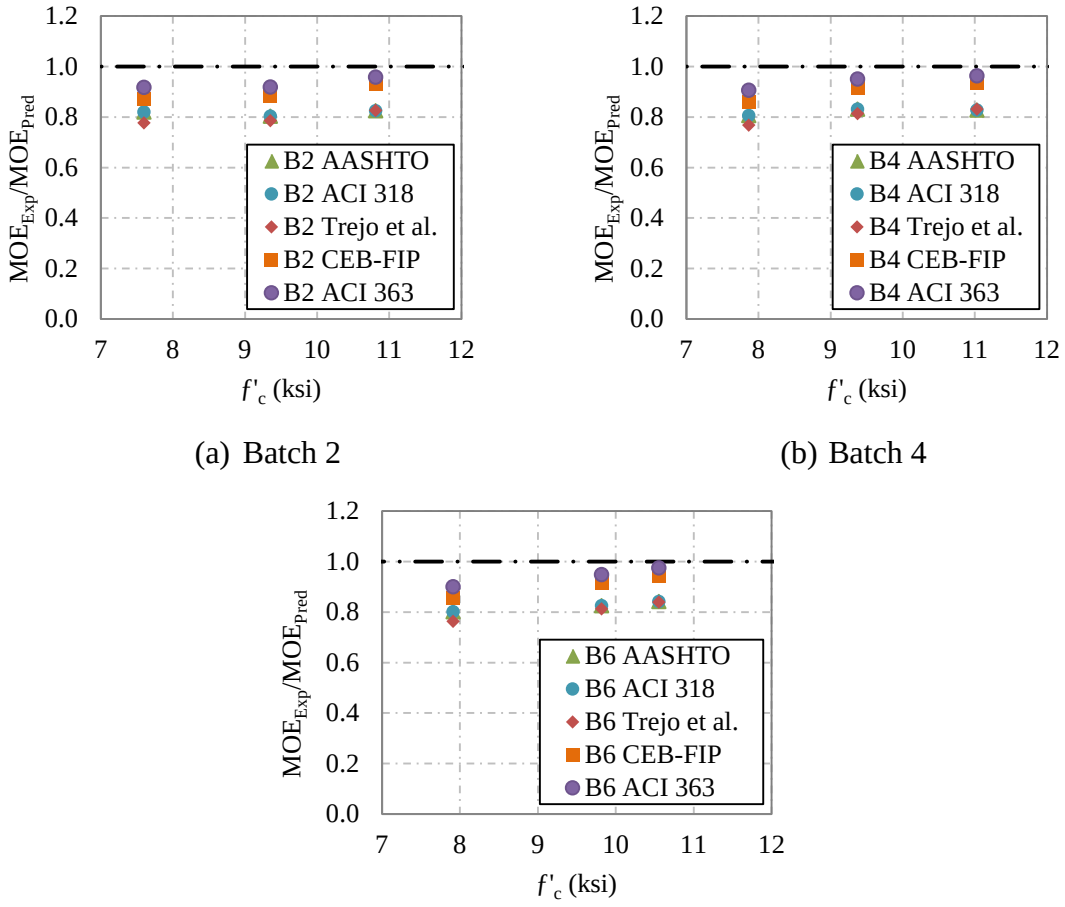

(a) Batch 2

(b) Batch 4

(c) Batch 6

Figure 6.13. Spliced Girder – Experimental-to-Predicted MOE Ratios.

Figure 6.13 shows that for the spliced girder SCC the models predict greater values of MOE than were achieved. The MOE is overestimated by the predictions, which would indicate that the girder is less stiff than expected. The coefficients corresponding to the form of the ACI 318 and AASHTO LRFD MOE relationships for normal strength concrete were calculated for each age, by batch, and illustrated in Figure 6.14.

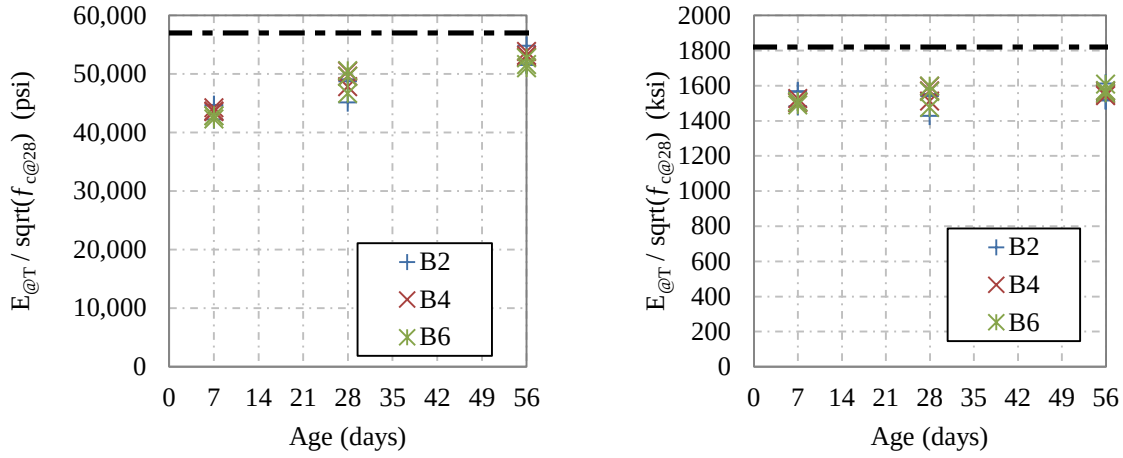

(a) ACI 318 (psi) (b) AASHTO LRFD (ksi)

Figure 6.14. Spliced Girder MOE Coefficients.

6.3.2.2 Connections

The CC experimental MOE data and the predicted MOE values from 7 to 56 days are presented in Figure 6.15 and Figure 6.16. The predicted values were calculated using the average compression strength for both the connection and deck concrete at 7, 28, and 56 days. The prediction equations from Tables 2.1 and 2.2 were applied to the connection concrete measured MOE data and the percent error can be seen in Table 6.6 at 28 days.

ACI 363 and CEB-FIP prediction models underestimate the measured MOE of the connection concrete. The AASHTO LRFD and ACI 318 prediction models underestimate the measured MOE for lower compression strength but had a smaller margin of error to the measured experimental MOE for concrete with compression strength of 8 ksi or higher. The Trejo et al. (2008) unified prediction model was the best fit for the measured MOE of the connection and deck concrete as compression strength increased. The AASHTO LRFD prediction model is a good fit for the measured MOE of the connection concrete, with compression strength between 7 and 10 ksi, without being overly conservative.

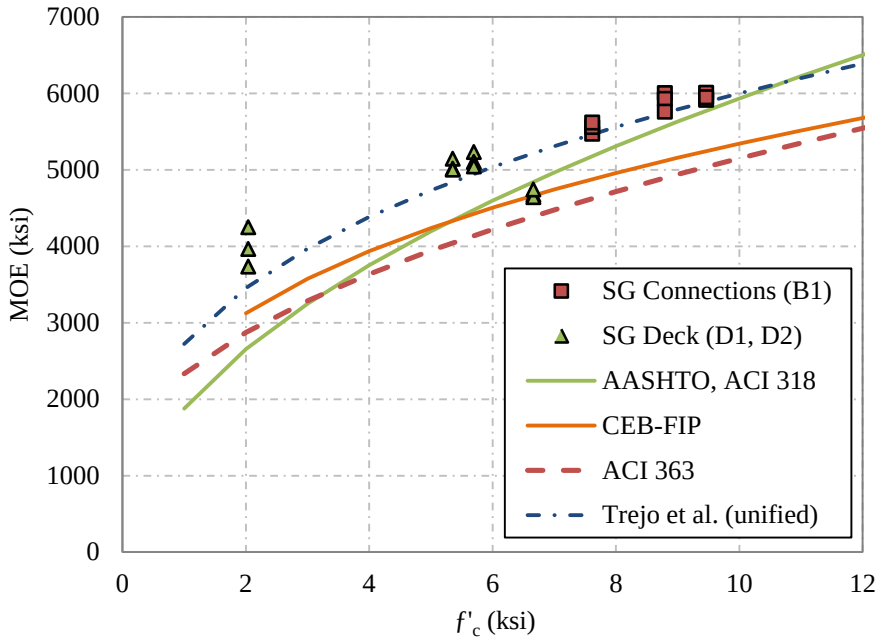

Figure 6.15. Connections and Deck Predicted and Experimental MOE versus f'_c.

Table 6.6. Connection Concrete Predictions for 28-Day MOE.

Equation Source		**ksi (% error)**
Average Experimental Results		5900
AASHTO (2012), ACI 318 (2011)		5570 (-5.6)
ACI 363 (1992)		4890 (-17)
CEB-FIP (2010)		5120 (-13)
Trejo et al. (2008)	River Gravel	6180 (4.8)
	Unified	5740 (-2.6)

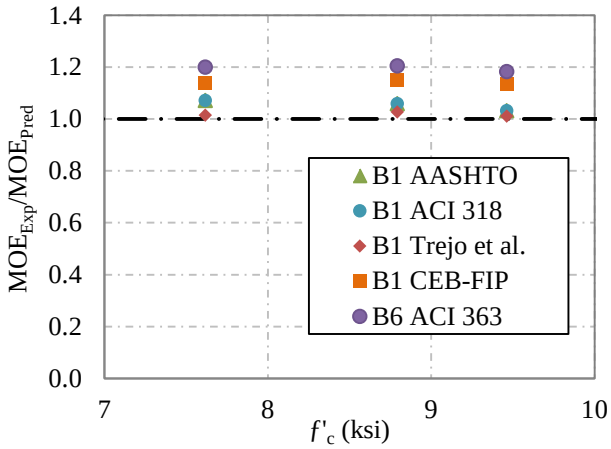

Figure 6.16. Connections – Experimental-to-Predicted MOE Ratios.

6.4 Splitting Tensile Strength

STS samples were fabricated and tested for the AFRP girder and deck SCC and the spliced girder SCC. All measured STS values for the AFRP girder and spliced girder projects have been graphed versus time and compressive strength, as shown in Figure 6.17.

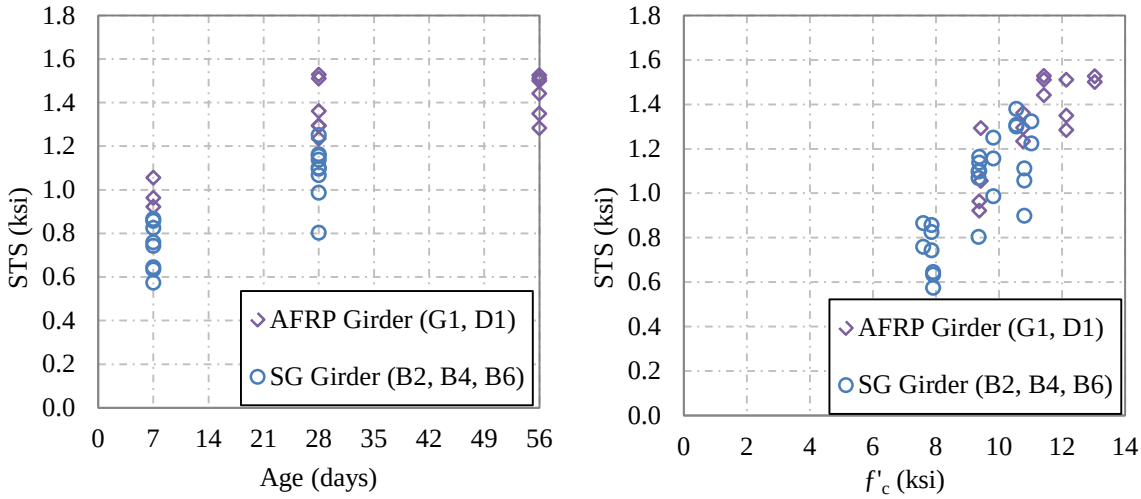

(a) STS versus time (b) STS versus f'_c

Figure 6.17. Measured STS Experimental Data for SCC.

6.4.1 AFRP Girder

The average experimental STS data for the AFRP girder and deck and the predicted STS values from 7 to 56 days are presented in Figure 6.18. The AASHTO (2010), ACI 318 (2011), and Trejo et al. (2008) lower bound (LB) equations were significantly lower than the experimental results by 0.4 to 0.6 ksi. Even the Trejo et al. upper bound (UB) equations were below the average STS experimental results although by a smaller margin of 0.2 to 0.4 ksi.

The prediction equations were applied to the girder and deck STS data and the percent error can be seen in Table 6.7 at 28 days. The ratios of the experimental STS to the predicted STS versus the compressive strength are shown in Figure 6.19.

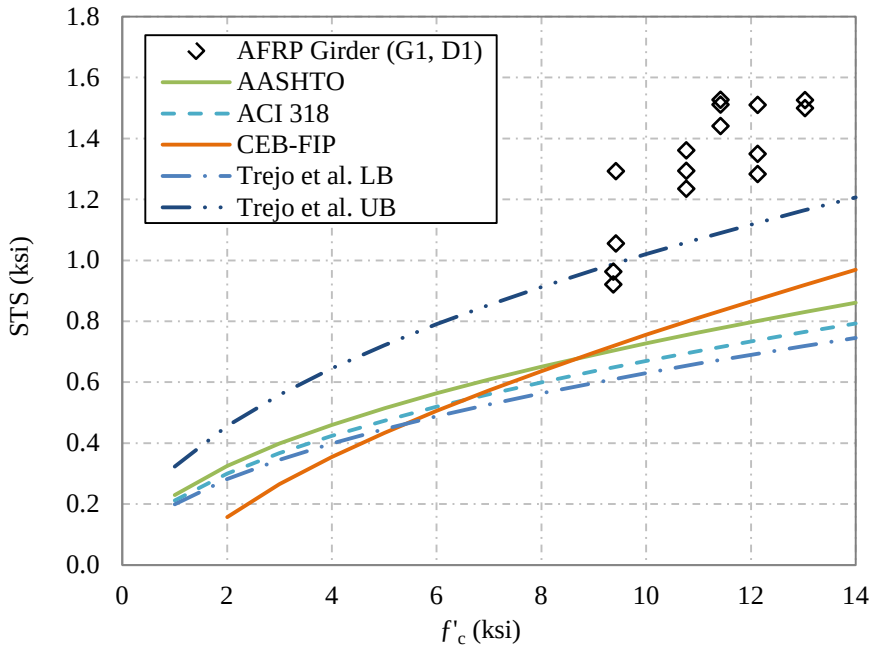

Figure 6.18. AFRP Girder and Deck Predicted and Experimental STS versus f'_c.

Table 6.7. AFRP Girder and Deck Predictions for 28-Day STS.

Equation Source		Girder, ksi (% error)	Deck (D1), ksi (% error)
Average Experimental Results		1.27	1.47
AASHTO (2012)		0.75 (-41)	0.78 (-47)
ACI 318 (2011)		0.70 (-45)	0.72 (-51)
CEB-FIP (2010)		0.80 (-37)	0.83 (-43)
Trejo et al. (2008)	Lower bound	0.65 (-49)	0.67 (-54)
	Upper bound	1.06 (-17)	1.09 (-26)

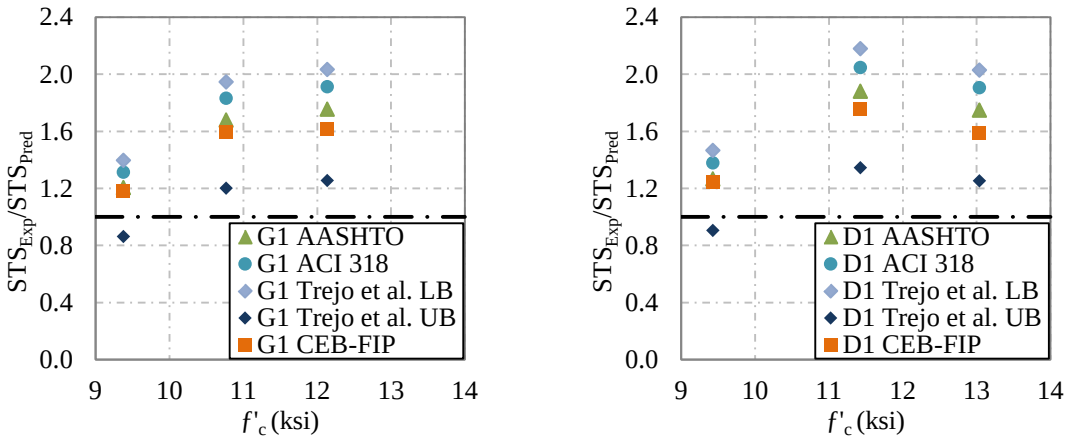

(a) Girder (b) Deck

Figure 6.19. AFRP Girder and Deck – Experimental-to-Predicted STS Ratios.

The ACI STS relationship for normal strength concrete is $6.7(f'_c)^{1/2}$ calculated with the 28-day f'_c in psi. The AASHTO LRFD STS relationship for normal strength concrete is $0.24(f'_c)^{1/2}$ calculated with 28-day f'_c in ksi. The coefficients based on the

experimental data were calculated for each age, by batch, and illustrated in Figure 6.20. For comparison, the ACI 318 and AASHTO LRFD coefficients are shown with a horizontal line.

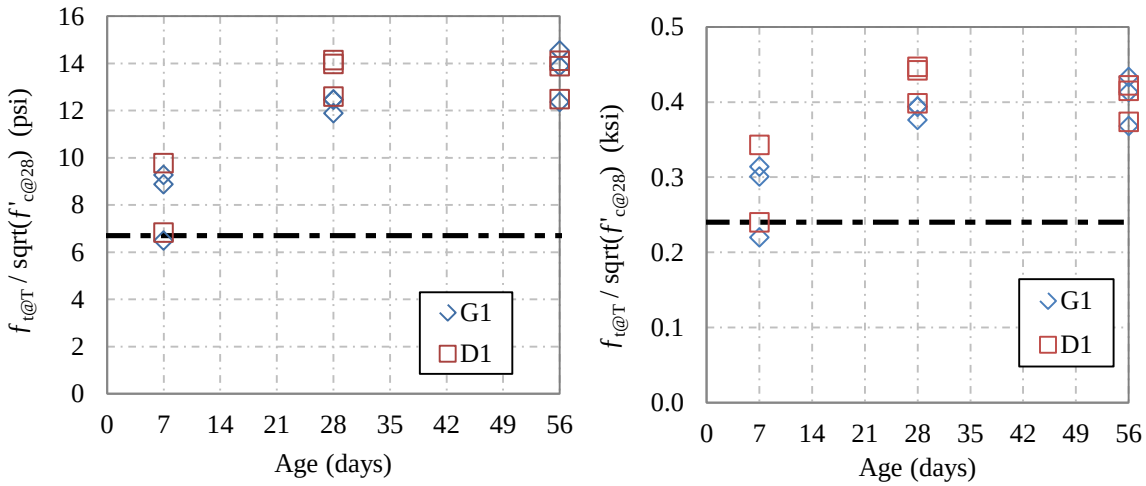

(a) ACI 318 (psi)

(b) AASHTO LRFD (ksi)

Figure 6.20. AFRP Girder and Deck STS Design Coefficients.

6.4.2 Spliced Girder

6.4.2.1 Girder Segments

The experimental STS data and the predicted STS values from 7 to 56 days are presented in Figure 6.21. The percent error can be seen in Table 6.8 for the 28-day data. Figure 6.22 shows the experimental STS to the predicted STS ratios versus the compressive strength for Batches 2, 4, and 6.

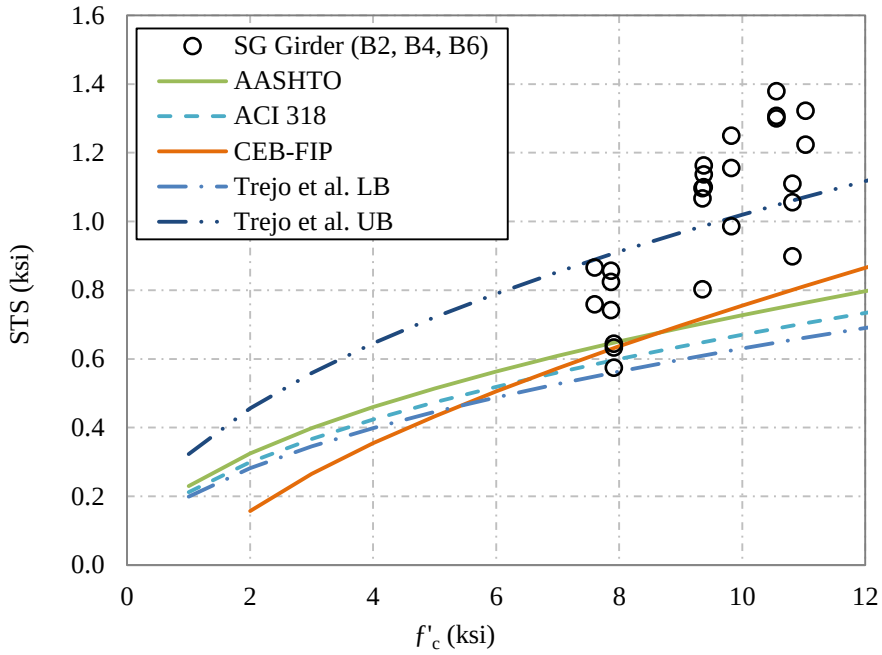

Figure 6.21. Spliced Girder Predicted and Experimental STS versus f'_c.

The coefficients for the STS as compared to the ACI 318 and AASHTO relationships were calculated for each age, by batch, and illustrated in Figure 6.23. The AASHTO LRFD (2012), ACI 318 (2011), and Trejo et al. (2008) LB equations underestimated the experimental STS by a range of 0.2 to 0.4 ksi on average for Batches 2 and 4. Batch 6 experimental 7-day STS was very close to AASHTO, ACI 318, and Trejo et al. LB equations but the STS increased significantly so that the average difference at 28 days and 56 days was at least 0.4 and 0.6 ksi, respectively.

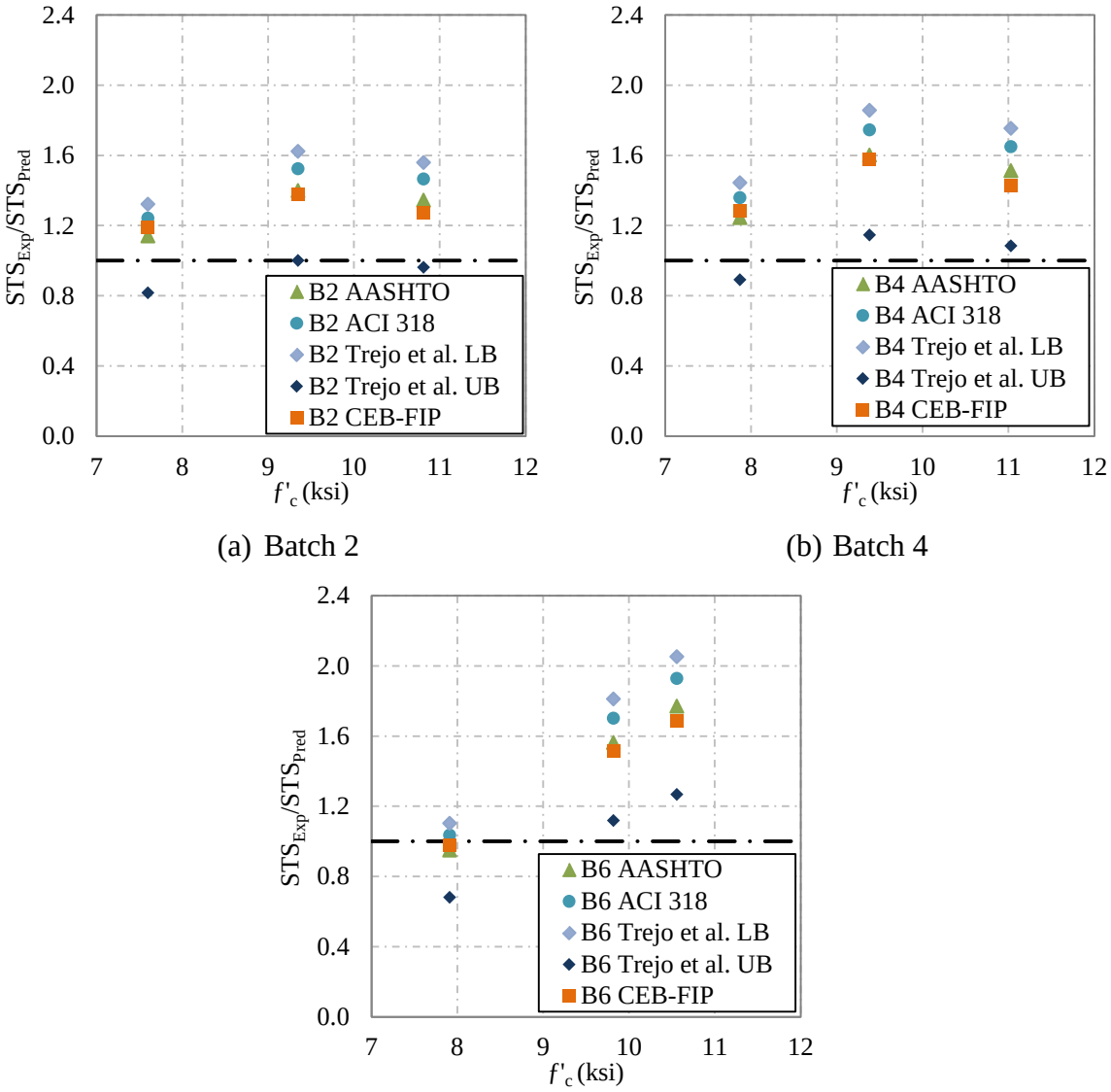

(a) Batch 2

(b) Batch 4

(c) Batch 6

Figure 6.22. Spliced Girder – Experimental-to-Predicted STS Ratios.

Table 6.8. Spliced Girder Predictions for 28-Day STS

Equation Source		Batch 2 ksi (% error)	Batch 4 ksi (% error)	Batch 6 ksi (% error)
Average Experimental Results		0.988	1.13	1.02
AASHTO (2012)		0.70 (-29)	0.70 (-38)	0.72 (-36)
ACI 318 (2011)		0.65 (-34)	0.65 (-43)	0.66 (-41)
CEB-FIP (2010)		0.72 (-27)	0.72 (-36)	0.75 (-34)
Trejo et al. (2008)	Lower bound	0.61 (-38)	0.61 (-46)	0.62 (-45)
	Upper bound	0.99 (-0.19)	0.99 (-13)	1.01 (-11)

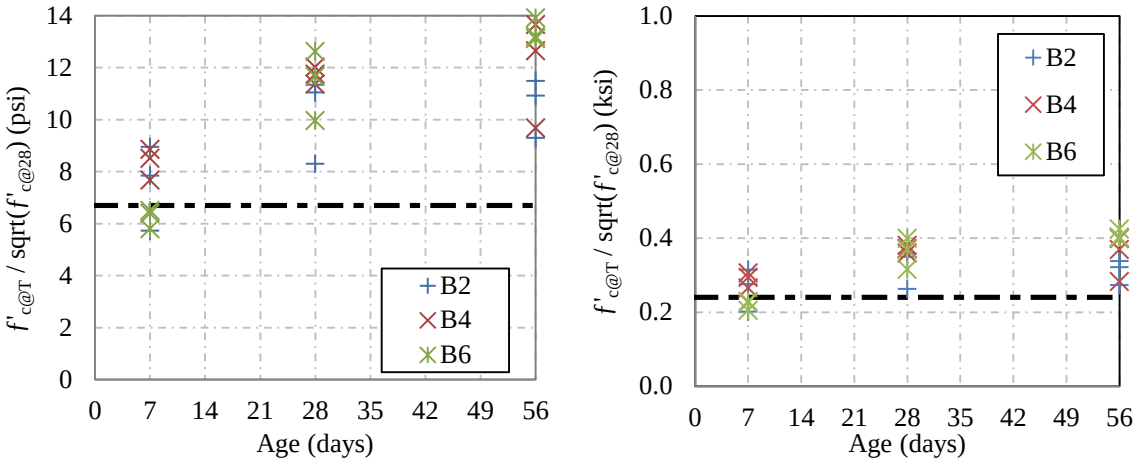

(a) ACI 318 (psi) (b) AASHTO LRFD (ksi)

Figure 6.23. Spliced Girder STS Coefficients.

6.4.2.2 Connections

The CC experimental STS data and the predicted STS values from 7 to 56 days are presented in Figure 6.24 and Figure 6.25. The predicted values were calculated using the average compression strength for both the connection and deck concrete at 7, 28, and 56 days. The percent error for the connection concrete predicted STS can be seen in Table 6.9 for the 28-day data.

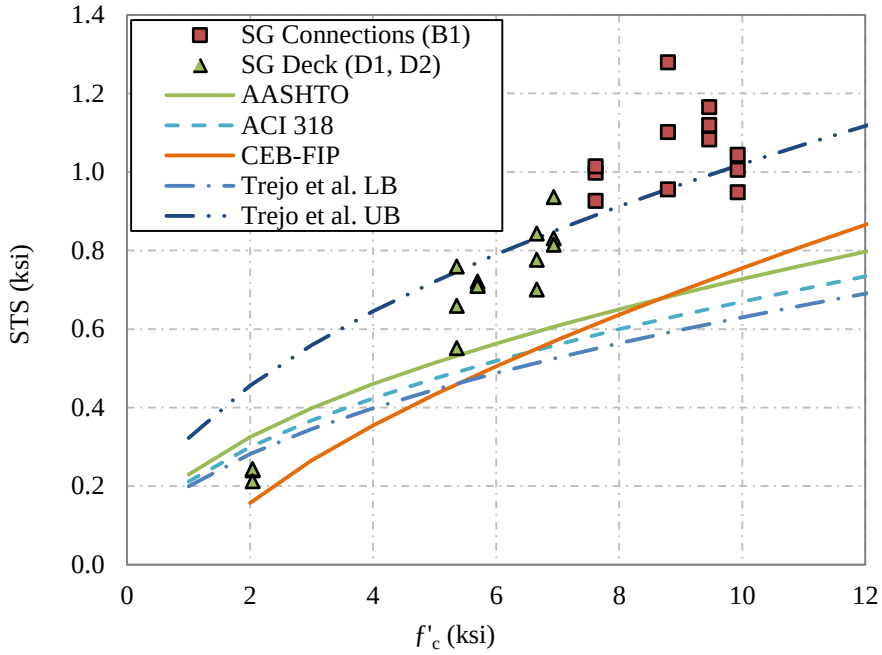

Figure 6.24.Connections and Deck Predicted and Experimental STS versus f'_c.

Table 6.9. Connection Concrete Predictions for 28-Day STS.

Equation Source		ksi (% error)
Average Experimental Results		1.11
AASHTO (2012)		0.68 (-39)
ACI 318 (2011)		0.63 (-43)
CEB-FIP (2010)		0.68 (-38)
Trejo et al. (2008)	Lower bound	0.59 (-47)
	Upper bound	0.96 (-14)

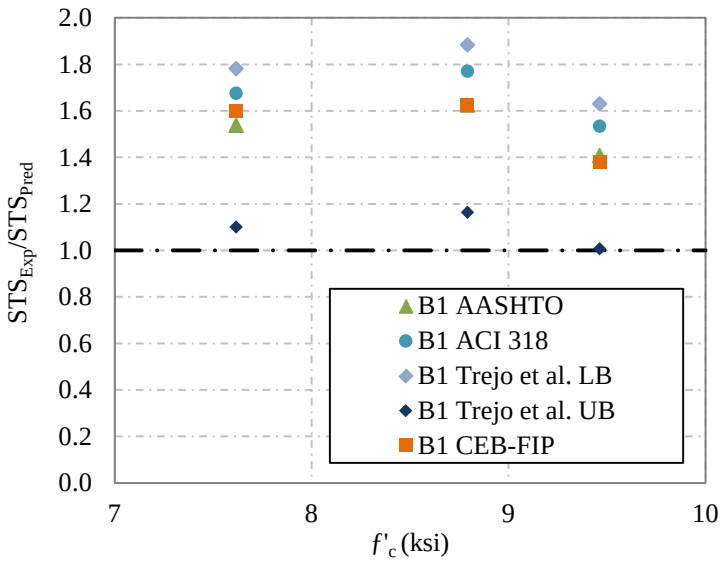

Figure 6.25. Connections – Experimental-to-Predicted STS Ratios.

The AASHTO LRFD (2012), ACI 218 (2011), and the Trejo et al. (2008) prediction models underestimate the measured STS of the connection concrete. The Trejo et al. (2008) model bounds the average measured STS of the deck concrete with

compression strength between 5 and 7 ksi. However, the measured STS values for the connection concrete exceed the upper bound of the Trejo et al. (2008) model. The AASHTO LRFD model was conservative and underestimated the measured STS for the connection concrete by at least 50 percent for concrete with compression strength between 7.5 and 10 ksi.

6.5 Modulus of Rupture

MOR samples were fabricated and tested for the AFRP girder and deck SCC and the spliced girder SCC. The measured MOR for all batches of the AFRP girder and spliced girder projects have been graphed versus time and compressive strength, as illustrated in Figure 6.26.

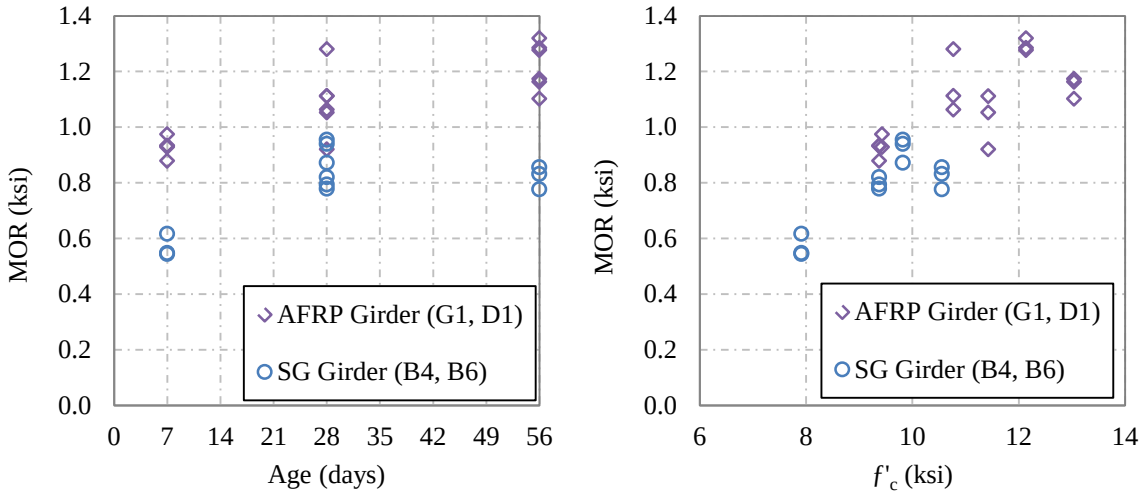

(a) MOR versus time (b) MOR versus f'_c

Figure 6.26. Measured MOR Experimental Data for SCC.

6.5.1 AFRP Girder

The AFRP girder experimental MOR data and corresponding predicted MOR values from 7 to 56 days are presented in Figure 6.27. The AASHTO (2010) LB, ACI 318 (2011), and Trejo et al. (2008) LB equations are all at least 200 psi lower than the experimental results. The AASHTO (2010) UB and Trejo et al. (2008) UB equations were within 100 psi of the girder SCC experimental results and about 200 psi of the deck SCC experimental results.

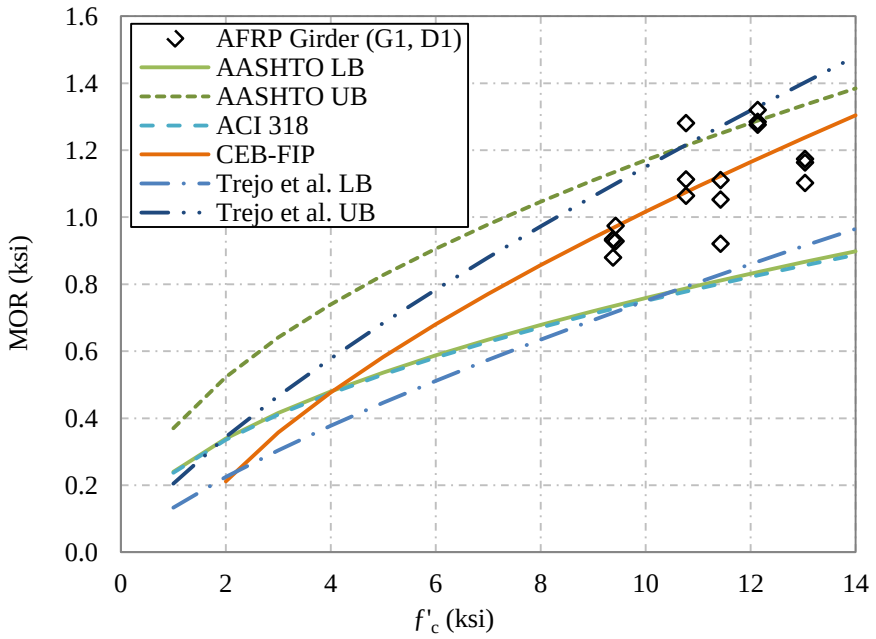

Figure 6.27. AFRP Girder and Deck Predicted and Experimental MOR versus f'_c.

The prediction equations were applied for the girder and deck MOR data and the percent error can be seen in Table 6.10 for the 28-day data. The ratios of the experimental MOR to the predicted MOR versus the compressive strength are shown in Figure 6.28.

Table 6.10. AFRP Girder and Deck Predictions for 28-Day MOR.

Equation Source		Girder, ksi (% error)	Deck (D1), ksi (% error)
Average Experimental Results		1.15	1.03
AASHTO (2012)	Lower bound	0.79 (-32)	0.81 (-21)
	Upper bound	1.21 (5.4)	1.25 (22)
ACI 318 (2011)		0.78 (-32)	0.80 (-22)
CEB-FIP (2010)		1.08 (-6.7)	1.12 (9.3)
Trejo et al. (2008)	Lower bound	0.79 (-31)	0.83 (-19)
	Upper bound	1.22 (5.5)	1.27 (24)

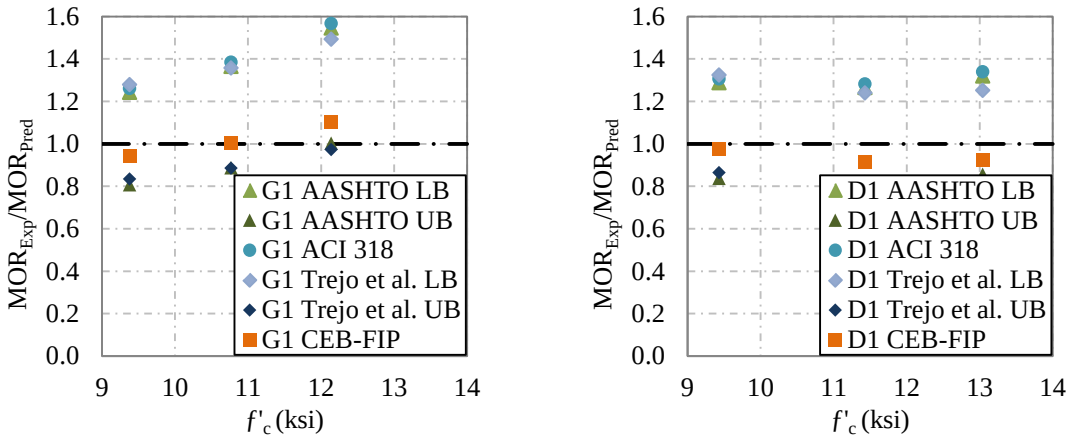

(a) Girder (b) Deck

Figure 6.28. AFRP Girder and Deck – Experimental-to-Predicted MOR Ratios.

The ACI MOR relationship for normal strength concrete is $7.5(f'_c)^{1/2}$ calculated with the 28-day f'_c in psi. The AASHTO LRFD coefficient for the MOE relationship is

$0.23(f'_c)^{1/2}$ for normal strength concrete (up to 10 ksi) or $0.37(f'_c)^{1/2}$ for HSC (up to 15 ksi), calculated with the 28-day f'_c in ksi. The coefficients based on the experimental data were calculated for each age, by batch, and illustrated in Figure 6.29. For comparison, the ACI 318 and AASHTO LRFD coefficients are shown with a horizontal line.

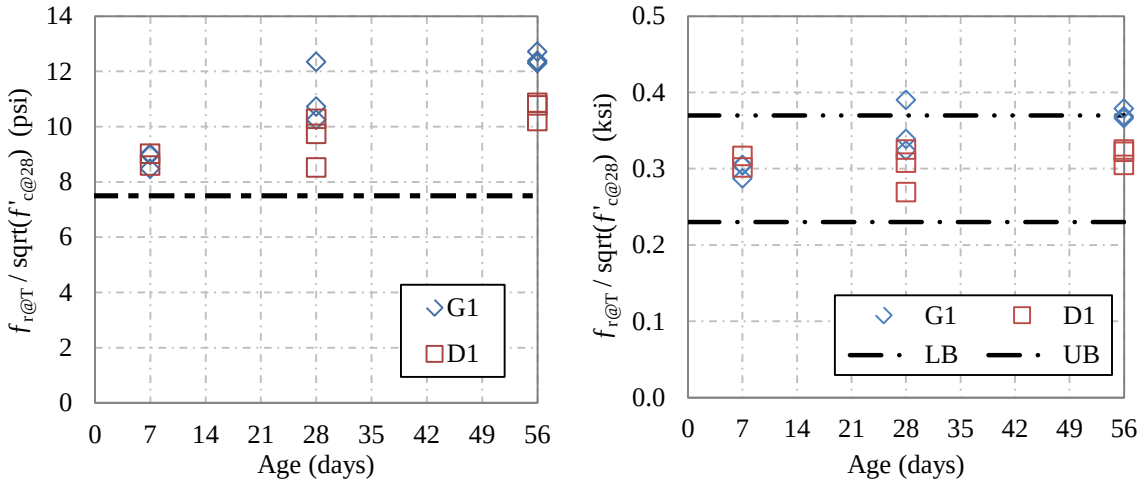

(a) ACI 318 (psi) (b) AASHTO LRFD (ksi)

Figure 6.29. AFRP Girder and Deck MOR Design Coefficients.

6.5.2 Spliced Girder

6.5.2.1 Girder Segments

The experimental MOR data and the predicted MOR values for 7 to 56 days are presented in Figure 6.30 and Figure 6.31. The percent error for the 28-day data is given in Table 6.11. The average experimental 7-day MOR of Batch 6 was below all prediction equation values, even the lower bounds, for both AASHTO (2012) and Trejo et al. (2008).

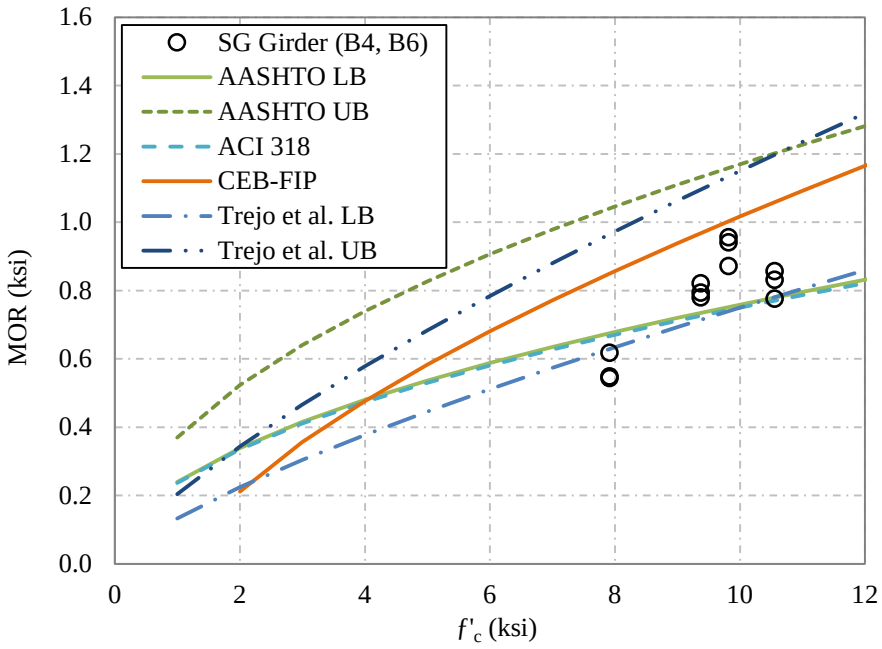

Figure 6.30. Spliced Girder Predicted and Experimental MOR versus f'_c.

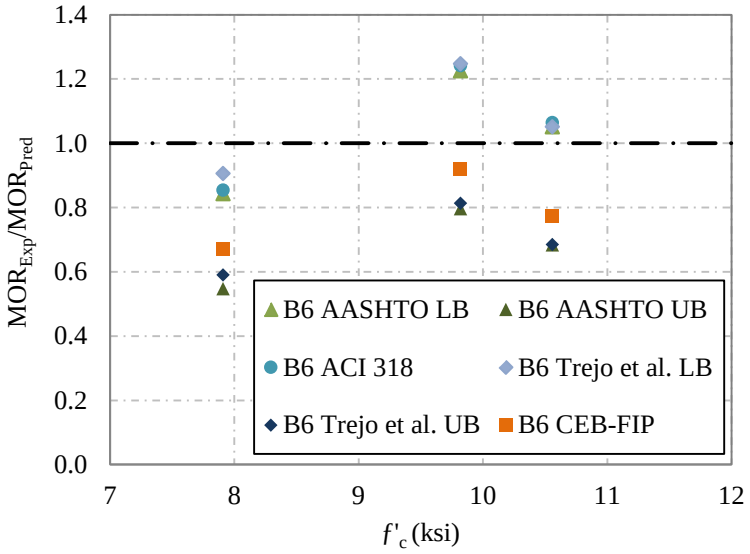

Figure 6.31. Spliced Girder Batch 6 – Experimental-to-Predicted MOE Ratios.

Table 6.11. Spliced Girder Predictions for 28-Day MOR.

Equation Source		Batch #4 ksi (% error)	Batch #6 ksi (% error)
Average Experimental Results		0.798	0.923
AASHTO (2012)	Lower bound	0.73 (-7.9)	0.82 (-18)
	Upper bound	1.13 (42)	1.16 (26)
ACI 318 (2011)		0.73 (-9.0)	0.74 (-19)
CEB-FIP (2010)		0.97 (21)	1.00 (8.7)
Trejo et al. (2008)	Lower bound	0.71 (-10)	0.74 (-20)
	Upper bound	1.10 (37)	1.13 (23)

The coefficients for the MOR as compared to the ACI 318 and AASHTO relationships were calculated for each age, by batch, and illustrated in Figure 6.32.

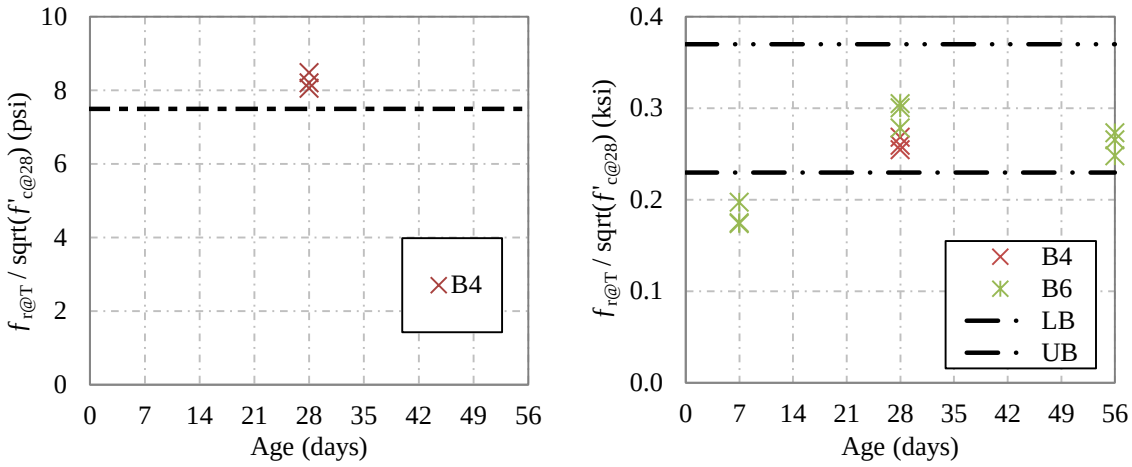

(a) ACI 318 (psi) (b) AASHTO LRFD (ksi)

Figure 6.32. Spliced Girder MOR Coefficients.

6.5.2.2 Connections

The experimental MOR data and the predicted values from 7 to 56 days are presented in Figure 6.33 and Figure 6.34. The predicted MOR values were calculated using the average compression strength of the connection concrete at 7, 28, and 56 days. The percent error for the connection concrete predicted MOR can be seen in Table 6.12 for the 28-day data.

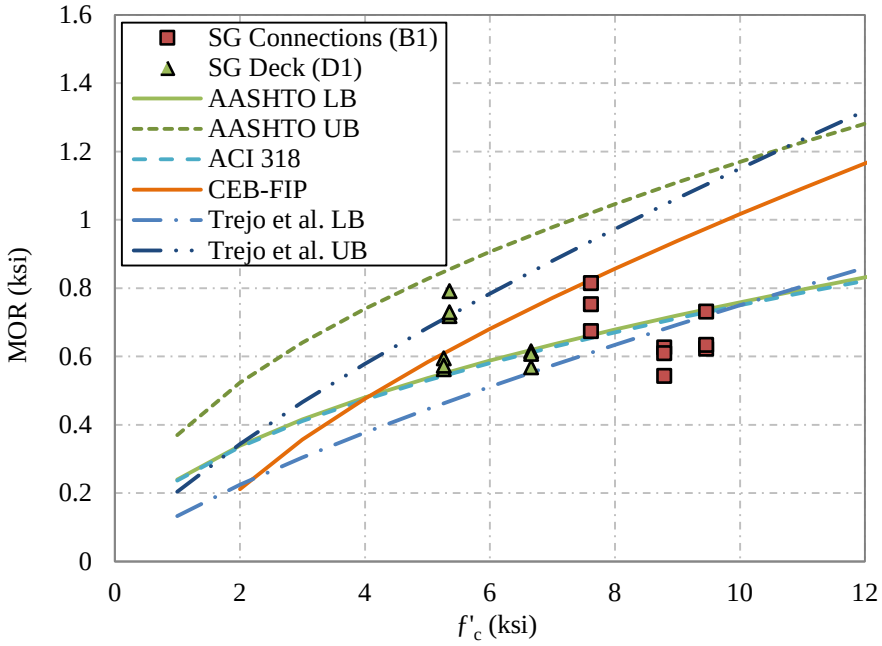

Figure 6.33. Connections and Deck Predicted and Experimental MOR versus f'_c.

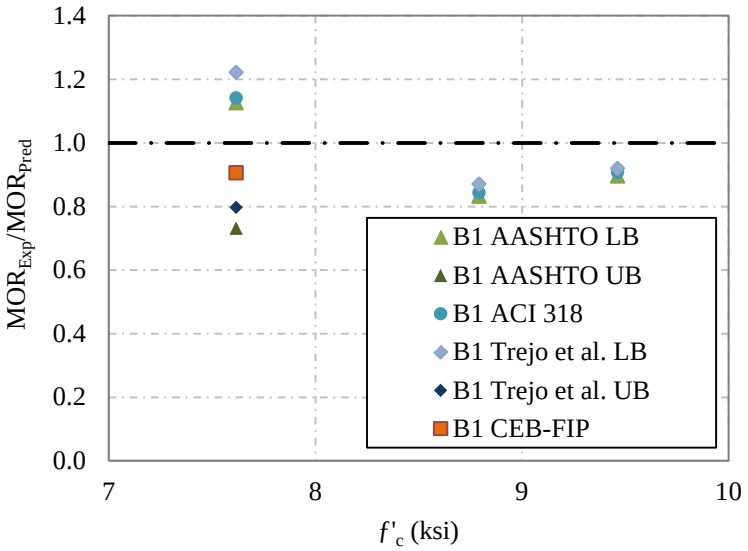

Figure 6.34. Connections – Experimental-to-Predicted MOR Ratios.

Table 6.12. Connection Concrete Predictions for 28-Day MOR.

Equation Source		**ksi (% error)**
Average Experimental Results		0.593
AASHTO (2012)	Lower bound	0.71 (20)
	Upper bound	1.10 (85)
ACI 318 (2011)		0.70 (19)
CEB-FIP (2010)		0.92 (56)
Trejo et al. (2008)	Lower bound	0.68 (15)
	Upper bound	1.04 (76)

The AASHTO LRFD (2012) expressions bound the average measured MOR for the connection concrete with compression strength between 5 and 7 ksi. However, the AASHTO LRFD expressions do not bound the measured MOR of the connection

concrete; the lower bound equation overestimates the measured MOR for compression strengths greater than 8 ksi. The ACI 318 (2011) prediction model underestimates the measured MOR for the connection and deck concrete with compressive strength between 5 and 8 ksi, while overestimating the measured MOR for the connection concrete with compressive strength greater than 8 ksi. The CEB-FIP (2010) model overestimates the measured MOR for the connection concrete, but significantly overestimates the measured MOR when the compression strength is 8 ksi or greater.

6.6 Shrinkage

Typical shrinkage strain values at 280 days for the SCC in this research range from 0.00052 to 0.00078 in./in. Research suggests that for high strength concrete (6-12 ksi), the typical range is 0.00058 to 0.00095 in./in. (Oliva and Cramer 2008, Mertol et al. 2010).

6.7 Summary

Power regression models were developed for the AFRP and spliced girder projects by individual batch and for combined data sets, and these models were compared. Prediction equations and design equations were modeled and related to the experimental data measured for the hardened property samples of both projects. MOR decreased at later ages for the spliced girder and connection concrete. The lower MOR of the connection concrete from 28 and 56 days as compared to 7 days may be attributed to the curing conditions.

The Trejo et al. (2008) prediction model was the best fit for the measured MOE of the experimental data obtained in this research, as compared to the AASHTO LRFD (2012), ACI 318 (2011), ACI 363 (1992), and CEB-FIP (2010) prediction models for MOE. The AASHTO LRFD prediction model underestimated the measured MOE with concrete less than 6 ksi compression strength but the model was the best fit for the AFRP girder and deck SCC and the spliced girder connection concrete, for concrete with a compressive strength of 8 ksi and above. However, for the spliced girder SCC, with compression strength between 8 to 12 ksi, the AASHTO LRFD prediction model was

significantly conservative (compared to the other models) and the ACI 363 model provided a better representation of the measured MOE.

The AASHTO LRFD (2012), ACI 318 (2011), CEB-FIP (2010), and Trejo et al. (2008) prediction models were significantly conservative on the estimation of the measured STS obtained in this research. However, the Trejo et al. (2008) models bounded the measured data well for concrete with compression strength between 4 and 8 ksi. For higher strength concrete, including SCC and connection concrete with compressive strength greater than 8 ksi, the prediction models compared did not match well with the measured STS in this research.

The measured MOR obtained in this research was modeled well by the bounds of the AASHTO LRFD (2012) and the Trejo et al. (2008) prediction model for concrete with compression strength between 5 to 14 ksi, except for the connection concrete when the compression strength was between 8 to 10 ksi. The CEB-FIP model overestimated the average measured MOR but provided a good indication as an upper bound model for the SCC.

7. SUMMARY, CONCLUSIONS, AND RECOMMENDATIONS

7.1 Summary

This section summarizes the results of a study that has been conducted to characterize advanced construction materials such as SCC and AFRP for use in bridge girders. First, a review of literature on SCC origins and growing acceptance of implementation in the precast sector was conducted. Second, a detailed review was done for all the fresh and hardened property concrete tests performed for this project. SCC possesses different inherent qualities than CC that require alternative methods of testing. Third, an analysis of results was conducted for the AFRP girder and spliced girder project, respectively. Based on the results, an analysis was performed to compare experimental data to the current design prediction equations used in practice today. Additional information and recommendations for these equations have been provided to assist in the implementation of SCC. Several areas requiring further study are identified based on the comparative analysis.

7.2 Conclusion

Based on the research presented in this thesis, the following conclusions may be drawn:

1. AFRP Girder
    - The AFRP strands used in the AFRP girder were found to have an average of 18 kips axial force capacity. The optimal grout mixture used for the couplers was 3:8, water-to-powder ratio, with an average 7-day compressive strength of 5 ksi.
    - The final coupler anchorage system designed for extending the AFRP strands for prestressing included welding the ends of the pipes used for the coupler and dead ends, rather than epoxying plastic end caps, to prevent grout pullout. Threaded rod, instead of conventional steel strand, was found to

counteract the torsional action of the pipes to prevent the twisting of the AFRP strand.

- The measured compressive strength for the SCC in the girder concrete exceeded the design strength but not the expected strength (based on the pilot batch data provided by the precasters). However, the compressive strength of SCC in the deck was above the expected strength.
- The AASHTO LRFD and ACI 318 prediction models were the same in this case and were the best fit for the measured MOE experimental data for all the prediction models compared. The Trejo et al. (2008) prediction equations for SCC overestimated the MOE for the SCC used in the girder and deck. The CEB-FIP prediction model underestimated the measured MOE by more than any other prediction model.
- The AASHTO LRFD, ACI 318, CEB-FIP, and Trejo et al. (2008) prediction models heavily underestimated the measured STS for the SCC. The upper bound Trejo et al. (2008) model was the closest to the measured STS but still had 20 percent error, as opposed to the lower bound model (Trejo et al. 2008) that underestimated the measured STS by more than 90 percent.
- The AASHTO LRFD upper bound and Trejo et al. (2008) upper bound prediction models were within range of the measured MOR values for the SCC. The AASHTO LRFD lower bound, ACI 318, and Trejo et al. (2008) lower bound equations all underestimated the measured MOR. The CEB-FIP equation was the best fit prediction model for this set of data.

2. Spliced Girder
    - The measured compressive strength for the SCC girder exceeded the design strength but not the expected strength (based on the pilot batch data provided by the precasters).
    - The AASHTO LRFD, ACI 318, Trejo et al. (2008), and CEB-FIP prediction models overestimated the measured MOE of the SCC used in the girder.

- The measured MOE for the connection concrete was close to the predicted values of the AASHTO LRFD, ACI 318, and the unified Trejo et al. (2008) prediction models. The CEB-FIP prediction model underestimated the measure MOE of the connection concrete.
- The AASHTO LRFD, ACI 318, CEB-FIP, and Trejo et al. lower bound (2008) prediction equations underestimated the measured STS for the SCC in the girder and for the connection concrete.
- The Trejo et al. (2008) upper bound equation was the closest model to accurately predict the average measured STS for the SCC in the girder and the connection concrete.
- The AASHTO LRFD lower bound, ACI 318, and Trejo et al. (2008) lower bound prediction equations provided the best model for the measured MOR values for the SCC used in the spliced girder. The AASHTO upper bound, Trejo et al. (2008) upper bound, and the CEB-FIP prediction models overestimated the measured MOR for the SCC used in the girder.
- While AASHTO LRFD, ACI 318, CEB-FIP, and Trejo et al. (2008) prediction models were close to the early age, measured MOR for the connections, the AASHTO upper bound, Trejo et al. upper bound, and the CEB-FIP models were greatly different than the later age, measured MOR for the connection concrete. However, data was limited to only one batch; therefore, more samples may be beneficial in the future for a better indication of the behavior of the connection concrete and prediction model evaluation.

3. Comparisons
    - As expected, measured MOE values tended to increase as the concrete compressive strength increased.
    - The CEB-FIP prediction model consistently underestimated the measured MOE of the SCC used in the AFRP girder and deck, as well as the connection CC, but overestimated the measured MOE of the SCC used in the

spliced girder. The AFRP girder and the spliced girder were less stiff than expected based on the prediction models.

- The Trejo et al. (2008) upper bound prediction model was the closest model for the measured STS for the AFRP girder and spliced girder projects.

It is important to note that the trends and models discussed in this thesis are limited to the behavior of the concrete tested for this research and the measured experimental data obtained.

7.3 Recommendations

The experimental data collection and comparison to design and prediction equations provides useful data in the overall evaluation of the large scale specimens of the two projects considered in this study. However, further research into the behavior of SCC, curing conditions, and alternative test methods for mechanical properties of SCC would be beneficial for the future concrete industry. Information concerning the longevity of AFRP use in bridge girder as well as retrofitting existing girders using these construction materials is currently limited. Longer term tests of AFRP and SCC in bridge girders needs to be conducted to discern the behavior of the material after a number of years in service.

REFERENCES

ACI Committee 209 (2010). *Prediction of Creep, Shrinkage, and Temperature Effects in Concrete Structures (ACI 209R).* American Concrete Institute, Farmington Hills, MI.

ACI Committee 237 (2007). *Self -Consolidating Concrete (ACI 237R).* American Concrete Institute, Farmington Hills, MI.

ACI Committee 238 (2008). *Report on Measurements of Workability and Rheology of Fresh Concrete (ACI 238.1R-08).* American Concrete Institute, Farmington Hills, MI.

ACI Committee 301 (2010). *Specifications for Structural Concrete (ACI 301R).* American Concrete Institute, Farmington Hills, MI.

ACI Committee 308 (2001). *Guide to Curing Concrete (ACI 308R-01).* American Concrete Institute, Farmington Hills, MI.

ACI Committee 318 (2008). *Building Code Requirements for Structural Concrete and Commentary (318R-08).* American Concrete Institute, Farmington Hills, MI.

ACI Committee 363 (1992). *State of the Art Report on High-Strength Concrete (363R-92).* American Concrete Institute, Detroit, MI.

ACI Committee 440 (2006). *Guide for the Design and Construction of Concrete Reinforced with FRP Bars (ACI 440.1R-06).* American Concrete Institute, Farmington Hills, MI.

Al-Omaishi, N., Tadros, M. K., and Seguirant, S. J. (2009). "Elasticity modulus, shrinkage, and creep of high-strength concrete as adopted by AASHTO."*PCI Journal*, 54(3), 44-63.

ASTM C31 (2003). "Standard Practice for Making and Curing Concrete Test Specimens in the Field." In *Annual Book of ASTM standards*. West Conshohoken, Pennsylvania: The American Society for Testing and Materials.

ASTM C39 (2004). "Standard test method for compressive strength of cylindrical concrete specimens." In *Annual Book of ASTM standards*. West Conshohoken, Pennsylvania: The American Society for Testing and Materials.

ASTM C78 (2010). “Standard Test Method for Flexural Strength of Concrete (using Simple Beam with Third-Point Loading).” In *Annual Book of ASTM standards*. West Conshohoken, Pennsylvania: The American Society for Testing and Materials.

ASTM C172 (2003). “Standard Practice for Sampling Freshly Mixed Concrete.” In *Annual Book of ASTM standards*. West Conshohoken, Pennsylvania: The American Society for Testing and Materials.

ASTM C318 (2009). “Standard test method for density (unit weight), yield, and air content of concrete.” In *Annual Book of ASTM standards*. West Conshohoken, Pennsylvania: The American Society for Testing and Materials.

ASTM C469 (2010). “Standard test method for static modulus of elasticity and Poisson's ratio of concrete in compression.” In *Annual Book of ASTM standards*. West Conshohoken, Pennsylvania: The American Society for Testing and Materials.

ASTM C496 (2011). “Standard Test Method for Splitting Tensile Strength of Cylindrical Concrete Specimens.” In *Annual Book of ASTM standards*. West Conshohoken, Pennsylvania: The American Society for Testing and Materials.

ASTM C1610 (2010). “Standard test method for static segregation of self-consolidating concrete using column technique." In *Annual Book of ASTM standards*. West Conshohoken, Pennsylvania: The American Society for Testing and Materials.

ASTM C1611 (2009). “Standard test method for slump flow of self-consolidating concrete." In *Annual Book of ASTM standards*. West Conshohoken, Pennsylvania: The American Society for Testing and Materials.

ASTM C1621 (2009). “Standard test method for passing ability of self-consolidating Concrete by J-ring." In *Annual Book of ASTM standards*. West Conshohoken, Pennsylvania: The American Society for Testing and Materials.

ASTM C1712 (2009). “Standard test method for rapid assessment of static segregation resistance of self-consolidating concrete using penetration test." In *Annual Book of ASTM standards*. West Conshohoken, Pennsylvania: The American Society for Testing and Materials.

ASTM C1758 (2013). “Standard practice for fabricating test specimens with self-consolidating concrete." In *Annual Book of ASTM standards*. West Conshohoken, Pennsylvania: The American Society for Testing and Materials.

Bažant, Z. P., and Novák, D. (2001). "Proposal for standard test of modulus of rupture of concrete with its size dependence." *ACI Materials Journal,* 98(1), 79-87.

CEB-FIP (2010). *CEB-FIP model code 2010,* Thomas Telford, London.

Daczko, J. A. (2012). *Self-consolidating concrete : applying what we know*. Spon Press, London; New York.

Domone, P. L. (2007). "A review of the hardened mechanical properties of self-compacting concrete." *Cement and Concrete Composites,* 29(1), 1-12.

Fowler, D. W. (2008). "Self- consolidating concrete for precast structural applications: Mixture proportioning, workability, and early-age hardened properties." *Report no. TX-0-5134-5141*.

Gutierrez, P. A., and Canovas, M. F. (1995). "The modulus of elasticity of high performance concrete." *Material Structures,* 28(10), 559-568.

Hameed, A.H. (2009). "The Effect of Curing Condition on Compressive Strength in High Strength Concrete." *Diyala Journal of Engineering Sciences,*2(1), 35-48.

Henault, J.W. (2014). " Self-Consolidating Concrete: A Synthesis of Research Findings and Best Practices – Final Report." *Rep. CT-2255-F-12-4.*

Hurlebaus, S., Pirayeh Gar, S., Mander, J.B., Cummings W., Prouty, M. (2014). "Sustainability of Transportation Structures using Composite Materials to Support Growth and Trade." *Rep. No. SWUTC/14/600451-00028,* Southwest University Transportation Center.

Khayat, K. H. (1999). "Workability, testing, and performance of self-consolidating concrete." *ACI Materials Journal,* 96(3), 346-353.

Kim, Y.H., Trejo, D., Atahan, H., Hueste, M.B. (2012). "Mechanical Property Prediction for High Early Strength Self-Consolidating Concrete." *J.Mater.Civ.Eng.,* 24(12), 1501-1512.

Long, W., Khayat, K. H., and Hwang, S. (2013). "Mechanical properties of prestressed self-consolidating concrete." *Materials and Structures/Materiaux Et Constructions*, 46(9), 1473-1487.

Mander, J. (2014), Personal communication, College Station, TX, May 2014.

Mehta, P.K., and Monteiro, P.J.M. (2006). *Concrete: Microstructure, Properties, and Materials.* 3rd. New York: McGraw-Hill Companies, Inc.

Mertol, H. C., Rizkalla, S., Zia, P., and Mirmiran, A. (2010). "Creep and shrinkage behavior of high-strength concrete and minimum reinforcement ratio for bridge columns Halit Cenan Mertol, Sami Rizkalla, Paul Zia, and Amir Mirmiran ." *PCI Journal*, 2-18.

Naik, T. R., Kumar, R., Ramme, B. W., and Canpolat, F. (2012). "Development of high-strength, economical self-consolidating concrete." *Constr.Build.Mater.*, 30 463-469.

Newbolds, S.A. and Olek, J. (2001). "Influence of Curing Conditions on Strength Properties and Maturity Development of Concrete." *Rep. No. FHWA/IN/JTRP-2001/23,* Indiana Department of Transportation.

Okamura, H., and Ouchi, M. (2003). "Self-Compacting Concrete." *Journal of Advanced Concrete Technology*, 1(1), 5.

Okamura, H., and Ozawa, K. (1996). "Self-compacting high performance concrete." *Structural Engineering International: Journal of the International Association for Bridge and Structural Engineering (IABSE)*, 6(4), 269-270.

Oliva, M. G., and Cramer, S. (2008). "Self-Consolidating Concrete: Creep and Shrinkage Characteristics." Department of Civil and Environmental Engineering University of Wisconsin.

Ozyildirim, C. and Carino, N.J. (2006). “Concrete Strength Testing.” In *Significance of Tests and Properties of Concrete and Concrete-making Materials – STP 169D.* West Conshohoken, Pennsylvania: The American Society for Testing and Materials.

Pirayeh Gar, S., Head, M., Hurlebaus, S., and Mander, J. B. (2013). "Comparative experimental performance of bridge deck slabs with AFRP and steel precast panels." *Journal of Composite Construction*, 17(6).

Pirayeh Gar, S. (2012), "Structural Performance of a Full-Depth Precast Bridge Deck System Prestressed and Reinforced with AFRP Bars," PhD Dissertation, Texas A&M Univ., College Station, TX.

Sesha Phani, S., Sekhar, S., Rao, S., and Sravana. (2013). "Evaluation of Relationship Between Mechanical Properties of High Strength Self Compacting Concrete." *American Journal of Engineering Research*, 2(4), 67.

Tex-407-A (2008). "Sampling Freshly Mixed Concrete." *Standard specifications for construction and maintenance of highways, streets, and bridges.* Texas Department of Transportation, Austin.

Tex-415-A (2008). "Slump of Hydraulic Cement Concrete." *Standard specifications for construction and maintenance of highways, streets, and bridges.* Texas Department of Transportation, Austin.

Tex-416-A (2008). "Air Content of Freshly Mixed Concrete by Pressure Method." *Standard specifications for construction and maintenance of highways, streets, and bridges.* Texas Department of Transportation, Austin.

Tex-417-A (2008). "Unit Weight, Yield, and Air Content (Gravimetric) of Concrete." *Standard specifications for construction and maintenance of highways, streets, and bridges.* Texas Department of Transportation, Austin.

Tex-418-A (2008). "Compressive Strength of Cylindrical Concrete Specimens." *Standard specifications for construction and maintenance of highways, streets, and bridges.* Texas Department of Transportation, Austin.

Tex-421-A (2008). "Splitting Tensile Strength of Cylindrical Concrete Specimens." *Standard specifications for construction and maintenance of highways, streets, and bridges.* Texas Department of Transportation, Austin.

Tex-422-A (2008). “Temperature of Freshly Mixed Concrete.” *Standard specifications for construction and maintenance of highways, streets, and bridges.* Texas Department of Transportation, Austin.

Tex-448-A (2008). “Flexural Strength of Concrete (using Simple Beam with Third-Point Loading).” *Standard specifications for construction and maintenance of highways, streets, and bridges.* Texas Department of Transportation, Austin.

Trejo, D., Hueste, M.B., Kim, Y.H., and Atahan, H. (2008). "Characterization of self-consolidating concrete for design of precast, prestressed bridge." *Rep. FHWA/TX-09/0-5134-2*.

Trejo, D., Aguiniga, F., Buth, C. E., Yuan, R., and Keating, P. (2000). "FRP Reinforcing Bars in Bridge Decks: State of the Art Review." *Rep. FHWA/TX-09/0-5134-2*.

TxDOT (2013). *Bridge design manual - LRFD*, Texas Department of Transportation, Austin.

Yang, C., Yang, Y., and Huang, R. (1997). "The Effect of Aggregate Volume Ratio on the Elastic Modulus and Compressive Strength of Lightweight Concrete." *Jmst*, 5(1), 31-38.

Zemajitas, J.Z. "Role of Concrete Curing." http://www.cement.org. Accessed April 2014.